NUMERICAL PREDICTION OF CHANNEL CHANGES IN LARGE, BRAIDED RIVERS DOMINATED BY SUSPENDED SEDIMENT

A Dissertation

Submitted to the Faculty of the National Graduate Institute for Policy Studies (GRIPS)

in Partial Fulfillment of the Requirements for the Degree of

DOCTOR OF PHILOSOPHY IN DISASTER MANAGEMENT

by

Robin Kumar Biswas

September, 2016

NUMERICAL PREDICTION OF CHANNEL CHANGES IN LARGE, BRAIDED RIVERS DOMINATED BY SUSPENDED SEDIMENT

A Dissertation

Submitted to the Faculty of the National Graduate Institute for Policy Studies (GRIPS)

and International Centre for Water Hazard and Risk Management (ICHARM),

Public Works Research Institute (PWRI)

in Partial Fulfillment of the Requirements for the Degree of

DOCTOR OF PHILOSOPHY IN DISASTER MANAGEMENT

by

Robin Kumar Biswas

September, 2016

Declaration

Except where specific reference has been made to the work of others, the work embodied in this thesis is the result of investigation carried out by the author. No part of this thesis has been submitted or is being concurrently submitted in candidature for any degree at any other institution.

(Robin Kumar BISWAS)

This page intentionally left blank

Abstract

The present study describes a numerical method for evaluating channel changes and acquiring suitable information to improve the management of those rivers dominated by suspended sediment. The influence of a lateral bed slope on suspended sediment transport is studied first, focusing on the erosion and deposition process in the near-bank region. An expression for the erosion term that includes the lateral bed slope is derived based on the principle of sediment transport by turbulent diffusion. The lateral profile of the sediment concentration is also derived theoretically from a depth-integrated convection equation in an idealized flow field. Numerical computations suggest that riverbed evolution, such as scour holes and ridges due to erosion and deposition in the bank area, is amplified by the effects of the lateral bed slope. As such, the present study proposes a modified erosion rate term in the governing equations for bed sediment and sediment within the flow body.

The formation and migration of sandbars in the Brahmaputra River are studied using a two-dimensional depth-integrated numerical model, remote sensing data, and measured cross-sections. To overcome the limited data availability, the initial channel topography are set from the remote sensing data. The performance of the model was verified using field data from field investigations and remote sensing data. The computed results suggest that the model captures the formation and deformation of sandbars, the maximum bed scouring and aggradation, the bedload and suspended load transport rate, and the suspended sediment concentration well. The simulated results are matched with field observation.

In the present study, I propose a bank erosion model that is capable of computing the bank shifting using coarse-sized grids. In developing the model, I assumed that the

riverbank erosion was continuous, despite the intermittent behavior of the riverbank's collapse. The eroded sediment in the near-bank region is instantly counterbalanced by the slip-type failure of the adjacent riverbank. To overcome the issue of movable boundaries, I used flexible grids in the near-bank region to maintain similarity in bank shape. The proposed model for riverbank erosion and the erosion term corrected with the lateral bed slope are introduced to a two-dimensional 2D depth-integrated model with general coordinate system developed by Takebayashi et al. The results suggest that proposed model captures the gradual shifting of a riverbank with a coarse-sized grid. The corrected erosion rate term is suitable for covering the bank erosion in the Brahmaputra River.

Remote sensing data are analyzed to validate the results obtained from the numerical simulations. Assuming that an edge exists between two land covers, I propose the modified gradient-based method (MGBM) to highlight the edge between water and soil for automatically detecting sandbar. The results obtained using the proposed method were verified by means of field investigations, which were conducted to identify edges by travelling along the sandbars with a manned boat tethered to a tetra-head boat mounting with an acoustic Doppler current profiler (ADCP) and global positioning system (GPS). The sizes and shapes of sandbars identified by the proposed method coincided with those in the field investigations.

In the final part of the study, water and river management policy in Bangladesh are reviewed. The findings of the present study are used to conceptually improve the existing policy practice.

Acknowledgement

I am extremely delighted to express my sincere gratitude to my supervisors, Dr. A. Yorozuya, associate professor at National Graduate Institute for Policy Studies (GRIPS) and senior researcher at the International Centre for Water Hazard and Risk Management (ICHARM), Public Works Research Institute (PWRI), and Professor S. Egashira, research and training advisor of ICHARM, PWRI, Japan, for their continuous support, invaluable advice, and incessant encouragement in completing the study.

Professor T. Koike and Professor K. Takeuchi, respectively the director and advisor of ICHARM, PWRI, Japan, have inspired me with positive suggestions and comments to integrate the findings of the present study to the river management, for which I express my gratefulness. Also, I am thankful to Professor H. Nakagawa of Kyoto University, Japan, for his careful review and positive advice. H. Takebayashi, associate professor at Kyoto University, Japan, provided the source code of the model and gave me valuable suggestions on how to treat the suspended sediment in the near-bank region. I acknowledge their contributions. Former researcher Dr. K. Kibler and former chief researcher Mr. M. Kamoto deserve special thanks for their support and valuable suggestions. I am indebted to PWRI and the National Graduate Institute for Policy Studies (GRIPS) for their financial support to carry out this study in Japan.

My beloved wife Ms. Soma Roy and son Aditya Kumar Biswas have sacrificed a considerable amount of time and supported me in my difficulties. I appreciate their precious contributions. Above all, I am thankful to the almighty God for the blessings that have made this study possible. I dedicate this thesis to my father and first teacher, the late Shanti Kumar Biswas, as well as my mother and beloved son.

Table of Contents

List of Tables

List of Figures

1. Introduction

1.1 Background

Protection of land from any disasters is important because of the high population density and agriculture-dependent socioeconomic activities in Bangladesh. Riverbank erosion remains one of the critical problems in Bangladesh. People living along the banks and on the islands of the major rivers such as the Ganges, the Brahmaputra, and the Meghna are always under a constant threat of losing their homesteads and livelihoods to riverbank erosion. The constant threat of riverbank erosion has contributed to the development of a substantial disaster subculture in the riverine zones of Bangladesh (Haque, 1988; Hutton & Haque, 2003). Figure 1.1 shows the locations of the river reaches that are susceptible to riverbank erosion in Bangladesh. It reveals that riverbank erosion is observed not only along the major rivers, but also along their tributaries and distributaries. The population of Bangladesh has doubled since the 1970s, so more people are exposed to this hazardous environment than before.

The total length of rivers up to 50 m wide is about 24,000 km, of which about 1,200 km and 500 km of riverbank are under active and severe erosion, respectively (Islam, 2006). According to NHC (2013), since 1973, major rivers have eroded about 2,600 km² of land, leaving 2 million people homeless in Bangladesh. To minimize the risk, usually the affected people involuntarily take shelter adjacent to the flood embankments and in villages, distant villages, big cities, and even the slum area located in the capital. Most of the time, the displacees experience socioeconomic destitution as a result of unintentional migration (Hutton & Haque, 2004).

Figure 1.2 shows the decadal pattern of riverbank erosion in the major rivers of Bangladesh obtained with Landsat image analysis. The results suggest that among the rivers in Bangladesh, the Brahmaputra River is the most erosion prone. A number of studies suggest that among the affected people, more than 60 percent are from the floodplain of the Brahmaputra River. According to World Bank (2015), in the last 40 years, about 1 million people were displaced due to channel changes in the Brahmaputra River. During this time, the river engulfed about 1,000 km^2 arable and 50 km^2 of homestead land. The sandbar and total river area increased from 424 km^2 to 710 km^2 and from 686 km^2 to 1,400 km^2, respectively, while the water area during the dry season remained unchanged (NHC, 2013), which suggests that the fertile floodplain has converted to unproductive sandbar. Many studies, such as those by Coleman (1969), Klaassen and Masselink (1992), CEGIS (2007), and Nakagawa et al. (2013), reported that the annual riverbank erosion rate in the Brahmaputra River, Bangladesh, is on the order of 10^2 to 10^3 meters per year. Apart from direct land losses, riverbank erosion exacerbates flooding, as well.

Figure 1.3 shows the changes of the riverbank line in the Brahmaputra River from 1973 to 2015, as well as the locations of the erosion and deposition areas based on the Landsat images. The results suggest that the right bank of the Brahmaputra River is more erosion prone than the left bank. In order to curb the riverbank erosion problem, a number of structural measures have been implemented in Bangladesh since the 1990s. The left part of Figure 1.3 shows the locations and types of the hydraulic structures that have been implemented along the right and left banks of the Brahmaputra River from 1995 onward. The structural measures on the right bank are higher than those of the left bank. It is noticeable that the hydraulic structures can broadly be categorized into two major groups

as follows: (i) structure parallel to the riverbank, for instance, hard point, revetment, guide bunds, and (ii) flow-diverting structures such as spur-dykes and groins. According to Sarker and Akter (2011), both types of structures have faced damages to some extent when exposed to the main channel. However, the degree of damage is higher for flow-diverting structures such as spur dykes. Figure 1.4 shows an example of the damaged spur in the Brahmaputra River. The picture suggests that the solid part of the structure may be strong enough to withstand the fluid forces. However, the channel shifting in the upstream of the spur is very severe. As a result, the river ultimately takes a new course, leaving the structure ineffective. This phenomenon is very common along the Brahmaputra River. Therefore, it is indispensable to predict channel changes and riverbank shifting.

Application of satellite images is a common tool to understand channel changes in Bangladesh. Several studies, such as those by Oya (1979), Klaassen and Masselink (1992), Best and Bristow (1993), Bristow (1993), Klaassen et al. (1993), Mosselman et al. (1993), Sarker (2009), Sarker and Akter (2011), Sarker et al. (2013), and Baki and Gan (2012), have employed Landsat images to understand the channel changes in the Brahmaputra River and to develop the empirical relationships among different parameters related to flow and sediment transport. In these studies, the satellite images were collected once a year during the dry season. Thereafter, images of the riverbank and sandbars were digitized and compared to the images of successive years to detect morphological changes. Using similar approaches and based on the shapes of the sedimentary features such as a contraction bar, sharpened bar, sand wing, sand tongue, and bankside sandbar from the dry season satellite images, the Centre for Environmental

and Geographic Information Services (CEGIS) has developed a methodology to forecast the morphological changes in the major rivers of Bangladesh (CEGIS, 2002).

In addition to the satellite-based information, physical and numerical models are the tools that have been used by researchers to evaluate the channel changes in the experimental channel as well as explain the behavior of the rivers in the actual field condition. Both approaches have their advantages and limitations. Physical modelling can provide directly specific results, but sometimes it is expensive and time consuming. The flow, sediment transport, and riverbed changes are very complex. The riverbed is dominated by sand and/or silt in most of the rivers in Bangladesh. Correspondingly, it is difficult to attain similarity with respect to sediment transport and flow resistance. Again, most of the model tests are performed using some distorted scale model, which creates difficulties in properly translating the experimental results into one prototype. On the other hand, prediction by means of a numerical simulation using governing equations of the water flow and sediment transport will give results directly without any scale factors. However, the simulation results must be validated using data from field investigations.

The application of the numerical models in suspended-sediment-dominated large braided rivers is challenging for the following reasons: (i) The river morphology behaves almost erratically, (ii) the characteristics of the suspended sediment transport are non-equilibrium, and (iii) the available data are not sufficient. These factors cause difficulties in specifying the initial and boundary conditions for the numerical model. Figure 1.5 shows the relationship between the non-dimensional suspended sediment transport rate to the relative fall velocity of sediment particle and non-dimensional bed load transport rate to the non-dimensional bed shear stress. The results suggest that the bedload transport rate follows the pattern of the bed shear stress. However, the suspended

sediment transport rate scatters with the relative fall velocities of sediment particles. This signifies that defining the initial condition for suspended sediment is difficult, which creates problems for the development of a numerical model for suspended sediment.

Many researchers in Japan and around the world, such as Ashida (1964), Ikeda (1975), Engelund (1974), Kikkawa et al. (1976), Hasegawa (1981), Ikeda et al. (1981), Parker et al. (1982), Fujita and Muramoto (1982), Kitanidis and Kennedy (1984), Johannesson and Parker (1985), Blondeaux and Seminara (1985), Hasegawa and Mochizuki (1989), and Kovacs and Parker (1994), have proposed several numerical models to predict and explain the channel changes. Researchers and river engineers such as Dietrich et al. (1979), Crosato (1989), Howard (1992), Nagata et al. (2000), Darby et al. (2002), Duan (2004), Jang and Shimizu (2005), and Duan and Julien (2010) have applied numerical models for evaluating the channel changes in bedload-dominated rivers. However, numerical models to study the mechanisms of channel changes in suspended-sediment-dominated large braided rivers are not common (Mosselman, 1995). Riverbed evolution corresponding to the erosion and deposition of suspended sediment is complex in the bank region due to the existence of a lateral bed slope.

The channel changes in the vicinity of the hydraulic structures such as the spur-dykes have been studied by several researchers, with some using a numerical model. For example, Zhang et al. (2011) predicted the consequences of bank protection measures along the Brahmaputra River. Therefore, efforts to understand the local phenomenon have been limited. There are no comprehensive studies that have been conducted to understand the channel changes in the large, suspended-sediment-dominated Brahmaputra River by means of the numerical model.

The present research applies a numerical model based on two-dimensional, depth-integrated governing equations developed by Takebayashi et al. (2000). Takebayashi et al. as well as other researchers applied the model to explain issues related to sediment transport in different hydraulic conditions. For example, Takebayashi et al. (2000) studied the formative condition and mechanism of a self-formed stream channel in a straight river course in terms of flume test and numerical analysis. In their study, formation of equilibrium multiple-row bars is investigated by means of numerical analysis under a wide range of hydraulic conditions. Takebayashi et al. (2003) analyzed the braided streams formed on beds with non-uniform sediment. Takebayashi (2008) also studied the instability of stream geometry using numerical analysis in a straight, open channel. Luu et al. (2004, 2005) applied the model to understanding the mechanism of river change of Tan Chau reach in the lower Mekong River using field data and numerical simulation. A new treatment of exchange layer thickness was introduced by Luu et al. (2006) to evaluate the sediment sorting and armoring process in experimental channels. However, the validity of the numerical model proposed by Takebayashi et al. (2000) has not been tested to analyze the channel changes in large braided rivers dominated by suspended sediment. In addition, Yorozuya et al. (2012, 2013) attempted to predict suspended sediment transportation, bank erosion, and sandbar behaviors in mega-size rivers such as the Ganges and the Brahmaputra, although they did not obtain notable results. Through these studies as well as review studies, I have learned that it would be better to modify the expression of the erosion term in mass conservation equations of sediment, both in fluid body and bed sediment, when I analyze sediment behavior in bank regions for suspended-sediment-dominated rivers.

1.2 Large Braided Rivers

The patterns of the river channel are classified as straight, meandering, and braided based on the planform view (Brice et al., 1978; Leopold & Wolman, 1957; Muramoto & Fujita, 1978; Schumm, 1981). The braiding intensity depends on the ratio of the channel length that is divided by islands or sandbars. In braided rivers, streams are divided into several channels with submerged and emerged bars, depending on the flood stage. The flow pattern and sediment transport are complicated in braided rivers due to the frequent occurrence of bifurcation and confluence.

The geometry and formation region of the braided river have been studied by many researchers. Muramoto and Fujita (1978) proposed a criterion for the formation of bed configuration in the river channel based on a simple relationship between the ratios of the width to depth and the depth to particle size for explaining the formative condition of the river channel pattern. They categorized the formation region of mesoscale bed form as semi bar (straight), alternating bar (meandering), and double-row bar (braided), with each fulfilling a specific condition. Kuroki and Kishi (1984) classified the bed forms as no occurrence, alternate bar, and multiple-row bar using the width, flow depth, riverbed slope, and non-dimensional bed shear stress. Both Muramoto et al.'s (1978) and Kuroki et al.'s (1984) methods are proposed for the flow field in the bedload dominated river.

A wide variety of criteria exists for defining large rivers. For example, large, braided rivers are characterized by a complex flow process and channel pattern (Mosley, 1982), high width-to-depth ratio, and extensive floodplains for channel shifting having low gradients (Ashworth & Lewin, 2012; Lewin & Ashworth, 2014). Potter (1978) described large rivers as having a large drainage basin or a long river course, or transporting a large volume of sediment and water. Potter plotted the drainage basin area

against the river length and suggested that an average river having a length of 1,000 km possesses a drainage basin of 100,000 km^2. Large rivers have drainage basins greater than 5×10^5 km^2 or mean annual discharge at the river mouth higher than 2,000 m^3 s^{-1} (WMO, 2006), whereas the lower limit is 1,000 m^3 s^{-1} (Latrubesse, 2008).

Lane et al. (2008) proposed that large rivers have high width-to-depth ratios 1 to 2 orders higher than small rivers. Their study described small rivers as having a width less than 10 m. Ruben et al. (2015) considered width-to-depth ratios higher and lower than 30 to classify small and large rivers, respectively. Considering the channel dimension threshold, Sambrook Smith et al. (2009) considered a width over 1,000 m for large rivers. Molinas and Wu (2010) designated large rivers as those having yearly average flow depths higher than 4 m. A hierarchy of mid-channel sandbars and islands, some of which are characterized by heavy vegetation, are observed in large rivers. The islands and bed forms are submerged during flows higher than that of the bankfull discharge and exposed during the low-flow condition. In terms of bed configuration, dunes are the representative bed form in the large rivers. The dune height and length in large rivers increase with discharge. However, the dune steepness is almost constant with discharge, and the ratio of dune wavelength to flow depth is 6.5 in large rivers (Julien, 1992).

Based on the discussion above, it is difficult to adopt a universal threshold in order to define a large river. In the present study, I compute the riverbed variations using a numerical model as the prediction tool. Several studies have been conducted using the tool in different hydro-morphological situations. Considering the environment of the previous application of the modeling tool, in this study, I refer to large rivers as those rivers that have high width to depth ratios, comparatively small diameters of transported

sand particles, and width on the order of 10^3 m, and the model has not been applied previously to predict channel changes in such morphological conditions.

1.3 Suspended-Sediment-Dominated Rivers

Understanding of the dominant sediment transport type is essential for explaining the formation and migration process of sandbars and bed forms. The sediment transport is categorized as bedload, mixed load, and suspended load by many researchers such as Schumm (1963, 1969). According to Einstein (1950), in the case of bedload, the sediment particles move in the bedload layer by rolling, by sliding, and occasionally by jumping. In suspended sediment transport, the sediment particles move outside the bedload layer and remain in suspension in a flow body under the action of the turbulence of the flow. The bedload transport rate is characterized by non-dimensional bed shear stress. The non-dimensional bed shear stress increases with discharge; thus, so does the rate of the bedload transport. In addition to the non-dimensional bed shear stress, relative fall velocity, which is defined as the ratio of the particle fall velocity to the shear velocity, is a key parameter to explain the characteristics of the suspended sediment transportation. A relative fall velocity greater than unity signifies dominance of the bedload, and less than unity shows dominance of the suspended sediment. In suspended-sediment-dominated river, the sediment transport in the form of bedload is small. Therefore, the erosion and deposition process controls the riverbed evolution and channel changes. The erosion rate is usually defined as the sediment transport by turbulent diffusion from the riverbed. The deposition rate is evaluated by the depth-averaged sediment concentration. Therefore, parameters that control the spatial and temporal sediment concentration within the flow body and the reference layer, initial conditions for sediment concentration, and direction of sediment

entrainment and deposition are to be determined critically in order to evaluate the channel change.

The mode of dominant sediment transport in a river is normally measured by the ratio of the transport rate of suspended to bedload. Schumm (1963) hypothesized that the probability of having maximum bedload in a river is 60–70% of the total load. The proportion of bed sediment ranges from 0% to 15% of the total load in suspended-sediment-dominated rivers. In the present study, a ratio higher than 10 is regarded as the indicator to define the dominance of the suspended sediment.

1.4 Objectives of the Research

The mechanism of channel change remains the same in all climatic conditions. However, the local factors such as sediment transport mode, physical dimensions of the channel, and mesoscale bed configuration influence the pattern and extent of the channel changes. Therefore, it is important to study the sediment transport and associated channel changes to develop a river management strategy and execute suitable countermeasure. With the present research, I aim to understand the mechanism for channel changes in suspended-sediment-dominated large braided river by means of two-dimensional depth-averaged governing equations for water flow and sediment transport. I also aim to develop and apply a numerical method for predicting channel changes in suspended-sediment-dominated large rivers using satellite-based information in order to obtain useful information for improving river management as well as to test the possibility of using the proposed method as a tool to improve the river management strategy of Bangladesh.

Figure 1.6 summarizes the methodology adopted in this study. The methodology applied in this study includes a two-dimensional depth-integrated numerical model,

fundamentals of sediment hydraulics, field observations, and remote sensing data analyses. The numerical model acts as a tool to predict and evaluate the target phenomenon. The remote sensing and field observation data are used to define the initial conditions, develop a method for sandbar monitoring, and validate results from numerical simulation.

1.5 Outline of the Thesis

The present study is conducted to achieve the stated objectives and is described in seven chapters. The current chapter introduces the background of the present research work, review of previous studies, criteria for delineating large rivers and braided rivers, and criteria for suspended-sediment-dominated rivers. Following the introduction, characteristics of the Brahmaputra River are discussed in terms of hydrograph, sediment characteristics, and planform changes in Chapter 2. Chapter 3 discusses the derivation of the two-dimensional, depth-integrated governing equations, modified erosion rate, and suspended sediment concentration profile in the transverse direction under steady-uniform and unidirectional flow conditions. Furthermore, Chapter 3 includes the effect of the modified erosion rate and sediment transport by turbulent diffusion in the lateral direction on the evolution of the riverbed configuration. Chapter 4 proposes a method for determining the dimensions of the sandbar automatically from remote sensing data such as the daily surface reflectance of the MODIS data set. This chapter also includes results to verify the proposed method and further applies the proposed method to monitor the formation and migration of sandbars in the Brahmaputra River. Chapter 4 also describes a method for conducting field investigations in the Brahmaputra River. Chapter 5 describes the application of two-dimensional depth-integrated governing equations for studying the formation and migration of sandbars in the study area of the Brahmaputra

River. Chapter 6 introduces a new bank erosion model that is capable of using the coarser grid to compute the bank erosion. This chapter also discusses the effects of the modified erosion rate term on riverbank erosion and results of the proposed bank erosion model. Finally, Chapter 7 draws conclusions by summarizing the outcomes of the research and explores the policy implications for future water resource management.

2. Characteristics of the Brahmaputra River

2.1 Introduction

Bangladesh is located at the outlet of the Ganges–Brahmaputra–Meghna (GBM) river system. Figure 2.1 shows the basin area of the GBM basin together with the location of Bangladesh. The total drainage basin area of the GBM river system is about 1.72 × 106 km^2 (Chowdhury & Ward, 2004) and supplies about 1.35×10^{12} m^3 of water (FAO, 2000) and 1.7×10^9 tons of sediment (Milliman & Meade,1983) annually to the Bay of Bengal. About 80% of the total water discharge is concentrated during the month of June to October (Ahmad & Ahmed, 2003). According to Islam et al. (1991, 2001), about 25% of the total sediment takes part actively in the process of channel changes. The riverbed materials are comprised of fine particles that are easy to entrain into the flow body. Therefore, the sediment particles easily entrain into the flow body. In fact, a number of studies, for example, those by Holeman (1968), Coleman (1969), and Mosselman (1995), suggest that most of the rivers in Bangladesh are dominated by suspended sediment and are subjected to frequent planform changes due to erosion and deposition.

The Brahmaputra River originates from the Chemayungdung glacier in the Kailas range of the southern Tibet at an elevation of 5,300 m above sea level. The total length of the Brahmaputra River is 2,880 km, with a drainage area of 560,000 km^2, and receives water from four countries: China, Bhutan, India, and Bangladesh. The shape of the basin is irregular, having a maximum width in the east-to-west direction of 1,540 km and in the north-to-south of 680 km (Mahanta et al., 2014). Out of the total basin area, only 8% lies in Bangladesh. The main river channel travels through China, India, and Bangladesh.

Flooding is recurrent in the Brahmaputra basin. As a consequence of flooding, channel changes are also common.

2.2 Flow Characteristics

In terms of discharge, the Brahmaputra is the fifth largest river in the world (Thorne et al., 1993). On average, each year, the Brahmaputra River carries about 5.4×10^{11} m^3 of water to the Bay of Bengal. The flooding season usually prevails during May to October, and the low flow season lasts from December to March. Figure 2.2 shows a box-and-whisker plot depicting the range of flood variability for each month together with the average hydrograph and flood hydrograph of large flood events (such as 1988, 1998, and 2008) based on the data collected by Bangladesh Water Development Board (BWDB) at the Bahadurabad gauging station. Figure 2.2 suggests that the mean annual peak of flood is about 65,000 $m^3 s^{-1}$ (Delft Hydraulics & DHI, 1996); the maximum discharge was 102,535 $m^3 s^{-1}$, observed in September 1998; and the minimum discharge was 3,095 $m^3 s^{-1}$, observed in May 2000. The average annual discharge is 20,200 $m^3 s^{-1}$ (Sarker et al., 2003).

Figure 2.3 shows a relation between annual maximum discharge and exceedance probability. The discharge having a return period of one year represents the bankfull discharge, as flooding occurs every year in the Brahmaputra basin. In the present study, the bankfull discharge is estimated as 44,000 $m^3 s^{-1}$. In 1996, Delft Hydraulics and Danish Hydraulic Institute (DHI) estimated bankfull discharge at 48,000 $m^3 s^{-1}$. Figure 2.4 shows the inter-annual variability of the flow in the Brahmaputra River in terms of the year-wise maximum discharge, year-wise average discharge, and ratio between year-wise maximum to minimum discharge. Figure 2.4 indicates that discharge varies widely in the Brahmaputra River between years. The maximum discharge in the river is 3 to 30 times

higher than the minimum discharge. Therefore, the sediment transport and channel changes vary significantly between years and seasons.

Figure 2.5 shows the relationship between discharge and water levels, which is obtained by plotting the data from long-term monitoring of water levels and corresponding discharge. The array of the points almost lays on a curve that is approximately parabolic and can be represented by $H = 3.9542Q^{0.1443}$. Bangladesh Water Development Board (BWDB) forecast the water levels in the river system of Bangladesh. According to Flood Forecasting and Warning Centre of Bangladesh, the danger level and discharge corresponding to the danger level are 19.33 m and 63,199 m^3 s^{-1} (FFWC, 2013), respectively. In addition to the danger level, the barfull and dominant discharge in the Brahmaputra River are 20,000 m^3 s^{-1} and 38,000 m^3 s^{-1} (FAP1, 1994; FAP 21, 1994).

2.3 Sediment Transport Characteristics

The bank material is one of the major sources of sediment to the river, which may influence the sediment budget. Many properties of the river are determined by the size and other characteristics of the bed and bank materials. For example, the bed materials reflect the types of sediment that are transported in the river. The sediment transport rate is inversely proportional to the size of the sediment particles. Therefore, in the case of the coarser bed materials, the sediment transport will be smaller. Again, the state of sediment transport depends on the intensity of the fluid forces on the sediment particles. In the case of deposition, sediment size is also important. The deposition at sandbars, the composition of banks and floodplains, and the channel geometry and planform of the river are influenced by the characteristics of the sediment particles. The bed material in the major rivers of Bangladesh is fine, fairly uniform sand (Delft Hydraulics & DHI, 1996).

Brahmaputra carries a very high amount of sediment compared to other rivers in the world. According to Schumm and Winkley (1994), it is the third-highest river in terms of total sediment load transport. On average, each year, the river carries about 540 $\times 10^9$ kg of sediment (Coleman, 1969) which ranges up to 725 $\times 10^9$ kg per year (Schumm & Winkley, 1994; Thorne et al., 1993). Subramanian and Ramanathan (1996) stated that the difference in sediment transport originates in the river mainly due to the variation seasonally and interannually of suspended sediment load. According to Klaassen and Vermeer (1988), most of the sediment remains under suspension in the Brahmaputra River. Based on the data collected during the period 1958 to 1962, Coleman (1969) estimated the suspended sediment concentration in the Brahmaputra River to be 1,000 mg l^{-1}. Such high sediment load also relates the large sediment yield of the river basin produced by heavy monsoon rainfall over the years (Saito, 2001). The riverbed comprises sediment with fine sand and silt. Based on the data collected during 1993-1994, the diameters of the sediment particles not exceeding 16%, 35%, 50%, 84%, and 90% by weight are 0.13, 0.16, 0.26, 0.29, and 0.34 mm respectively. The geometric standard deviation, which is defined as $0.5\left(d_{84}/d_{50}+d_{50}/d_{16}\right)$ of the bed material, is 1.50, where d_{84}, d_{50}, and d_{16} are diameters of the sediment particles not exceeding 84%, 50%, and 16% by weight.

The relationship between the discharge and sediment transport is expressed by an average curve and is generally referred to as a sediment rating curve. The rating curve is usually an exponential function and can be determined once the repressors are obtained by regression analysis or from a graph of data points. Since 1966, sediment data have been collected by BWDB. Using the data, a rating curve for sediment particles was

developed in the River Survey Project (RSP), which is expressed as $S = 0.35Q^{-1.42}$ and is used for making sediment balance studies (Delft Hydraulics & DHI, 1996). Because the river flow is strongly seasonal, the largest amounts of sediment are transported during flood season. The sediment transport capacity reduced rapidly with the decrease of velocities during the falling stage of the river. In the low stage, deposition takes place due to decreases in transport capacity.

2.4 Bedform and Cross-Sectional Characteristics

Understanding of the bedform is important for explaining river behavior such as the sediment transport rate, analysis of resistance factors, and prediction of local scour depth (Klaassen & Vermeer 1988; Peters, 1993). Furthermore, the bedform influences the growth of large-scale sandbar features and erosion or channel incision, which are keys to understanding river behavior. Coleman (1969) and Klaassen and Vermeer (1988) suggest that a wide range of bedforms starting from ripples to dunes and upper-stage plane beds exist in the Brahmaputra River. However, dunes are the predominant bedform in the Brahmaputra River. Over 40% of the bed is always occupied by dunes at any flow stage, which increases up to 70%. In the Brahmaputra River, the dune height and wavelength range from 0.15 to 6.3 m and 4.6 to 350 m, respectively and follow a log-normal distribution (Delft hydraulics & DHI, 1996). Delft Hydraulics and DHI (1996) also estimated the bedform migration rate at high stage range from 1.11 to 16.8 m hr^{-1}.

The nature of Brahmaputra is braiding. It has a number of channels and sandbars along its course of flow. It often shifts its course of main flow from one channel to another. The sandbar size ranges from a few meters to a few kilometers. Figure 2.6 shows the study area and the braided morphology of the Brahmaputra River in 2005 based on the Panchromatic Remote-Sensing Instrument for Stereo Mapping Digital Surface Model

(PRISM-DSM) data of the Advanced Land Observing Satellite (ALOS) provided by Japan Aerospace Exploration Agency (JAXA). As explained in the earlier sections, the seasonal variabilities in river discharge are high. During the periods of high discharge, the entire stream channel contains water, with the islands covered to become submerged bars. Some of the islands are eroded, but the sediment redeposits as the discharge decreases, forming new islands or submerged bars. Figure 2.7 shows the spatial and temporal planform changes in a part the Brahmaputra River within the study area based on the Landsat images of United States Geological Survey (USGS). Figure 2.7 is obtained from the Landsat images collected during the dry season. Arc Map, a GIS software, was used to estimate the riverbank migration and island dynamics within the study reach of the Brahmaputra River focusing on the changes before and after large flood events such as 1974, 1988, and 1998. As such, Figure 2.7 includes the planform of the Brahmaputra River for 1973, 1975, 1987, 1989, 1995, and 2000, which suggests active sandbar movement and river bank erosion.

Figure 2.8 shows that the river encompasses braided channels with multiple-row bars based on the criteria proposed by Kuroki and Kishi (1984) and Muramoto and Fujita (1978), and was obtained by using data as specified in Table 2.1. In Figure 2.8, I_0 is the bed slope, h is the flow depth, τ_* is the non-dimensional bed shear stress, A is the zone with no occurrence, B is the zone with alternate bar (single-row bar), and C is the zone having a multiple-row bar. The star marks show the bedform region based on the specific criteria for different flow discharge in the Brahmaputra River with mean sediment size d_{50} = 0.26 mm, average gradient I_0 = 0.0001, and Manning's n = 0.025. According to Muramoto and Fujita's (1978) criterion, the bedforms in the Brahmaputra River fall in the region of an alternate bar for all hydraulic conditions. Kuroki and Kishi's (1984)

criterion shows that bedforms in the river can be considered as multiple-row bars. Therefore, the Brahmaputra is comprised of a complex channel having combined bedforms characteristic of alternate bars and multiple-row bars.

Evolution and displacement of sandbars, channel abandonment, channel shrinking, and riverbank erosion are common in the river, making complicated morphological features in the Jamuna River. BWDB measures the cross-sectional data in the Brahmaputra River. The locations where BWDB is conducting measurement are indicated in Figure 2.6. Figure 2.6 also suggests that the cross-sectional shapes vary significantly between two measured sections. Figure 2.9 shows the changes in the river morphology with time based on measured cross-sections. The cross-sectional profile shows high mobility and the active nature of the bed. There exist multiple channels and sandbars that shift almost randomly between years. Because of the random behavior of the morphology, it is difficult to derive a solution for managing large rivers like the Brahmaputra River (Mosselman et al., 1995). Figure 2.10 shows typical changes in the morphology of the Jamuna River comparing the cross-section for 2008 to 2006 at RMJ 7, which suggests active riverbed changes after floods. The dominant channel in the right bank area widens significantly with riverbank erosion and riverbed scouring of about 5 m. The mid-channel turns to a narrow channel, and a big sandbar appears newly in the place of the channel. On the other hand, deposition is followed by channel shifting and channel splitting in the left bank region. The morphology of the second channel starting from the left bank also changes. Both channels are silted up, and old sandbars suffer from erosion. Considering sediment properties and flow variability, such shifting is not surprising and is common all over the study area.

3. Effect of Lateral Bed Slope on Suspended Sediment Transportation

3.1 Introduction

Riverbed evolution takes place through erosion and deposition processes. Bed materials composed of non-cohesive fine sediment such as non-cohesive sand and silt are entrained easily into the flow body because the fluid forces acting on sediment particles normally exceed their resisting forces during floods. Suspended sediment transportation, one of the key phenomena in river morpho-dynamics, has been studied by many researchers and professionals in relation to sediment-induced issues in river channels, reservoirs, artificial channels, etc. Representative results were obtained for sediment concentration profile, equilibrium concentration at a reference level near the bed, erosion rate, deposition rate, and turbulent structure of the flow field through those studies. The relation between suspended sediment transportation and channel morphology was studied also. Parker (1978) formulated a formation process of equilibrium cross-sectional shape. Ikeda and Izumi (1991) extended Parker's idea to the equilibrium cross-sectional shape with modified diffusion term. Figure 3.1 is a schematic diagram that shows a control volume for lateral sediment budget in which F_s is the suspended sediment transport by turbulent diffusion and q_{by} is the lateral component of bed load transport rate, E_n is the erosion rate of bed sediment, and D is the deposition rate of suspended sediment. Parker (1978) derived a differential equation for equilibrium cross-sectional shape assuming that the lateral transport rate of suspended sediment should be equal to lateral transport of bed load. Based on Parker's (1978) idea, Ikeda and Izumi (1991) developed a more rigorous model that predicts also an equilibrium cross-section with modified diffusion term.

3.2 Conventional Method for Bed Variation

Conventionally, the riverbed variation is computed using the mass conservation equation of sediment at the bed layer. Figure 3.2 shows the schematic diagram for sediment balance at the bed layer. The mass conservation equation for bed layer is expressed as follows:

$$\frac{\partial z_b}{\partial t} + \frac{1}{1-\lambda}\left(\frac{\partial q_{bx}}{\partial x} + \frac{\partial q_{by}}{\partial y} + E_n - D\right) = 0 \tag{3.1}$$

where t is the time, x is the coordinate in flow direction, y is the transverse direction, z_b is the riverbed elevation, q_{bx} and q_{by} are the component of the bed load transport rate in the x and y directions, respectively, E_n is the erosion rate, and D is the deposition rate.

In the case of suspended-sediment-dominated river, sediment transport in the form of bedload can be ignored. Under this circumstance, Equation 3.1 can be treated as follows:

$$\frac{\partial z_b}{\partial t} + \frac{1}{1-\lambda}\left(E_n - D\right) = 0 \tag{3.2}$$

According to Equation 3.2, the riverbed variation in suspended-sediment-dominated river is controlled by the erosion and deposition rate term. Erosion and deposition rates are defined as eroding and depositing sediment volume in unit time and unit area. The deposition rate is evaluated in terms of the sediment concentration in the reference layer in the vicinity of the bed surface and particle fall velocity. The erosion rate is determined by the turbulent characteristics near the bed. Conventionally, the erosion rate is evaluated using equilibrium sediment concentration at the reference layer. The equilibrium sediment concentration at the reference layer is determined, supposing an equilibrium state so that the sediment concentration does not change temporarily,

longitudinally, and transversely by using Rouse's (1937) profile for sediment concentration. Itakura and Kishi (1980) also proposed a formula based on the force balance on sediment particles in the vicinity of the bed layer. In both cases, the erosion rate is evaluated in the vertical direction.

As shown in Figure 3.1, sediment erosion takes place toward the normal direction of the bed boundary, and sediment deposition from the fluid body may occur vertically and is normally evaluated in terms of the product of fall velocity and reference sediment concentration. Correspondingly, the erosion term should be corrected, taking the lateral bed slope into consideration. In this chapter, I aim to modify the erosion terms in mass conservation equations of sediment for flow body and bed sediment as well as to investigate the effect of modified erosion term on bed variation numerically.

3.3 Derivation of 2-D Depth-Integrated Form of Mass Conservation Equation

The mass conservation of sediment within the flow body using Cartesian coordinate system is as follows:

$$\frac{\partial c}{\partial t}+\frac{\partial cu}{\partial x}+\frac{\partial cv}{\partial y}+\frac{\partial c(w-w_0)}{\partial z}=\frac{\partial}{\partial x}(\varepsilon_x\frac{\partial c}{\partial x})+\frac{\partial}{\partial y}(\varepsilon_y\frac{\partial c}{\partial y})+\frac{\partial}{\partial z}(\varepsilon_z\frac{\partial c}{\partial z}) \tag{3.3}$$

where c is the sediment concentration, t is the time, x is the coordinate in flow direction, y is the transverse direction, z is the coordinate in the vertical direction, u, v, and w are the x, y, and z components of depth-averaged velocity, respectively, w_0 is the fall velocity of sediment particles in the vertical direction, and ε_x, ε_y, and ε_z are the x, y, and z components of the diffusion coefficient, respectively.

The depth-integrated form for Equation (3.3) is as follows.

$$\frac{\partial ch}{\partial t}+\frac{\partial cuh}{\partial x}+\frac{\partial cvh}{\partial y}=\frac{\partial}{\partial x}\left(\in_x \frac{\partial c}{\partial x}h\right)+\frac{\partial}{\partial y}\left(\in_y \frac{\partial c}{\partial y}h\right)-cw_0\big|_{z_b}$$
$$+\varepsilon_x \frac{\partial c}{\partial x}\Big|_{z_b}\frac{\partial z_b}{\partial x}+\varepsilon_y \frac{\partial c}{\partial y}\Big|_{z_b}\frac{\partial z_b}{\partial y}-\varepsilon_z \frac{\partial c}{\partial z}\Big|_{z_b} \tag{3.4}$$

where c is the depth-averaged sediment concentration, u and v are the x and y components of depth averaged velocity, respectively, $\in_x$ and $\in_y$ are the x and y component of dispersion coefficient of suspended sediment, respectively, h is the flow depth, ε_x, ε_y, and ε_z are the x, y, and z components of the turbulent diffusion coefficient, respectively, z_b is the elevation of channel bottom, $cw_0\big|_{z_b}$ is the value of cw_0 at $z=z_b$, and w_0 is the particle fall velocity. All terms in all equations with a vertical bar indicates value at $z=z_b$.

In Equation (3.4), the x and y components of dispersion terms that include the turbulent diffusion terms are defined for simplicity as follows.

$$\in_x \frac{\partial c}{\partial x}h=\int_{z_b}^{z_h}\left(-c'u'+\varepsilon_x \frac{\partial c}{\partial x}\right)dz \tag{3.5}$$

$$\in_y \frac{\partial c}{\partial y}h=\int_{z_b}^{z_h}\left(-c'v'+\varepsilon_y \frac{\partial c}{\partial y}\right)dz \tag{3.6}$$

where c' is the deviation from the depth-averaged sediment concentration and u' and v' are the deviations of x and y components from depth-averaged velocity, respectively. The lateral transport term by turbulent diffusion in Equation (3.6) is as follows:

$$\int_{z_b}^{z_h}\varepsilon_y \frac{\partial c}{\partial y}dz=\varepsilon_y \frac{\partial}{\partial y}\int_{z_b}^{z_h}cdz+\varepsilon_y c\big|_{z_b}\frac{\partial z_b}{\partial y} \tag{3.7}$$

The second term of the right-hand side of Equation (3.7) is dropped in Parker's (1978) study. Figure 3.3 (a) and (b) are schematic diagrams that show the sediment

transportation by turbulent diffusion and sediment erosion–deposition at the bed surface. Sediment transportation by turbulent diffusion at the bed surface are defined by the fifth and sixth terms in the right-hand side of Equation (3.4), and each term is written by Equations (3.8) and (3.9), respectively. Correspondingly, these two terms reduce to Equation (3.10).

$$\varepsilon_y \left.\frac{\partial c}{\partial y}\right|_{z_b} \frac{\partial z_b}{\partial y} = -\varepsilon_n \frac{\partial c}{\partial n} \frac{\sin^2\theta}{\cos\theta} \tag{3.8}$$

$$-\varepsilon_z \left.\frac{\partial c}{\partial z}\right|_{z_b} = -\varepsilon_n \frac{\partial c}{\partial n} \cos\theta \tag{3.9}$$

$$\varepsilon_y \left.\frac{\partial c}{\partial y}\right|_{z_b} \frac{\partial z_b}{\partial y} - \varepsilon_z \left.\frac{\partial c}{\partial z}\right|_{z_b} = -\frac{1}{\cos\theta} \varepsilon_n \frac{\partial c}{\partial n} \tag{3.10}$$

Where ε_n is the *n*-component of turbulent diffusion coefficient at the bed surface, *n* is the coordinate toward normal direction, and θ is the lateral bed slope. Introducing Equation (3.10) into Equation (3.4) and using the definition such as $E_n = -\varepsilon_n \, \partial c / \partial n$, Equation (3.4) is rewritten as follows.

$$\frac{\partial ch}{\partial t} + \frac{\partial cuh}{\partial x} + \frac{\partial cvh}{\partial y} = \frac{\partial}{\partial x}\left(\in_x \frac{\partial c}{\partial x} h \right) + \frac{\partial}{\partial y}\left(\in_y \frac{\partial c}{\partial y} h \right) + \frac{E_n}{\cos\theta} - D \tag{3.11}$$

where E_n is the erosion rate of bed sediment and *D* is the deposition rate defined as shown in Equation (3.12). Similarly, mass conservation equation of bed sediment is described as shown in Equation (3.13).

$$D = c w_0 \big|_{z_b} \tag{3.12}$$

$$\frac{\partial z_b}{\partial t} + \frac{1}{1-\lambda}\left(\frac{E_n}{\cos\theta} - D \right) = 0 \tag{3.13}$$

where λ is the porosity of the bed sediment and cos θ is defined as $\cos\theta = \Delta y/\Delta s$, referring to Figure 3.3 (b). The effect of lateral bed slope on erosion rate has not been included in the mass conservation equation of sediment for fluid body and bed layer. Equations (3.11) and (3.12) may play an important role in treating sediment behavior in bank regions.

3.4 Lateral Concentration Profile for Suspended Sediment

The sediment transport by turbulent diffusion depends on the gradient of the depth-average sediment concentration in the transverse direction. For deriving the sediment concentration profile, the present study employs steady-uniform and unidirectional flow with no secondary current in a straight, open channel. Therefore, the convective sediment transport in the lateral direction in the mass conservation of suspended sediment in Equation (3.11) can be ignored. Assuming a constant sediment concentration for the upstream boundary condition, the diffusive sediment transport in the flow direction is also dropped. In this situation, the dispersion coefficient also changes into the turbulent diffusion coefficient. To investigate the role of turbulent diffusion on lateral sediment transportation, the mass conservation of the suspended sediment is simplified as

$$\frac{\partial c}{\partial t} + u\frac{\partial c}{\partial x} = \varepsilon_y \frac{\partial^2 c}{\partial y^2} + \frac{1}{h}\left(\frac{E_n}{\cos\theta} - D\right) \tag{3.14}$$

Itakura and Kishi's (1980) formula is used to compute the erosion rate. The deposition rate is evaluated by Rubey's (1933) formula. The local sediment concentration at the reference level is obtained by using Equation (3.15). The turbulent diffusion coefficient in Equation (3.14) is specified by Equation (3.16).

$$c_b = \frac{c_b''}{c''}c \tag{3.15}$$

$$\varepsilon_y = \frac{\kappa}{6}u_{*max}h_{max} \tag{3.16}$$

where c_b is the local sediment concentration at reference level, c_b''/c'' is the ratio of sediment concentration in the vicinity of the bed surface to the depth averaged one, and c is the locally depth-averaged sediment concentration. c_b''/c'' is evaluated by Lane and Kalinske's (1941) formula, assuming a similarity between the sediment concentration profiles in equilibrium regions and non-equilibrium regions, $\kappa(=0.4)$ is the von-Karman constant, and u_{*max} is the maximum shear velocity at channel center.

In order to investigate the role of lateral diffusion on bed evolution, the location where the maximum sediment concentration is taking place in the flow field under consideration is determined by neglecting the lateral diffusion term in Equation (3.14) and using the deposition rate in Equation (3.12). One of the steady solutions is derived with the upstream boundary condition of c = 0 as follows in Equation (3.17). With increase of flow distance, Equation (3.17) reduces to Equation (3.18).

$$c(x,y) = \frac{c''}{c_b''} \frac{E_n}{w_0 \cos\theta} \left\{ 1 - e^{-\frac{w_0}{uh}\left(\frac{c_b''}{c''}\right)x} \right\} \tag{3.17}$$

$$c(y) = \frac{c''}{c_b''} \frac{E_n}{w_0 \cos\theta} \tag{3.18}$$

3.5 Results on the Effect of Turbulent Diffusion

There are several methods for evaluating bed shear stress in temporarily averaged flow. In this study, the area method is employed for simplicity. For a cross-sectional shape of the straight, open channel that is part of a circle, the bed shear stress is expressed as follows:

$$\tau_b = \rho g \frac{\partial A}{\partial s} i = \frac{\rho g r i}{2} \left(1 - \frac{\cos^2 \beta_c}{\cos^2 \theta} \right) \tag{3.15}$$

where r is the arc radius, φ is the internal friction angle of fine sediment, β_c is the lateral bed slope at water edge on the bank, ρ is the mass-density of water, g is the gravitational acceleration, θ is the local lateral bed slope, and i is the bed slope along the flow direction.

All results hereafter are obtained from the flow specified using parameters such as sediment size d = 0.2 mm, Manning's roughness coefficient n = 0.021 (s/m$^{1/3}$), radius r = 40 m, $\beta_c = 40^0$ and channel bottom inclination i= 0.00009, 0.0002, 0.0008, and 0.003, respectively.

Figure 3.4 shows the lateral profile of sediment concentration that is obtained theoretically using Equation (3.18). The sediment concentration profile suggests that a maximum value takes place in the bank region, and thus two peaks are formed. Two peaks mean that the sediment transportation takes place from the bank region to the bank edge as well as to the channel center. The results on sediment concentration, erosion, and deposition rates at the location in a section where sediment concentration takes maximum value is shown in Figures 3.5 (a) and (b). The predicted curves are computed with and without a lateral diffusion term for two relative fall velocities w_0/u_{*max} of 0.10 and 0.20. The results suggest that a longitudinal uniformity for sediment concentration and the corresponding deposition rate are attained. The sediment concentration that is computed with the lateral diffusion term is small in comparison to the result without the diffusion term. Corresponding to the decrease of sediment concentration in the fluid body, the deposition rate is also smaller than the result computed without the diffusion. Sediment erosion and deposition take place laterally in response to the profile of sediment concentration illustrated in Figure 3.4 even if sediment transportation attains equilibrium

in the flow direction. Therefore, the erosion is not balanced by the deposition in the case of computation with lateral diffusion term.

The turbulent diffusion in the lateral direction of erosion deposition is important for explaining riverbed evolution in suspended-sediment-dominated rivers. We also discuss the role of lateral sediment transportation by turbulent diffusion in attaining the equilibrium condition in sediment concentration profile along the flow direction and transverse direction in completely suspended-sediment-dominated river reaches in this section.

3.6 Results on the Effect of Lateral Bed Slope

Figure 3.6 shows the erosion rates that are computed by Itakura and Kishi's (1980) method with and without the effect of lateral bed slope. The erosion rate predicted by the present method is larger than that obtained with the normal one in the bank region. Figures 3.7 (a) and (b) show the accumulated bed evolution normalized by the flow depth at the channel center. The results, which are illustrated by $\lambda=0$ for simplicity, are computed for the case with the effect of lateral bed slope and without it. All curves show that two scoured areas are formed at the bank regions, that the ridges are formed at their outsides, and that sediment deposition takes place in the area of the channel center. The scoured areas that were computed with $\cos\theta = 1$ shift a little to the center and shallower than the result predicted with $\cos\theta \neq 1$.

As shown in Figures 3.7 (a) and (b), the ridge and the scoured area are formed at both sides, and the deposition area is formed widely in the region of the channel center. Such configuration becomes representative in the results computed with the effect of cos θ on the erosion rate. All results are computed neglecting the influence of bed evolution

on the flow field, so these results may change corresponding to initially specified flow field such as the cross-sectional shape.

Based on the result from the experimental channel and the theoretical analysis, it is found that riverbed variations are influenced by lateral bed slope even in the region where the sediment concentration profile, erosion rate term, and deposition rate term attain steady and uniform conditions. Based on the results of the present study, I suggest to modify the erosion rate term for the bank region considering the lateral slope.

3.7 Summary

In this chapter, I have discussed the influence of lateral bed slope and lateral turbulent diffusion on erosion-deposition processes that treat river bed evolution in suspended-sediment-dominated rivers. The results are summarized as follows.

A new form for the erosion term in the mass-conservation equation is derived based on the mechanism of sediment transportation by turbulent diffusion near the laterally sloped bed boundary. Similarly, the erosion term of mass conservation equation of bed sediment is modified. The proposed erosion term is considered to be responsible for the treatment of sediment transport processes in laterally sloped regions.

A solution is derived for the lateral profile of sediment concentration in an idealized flow field. The profile shows that there are two peaks for sediment concentration. These peaks determine the direction of sediment transportation due to turbulent diffusion.

The sediment concentration as well as the deposition rate attain uniform condition in the longitudinal direction. In the case of computation without lateral diffusion, the sediment erosion from the channel bottom is balanced by the deposition of sediment from the flow body. However, sediment transport by turbulent diffusion creates an overloading

condition in the channel center and in the areas close to the near-bank. Locations where the sediment concentration takes the peak, the erosion is higher than the deposition.

The numerical results on bed evolution with a simple channel that is part of a circle suggest that the ridge is formed due to sediment deposition, the eroded area is formed at the inside of the ridge, corresponding to aforementioned two peaks of sediment concentration, and the deposition area is created in the channel center region by sediment transportation from both sides. Such lateral bed configuration is amplified by means of computation with the proposed erosion term.

4. Channel Changes Study Using Remote Sensing Data

4.1 Introduction

Migration of sandbars influences erosion and deposition in the near bank. Therefore, continuous monitoring of sandbars is important for obtaining information on adverse conditions such as riverbank erosion. Researchers commonly use field measurement, numerical simulations, and satellite-based observations in monitoring sandbars. Considering budgets, time, environmental constraints, and unstable river planforms, intensive field measurements are not a sensible choice, especially for large, braided rivers where the river planform changes very frequently within a short distance. Again, there are few predictive models for suspended-sediment-dominated braided rivers that can provide accurate information about real-time changes in river geometry. In these circumstances, the aerial-photo type, such as satellite-based information, is very helpful. The monitoring of the sandbars in a river depends on the identification of the surface types from the remote sensing data. This chapter introduces a method to detect sandbars automatically. The results obtained from the method are verified by means of field observations and Landsat images.

4.2 Index-Based Method (IBM)

The methods for identifying water and other surfaces from satellite-based information mainly fall into two broad categories: automatic and threshold-based. The spectral water index (SWI)-based methods include computing an index from two or more spectral bands, defining the best threshold and classifying each pixel either as water- or non-water-based on the threshold. Many researchers employed supervised and unsupervised methods such as artificial neural network, maximum likelihood, k-means

clustering, principal component analysis, and fuzzy clustering for detecting surface types (Li et al., 2014; Lira, 2006; Olaode et al., 2014; Zhang et al., 2012). The first- and second-order derivatives are common for detecting edges in digital image processing (Vernon, 1991).

Several researchers have employed moderate resolution imaging spectroradiometer (MODIS) surface reflectance for separating water from other surface types. For example, Sakamoto et al. (2007) detected temporal changes in the annual flooding extent for the Mekong delta. In their study, wavelet-based filter and linear interpolation are used for smoothing and filling the missing information in the time series of the enhanced vegetation index (EVI), the land surface water index (LSWI), and the difference between EVI and LSWI. Sun et al. (2011) used the linear mixture model and decision tree for deriving the flood map. Ticehurst et al. (2014) introduced the MODIS open water likelihood (OWL) method to compute the water fraction in each pixel. Kwak et al. (2014) introduced the modified land surface water index (MLSWI) to estimate inundation area using MODIS data.

Among the available threshold-based methods, many researchers such as McFeeters (1996), Gao (1996), Xu (2006), Xiao et al. (2002), Ji et al. (2009), and Kwak et al. (2014) have proposed the spectral water index (SWI) for identifying the surface types such as water, land, and vegetation and are applied widely. The SWI is computationally simple and can be applied to only a pixel. However, the challenging task is to define a suitable threshold. We employ the modified land soil water index (MLSWI) proposed by Kwak et al. (2014) for identifying the sandbars in the study area of the Brahmaputra River. The arithmetic relation between bands 2 and 7 for computing the

MLSWI using Moderate Resolution Imaging Spectroradiometer (MODIS) data is as follows.

$$MLSWI = \frac{(1 - 0.0001\rho_{2.13}) - 0.0001\rho_{0.865}}{(1 - 0.0001\rho_{2.13}) + 0.0001\rho_{0.865}} \tag{4.1}$$

where $\rho_{0.865}$ and $\rho_{2.13}$ are the surface reflectance for bands 2 and 7 of the MODIS satellite imagery and 0.0001 is a scale factor for converting the MODIS data into actual surface reflectance. A suitable threshold is determined by a trial and error method for which the water area is matched best corresponding to the actual field condition.

4.3 Gradient-Based Method (GBM)

Figure 4.1shows schematically typical surfaces such as green vegetation (GV), dry soil (DS), wet soil (WS), and turbid water (TW) existing within a braided channel. Assuming that each surface type responds differently to a specific wavelength of the electromagnetic spectrum, the variation of surface reflectance within a river can be expressed as a step function. Figure 4.2 is a schematic diagram that shows the difference between the surface reflectance of MODIS bands 2 and 1 along AA' or BB' in Figure 4.1. In Figure 4.2, the homogeneous areas such as GV, DS, and WS and edges between GV-DS, DS-WS, and WS-TW are shown with solid and dotted lines, respectively, where *x* and *y* are the coordinate of the location along the flow and transverse to the flow direction, respectively. The surface reflectance of water at MODIS band 2 is lower than at band 1. Therefore, Figure 4.2 shows that water areas have negative value and follow the pattern of a step function.

The properties of the step function are basic for edge detection by the gradient-based method (GBM). On the contrary, the SWI-based approach is a method to detect each surface type, such as water, soil, or vegetation, directly as indicated by the black

circle of Figure 4.2. GBM focuses on edges such as GV-DS, DS-WS, and WS-TS, whereas the index-based method emphasizes the surface type directly as demarcated by red and black circles in Figure 4.2.

The gradient or first-order derivatives that enhance the edge between two homogeneous regions is described as follows.

$$G(x,y) = \left(i\frac{\partial}{\partial x} + j\frac{\partial}{\partial y} \right) f(x,y) \tag{4.2}$$

Where *G (x,y)* is the gradient vector at a location defined by *x* and *y*, *f(x,y)* is the intensity of the difference between surface reflectance of MODIS band 2 and 1 dataset, and ***i*** and ***j*** are the coordinated unit vectors along and transverse to the flow direction, respectively.

The magnitude of the gradient vector that takes a maximum value at the edges is defined as follows.

$$M(x,y) = \sqrt{\left(\frac{\partial f(x,y)}{\partial x} \right)^2 + \left(\frac{\partial f(x,y)}{\partial y} \right)^2} \tag{4.3}$$

where *M(x,y)* is the magnitude of the gradient vector.

There are several methods for computing the directional derivatives in the *x* and *y* directions. Many textbooks such as Vernon's (1991) recommended that the derivatives in the *x* and *y* directions are to be computed in terms of *f(x,y)* at 3×3 regions. The first-order derivatives are very suitable for detecting edges with sharp discontinuity. For gradual variation, however, it is difficult to identify edges using first-order derivatives. Therefore, the second-order derivative known as the Laplacian is employed as well for finding the local edges and compared with the former one.

$$L(x,y) = \frac{\partial^2 f(x,y)}{\partial x^2} + \frac{\partial^2 f(x,y)}{\partial y^2} \tag{4.4}$$

where *L(x,y)* is the Laplacian of the enhanced surface reflectance.

In the homogeneous areas, as shown by solid black lines in Figure 4.2, the first- and second-order derivatives are close to zero. Consequently, the edges as shown schematically in Figure 4.3 are highlighted. However, it is difficult to separate the surface types only from the edges due to similar gradients in the homogeneous area. On the other hand, if I am able to highlight the edge in the original image, keeping the background, it will be easier to classify the surface types. To facilitate detection of edges and surface types, in this study, I modify Equations (4.2) and (4.3) by introducing a weightage average that is able highlight the edges between surface types and preserve the background information at the same time.

$$G_1(x,y) = \left\{ i\left(\frac{\partial}{\partial x} + w \right) + j\left(\frac{\partial}{\partial y} + w \right) \right\} f(x,y) \tag{4.5}$$

$$M_1(x,y) = \sqrt{\left(\frac{\partial f(x,y)}{\partial x} + W \right)^2 + \left(\frac{\partial f(x,y)}{\partial y} + W \right)^2} \tag{4.6}$$

where $G_1(x,y)$ is the modified gradient vector, *w* is the operator for the weighted average in *x* and *y* directions, *W=[w]f(x,y)* is the weighted average normalized to unity and is computed using 3×3 regions centered at *f(x,y)*, and $M_1(x,y)$ is the magnitude of the modified gradient vector.

In the homogeneous areas such as the points demarcated by P and Q in Figure 4.1, both $\partial/\partial x$ and $\partial/\partial y$ are zero. Consequently, the weighted average restores the surface types such as water, vegetation, or soil. At other points, such as R and S, $\partial/\partial x = 0$ and $\partial/\partial y = 0$, respectively. According to Equation (4.6), the contrast is enhanced between edge and non-edge pixels. Herein, I define a modified gradient-based method (MGBM).

4.4 Specification of Data

4.4.1 Satellite-based information

In the present study, I have used MODIS (MYD09GQ and MYD09A1) Landsat surface reflectance date. Surface reflectance of eleven spectral bands with 16-day repeat cycle at 30 m resolution was obtained from Landsat 8. Three of the bands, bands 5 (0.865 μm), 6 (1.610 μm) and 4 (0.655 μm), are combined together to obtain red, green, and blue (RGB) image in order to highlight the soil and water. The MYD09GQ of MODIS on board Aqua is a daily level 2 gridded (L2G) surface reflectance with the sinusoidal projection at 250 m resolution and provides data only from bands 1 (0.659 μm) and 2 (0.865 μm). The MYD09A1 provides the best possible L2G surface reflectance of seven spectral bands during the 8-day period at 500 m resolution. The MYD09A1 was used to compute the MLSWI. The MODIS surface reflectance data are radiometrically calibrated, are atmospherically corrected for gasses, aerosols, and Rayleigh scattering, and preserve data as observations. However, the performance during flooding seasons is not good due to cloud cover and often unsuitable for the smaller rivers. The MODIS data for the target area were downloaded from the NASA Land Processes Distributed Active Archive Center website at the time of the month that is relatively cloud free. The water levels at Sirajganj were also collected from Bangladesh Water Development Board (BWDB) to investigate the temporal variation of the water level. The recorded navigation tracks during the field survey in the Jamuna River were used to validate the results obtained from remote sensing analysis.

4.4.2 Data from field investigations

The field investigations are conducted to verify the results obtained from numerical simulation and remote sensing data analysis. Figure 4.4 shows instrumentation employed

for conducting the survey, recording the track along which the measurements were conducted, and points where photographs are taken for profiling the surface types such as sandbars, riverbank, and edges of the sandbars. The instrumentation for conducting the field investigations in the Brahmaputra River is composed of a RiverRay Acoustic Doppler Current Profiler (ADCP), Global Positioning System (GPS) with accuracy level of ± 15cm for determining water surface elevation and boat velocity, and a tethered boat. In addition, a manned boat for navigation and a smartphone control the navigation direction and record the measurement track for reference. The measuring track is obtained from the GPS as well. The tethered boat mounting with ADCP and GPS is tethered to the manned boat. The measurements are conducted only on the water surface and along sandbars in order to measure the bathymetry and discharge in the section and to identify edges of sandbars. Photographs are taken at many locations along the field measurement track in such a way that they can be used to verify the shape and size of the sandbars. The geo-referenced photograph points are then processed using ArcGIS and are used to compare the edges of the sandbars and banks of the river identified using the remotely sensed data.

4.5 Results from Remote Sensing Data Analysis

4.5.1 Sandbar identification by MGBM

The MYD09GQ data series of MODIS on board Aqua are daily level 2 gridded surface reflectance of bands 1 (0.659μm) and 2 (0.865μm) at 250 m resolution with sinusoidal projection. Figure 4.5 (a) and (b) show the variations of surface reflectance from band 1 and band 2 in a part of the study reach which are clipped from the MYD09GQ data set. Figure 4.5 (a) and (b) suggests the surface types such as water, sandbars, green vegetation, dry vegetation, and land. All the information obtained from Figure 4.5 (a)

and (b) is plotted in the manner of the histogram and is shown in Figure 4.6 (a) and (b). The histograms are unimodal and bimodal for bands 1 and 2, respectively, which means that the water and land area are distinguishable from the dataset of band 2. In Figure 4.6 (a), values around 200 and 1,000 are land and water, respectively. In Figure 4.6 (b), values around 500 and 2,500 are water and land, respectively. The bimodal characteristics of the histogram of band 2 offer a higher likelihood of separating water from the other surface types. To remove the noises from the images and to sharpen the image, median filter and the difference between bands 2 and 1 are implemented. Figure 4.5 (c) and Figure 4.6 (c) show the results obtained by applying these two operators. The undulation as in the histogram manner and differences as in surface types are clear, and the contrast between water and soil is increased, but the sizes and shapes of sandbars are not identifiable. In addition, Figure 4.5 (c) shows the improvement of thin cloud cover. Therefore, Figure 4.5 (c) is used as the fundamental input for further processing to detect sandbars. Figure 4.5 (d) shows the magnitude of the gradient computing by first-order derivatives that illustrates the edges between surface types. The edges that are the sharp boundary and form the regions following the shape of sandbars are apparent. However, the background surface types are missing. As a result, it is difficult to identify the surface types from Figure 4.5 (d). Figure 4.5 (e) shows the edges obtained by applying the Laplacian operator. The Laplacian is responding with zero value like the first-order derivative in homogeneous region, but with a positive and negative value simultaneously on either side of the edges. Comparing Figure 4.5 (e) to Figure 4.5 (d), the second-order derivatives result in many edges for different surface types, and noises are also higher than those of the first-order derivatives around the edges. To eliminate the edges, particularly differences between WS and TW, the first-order derivatives are applied with

the proposed modification. Figure 4.5 (f) shows the results obtained by applying the proposed modified gradient-based method (MGBM) as described in Equation (4.6), showing the distribution of sandbars with highlighted edges. The proposed modification does not affect the homogeneous area such as water, but increases the contrast between the edge and non-edge pixels. The results as seen in Figure 4.5 (f) also suggest that the proposed method improves the edge detection and shape-developing capacity.

Figure 4.7 (a) and (c) shows the sandbars and edges of sandbars that are obtained by applying the proposed method based on MODIS data as of 16 September 2014 and 9 September 2015, respectively. Figure 4.7 (d) is the Landsat image as of 30 July 2015 for the area in which the measurement tracks are indicated by pink curves. The edges of sandbars highlighted by the curves in Figure 4.7 (a) and (c) are obtained based on the measurement tracks from field investigations. During the measurement on 21–25 July 2015, the water levels at Sirajganj station were about 1.7 m higher than that of the Landsat data collection. Therefore, many sandbars were under submerged conditions as indicated in Figure 4.7 (c). Still, Figure 4.7 (c) identifies sandbars with different sizes in the study area. However, the shapes and sizes of sandbars are not exactly the same in Figure 4.7 (c) and (d).

Figure 4.7 (d) is clear enough to explain the actual river morphology in this area. However, the data are available at 15-day intervals. Therefore, the Landsat data may not be effective to understand the actual sandbar behavior during flood. On the other hand, MODIS image is available in a daily scale that enables researchers to monitor the real-time behavior of sandbars in the study area. Based on the results of the present study, I suggest the proposed method identifies sandbars and edges that coincide with field measurement, especially for the larger sandbars. However, it deviates slightly from the

smaller sandbars. For example, circles demarcated as 1, 2, 3, 4, and 5 are the channels and sandbars that are clear in the Landsat image as seen in Figure 4.7 (d), but those are not identifiable based on the proposed modified gradient-based method (MGBM). The present study employed the MODIS images that have a spatial resolution of 250 m. Therefore, features such as sandbars and channels that have a dimension less than 250 m are sometimes difficult to distinguish. On the contrary, the Landsat image is capable of identifying features having a dimension of 40 m. Despite this limitation, MODIS image and the proposed method provides useful information to monitor sandbars on a daily basis.

4.5.2 MLSWI on sandbar identification

Figure 4.7 shows the sandbars and water area that are detected by the proposed MGBM and index-based method (IBM) such as the MLSWI based on the MODIS image as of 16 September 2014. Figure 4.7 (b) shows water and other surface types by setting MLSWI higher than 0.84 as water using a trial-and-error method. Figure 4.8 shows the sensitivity of the threshold for defining water and other surface types. Figures 4.8 (a), (b), and (c) show the fluctuations in water area for MLSWI higher than 0.7, 0.8, and 0.84, respectively as the threshold for separating water. Focusing on the area demarcated by areas 1, 2, and 3, I noted a small change in the threshold affects the total water area considerably. Under such circumstances, without having any data from the field, it is difficult to select the best threshold for evaluating the water area perfectly. The results suggest sandbars 1, 2, 3, 4, and 5 with the edges clearly visible in Figure 4.7(a). Figure 4.9 shows the existing features at points 1 and 2. The results suggest that the proposed method identifies correctly the shapes and locations of the respective features. Similar accuracy near area 3, sandbars 3 and 4, are noticeable compared with the Landsat image. The results suggest the proposed method improves the detection of the shapes and sizes

of sandbars without any threshold. Therefore, the proposed method is applied for monitoring the real-time movement of sandbars using MODIS data.

4.5.3 Sandbar movement and planform change

Figure 4.10 shows the water levels at the Sirajganj station, the water surface slope and timing of MODIS image acquisition. The water level station is about 10 km upstream of the Jamuna Bridge and located at the Sirajganj Hard Point (SHP). The water surface slope is determined based on the recorded water levels at Bahadurabad and Sirajganj stations that are about 80 km apart. We noticed that the water surface slope at the rising limb of the flood is steeper than that of the peak water level, which means that the sediment movements are likely to be active during the rising limb of the flood period. Figure 4.11 shows the temporal changes of sandbars upstream of the Sirajganj Hard Point (SHP) and around the Jamuna Bridge areas for the year 2014. The MODIS images were downloaded once a month for the entirety of 2014; Figure 4.11 shows six of them only for simplicity. To estimate the rate of movement of sandbars, the coordinates of the head, middle, and tail of an existing sandbar are determined before and after flood season. The Euclidean distances of these points for all three positions provide the distances traveled by sandbars with time.

Figure 4.11 shows the sandbars around the Jamuna Bridge area such as S1 and S2. As seen in Figure 4.11 (a), a small channel separates S1 and S2 during the dry season. The erosion is dominant around the middle part of S1 and at the head of S2 at the rising phase of the water level. The water levels in January and November 2014 suggest similar inundation in this area. The Euclidian distances before and after the flood suggest that S2 migrates in the downstream direction about 1200 m with a deformed shape. The rate

and pattern of migration confirm the results obtained by previous studies such as Klassen and Masselink (1992).

Figure 4.11 (b) shows sandbars in the upstream area of the Sirajganj Hard Point (SHP) area. In Figure 4.11 (b), S1H1, S1H2, S1H3, S1H4, and S1H5 indicate sandbars in the main channel. However, these sandbars align differently to the flow. Results suggest the head areas of S1H1, S1H2, S1H3, and S1H4 suffered from erosion at the rising phase of the water level. The erosion continues and washes away the S1H3. At the same time, the flow attacks the riverbank in the area shown by dashed red circle. The riverbank line in this area is shifting to the westward direction. Usually, the dead water zone exists downstream of sandbars, where the deposition takes place. In the Brahmaputra River, dry vegetation is present in the dead water zones where sediment deposition is accelerated. The deposition pattern also depends on the angle between the two converging channels. Figure 4.11 (b) shows deposition taking place in the falling phase of the water level in the tail of sandbars; however, the pattern of deposition is not same for all sandbars.

4.5.4 Riverbank shifting based on MGBM

Figure 4.12 (a) shows the bank shift in the decadal scale based on Landsat image. The bank lines of the river are digitized based on the Landsat image collected during the dry season in order to avoid riverbank submergence from high water levels and noise from cloud cover. For keeping the reference of the digitized point the same, the study area was segmented by drawing straight lines at a 100-m interval. The chute channels originate from the main river and have a dimension less than 100 m, and the channels that do not merge with the main channel are ignored when digitizing the bank line.

The modified gradient-based method that highlights the edge between the water and soil automatically is employed for identifying the bank. Correspondingly, the right bank is digitized for computing the bank erosion rate, focusing on the area where the bank shifting is relatively consistent. Figure 4.12 (b) shows the temporal shifting of the right bank based on MODIS data from 2005 to 2014 using the MGBM.

However, there are few limitations of using satellite information for evaluating the shifting of the riverbank especially for the braided channel river with active bank erosion and channel change. First of all, during the dry season, there is no water in some of the channels close to the bank area. Therefore, the bank area will appear further away from the actual bank. In the next season, the channel may be active, which means the bank is sifting higher than that of the actual bank shifting. It is difficult to handle this problem using the satellite-based approach. Secondly, cloud cover negatively impacts the digitization of the bank shifting.

4.6 Summary

In the present chapter, I propose a suitable method to detect automatically sandbars using MODIS daily data. Besides, I obtain the results from the proposed method together with the MLSWI-based approach, Landsat images, and field observations. Based on the result, I noted that the proposed method is useful to monitor sandbars on a short timescale. Results are summarized as follows.

First-order derivative-based GBM is modified by introducing the weighted average. Introduction of the weighted average to the computation of the gradient based on first-order derivatives influence the edge pixels only. Therefore, the proposed modification successfully highlights edges and provides the background simultaneously. The proposed method uses the daily surface reflectance with a 250 m resolution that enables continuous

mapping of sandbars in a daily scale. The sizes and shapes of sandbars identified by the proposed method coincide closely with the field investigation as well as the Landsat image. Sediment erosion is dominant at the head, and sediment deposition takes place at the tail respectively, but the pattern and extent are not similar for all sandbars. The present study observes riverbank shifting and change in the position of sandbars.

MLSWI is able to classify each pixel either as water or other based on reflectance even only from a single target pixel. In the present study, MLSWI higher than 0.84 as the global threshold produces good results. However, results are sensitive to the choice of the best threshold.

The proposed method has several limitations. For example, the proposed method is unable to identify the sandbars automatically from images contaminated with dense cloud cover. The method may not be suitable for investigating the morphological change of small rivers because of the resolution of the MODIS data. MLSWI higher than 0.7, 0.8, and 0.84.

5. Study of Sandbar Behavior in Suspended-Sediment-Dominated Reaches

5.1 Introduction

Changes in river morphology are unavoidable and frequent in suspended-sediment-dominated large rivers, for example, in the lower reaches of the Brahmaputra River. The evolution of new sandbars and the movement of old ones affect the sediment transport in the near bank region. Any change in the river morphology of a large river affects a number of social, economic, and environmental issues. Riverbank erosion is a key concern for river managers, engineers, and policymakers in Bangladesh. Numerical results that can accurately predict the formation process of sandbars in a suspended-sediment-dominated mega-river are not common. In the present chapter, I aim to predict the formation and migration of sandbars in the Brahmaputra River by means of numerical simulations, remote sensing data, and the measurement of cross-section data in order to obtain useful information for river management.

5.2 Methodology

5.2.1 Governing equations

In the present study, I employ two-dimensional depth-integrated governing equations for conducting the numerical simulation. The governing equations are composed of mass- and momentum-conservation equations for the flow body, and mass conservation equations of sediment for the bed layer and the flow body. Many studies, such as Takebayashi and Okabe (2002), Takebayashi (2008), and Takebayashi et al. (2003), have described governing equations in the Cartesian coordinate system. The mass- and momentum-conservation equations for the flow body are as follows:

$$\frac{\partial h}{\partial t}+\frac{\partial hu}{\partial x}+\frac{\partial hv}{\partial y}=0 \tag{5.1}$$

$$\frac{\partial hu}{\partial t}+\frac{\partial huu}{\partial x}+\frac{\partial huv}{\partial y}=-gh\frac{\partial(z_b+h)}{\partial x}-\frac{\tau_x}{\rho}+\frac{\partial h\sigma_{xx}}{\partial x}+\frac{\partial h\tau_{yx}}{\partial y} \tag{5.2}$$

$$\frac{\partial hv}{\partial t}+\frac{\partial huv}{\partial x}+\frac{\partial hvv}{\partial y}=-gh\frac{\partial(z_b+h)}{\partial y}-\frac{\tau_y}{\rho}+\frac{\partial h\tau_{xy}}{\partial x}+\frac{\partial h\sigma_{yy}}{\partial y} \tag{5.3}$$

where x and y are the coordinates in the flow direction and transverse to the flow direction, t is the time, h is the flow depth, u and v are the x and y components of the depth averaged velocity, respectively, g is the acceleration due to gravity, ρ is the mass density of water, σ_{xx}, σ_{yy}, τ_{xy}, and τ_{yx} are the depth-averaged Reynolds stresses, τ_x and τ_y are the x and y components of the bed shear stress (τ_b), and z_b is the bed elevation.

The mass conservation of suspended sediment is described by the following convection-dispersion equation.

$$\frac{\partial ch}{\partial t}+\frac{\partial uch}{\partial x}+\frac{\partial vch}{\partial y}=\epsilon_x\frac{\partial^2 ch}{\partial x^2}+\epsilon_y\frac{\partial^2 ch}{\partial y^2}+\frac{E}{\cos\theta}-D \tag{5.4}$$

where ϵ_x and ϵ_y are the x and y components of dispersion coefficient, respectively, c is the depth-averaged sediment concentration, E is the erosion rate, and D is the deposition rate of the suspended sediment.

The temporal changes in the riverbed variation are described by mass conservation of the bed sediment. This is as follows:

$$\frac{\partial z_b}{\partial t}=\frac{1}{1-\lambda}\left(-\frac{\partial q_{bx}}{\partial x}-\frac{\partial q_{by}}{\partial y}-\frac{E}{\cos\theta}+D\right) \tag{5.5}$$

where λ is the porosity, z_b is the bed elevation, and q_{bx} and q_{by} are the x and y components of the bedload transport rate, respectively.

The erosion rate term is conventionally derived from the continuity of the suspended sediment for the flat region. In the present study, the erosion rate term in Equations (5.4) and (5.5) has a factor of $1/\cos\theta$ where θ is the lateral bed slope, which is derived from a consideration of the erosion that takes place in the normal direction of the bed boundary (Biswas et al., 2015).

To compute the bedload transport rate, I have employed Ashida and Michiue's (1972) formula, in which the effect of local bed inclination on the threshold motion of the bedload is introduced according to Ashida et al.'s (1991) study. We have also determined the influence of the secondary current on the bedload transport direction in terms of Shimizu et al.'s (1991) study and Takebayashi et al.'s (2003) study.

The erosion rate (E) and deposition rate (D) of the suspended sediment in Equations (5.4) and (5.5) are evaluated in terms of one of the conventional methods, in which the fall velocity of sediment particles and the equilibrium concentration of suspended sediment at the reference level are determined by Rubey's (1933) formula and Lane and Kalinske's (1941) formula, respectively, as follows:

$$w_0 = \left(\sqrt{\frac{2}{3} + \frac{36\nu^2}{(s-1)gd^3}} - \sqrt{\frac{36\nu^2}{(s-1)gd^3}} \right) \sqrt{(s-1)gd} \tag{5.6}$$

$$C_{sbe} = 5.55 \left(\frac{1}{2} \frac{u_*}{w_0} \exp\left(-\frac{w_0}{u_*} \right) \right)^{1.61} \tag{5.7}$$

where w_0 is the particle fall velocity, C_{sbe} is the equilibrium concentration of suspended sediment at the reference level, ν is the kinematic viscosity with a value of 0.01 $cm^2 s^{-1}$ at a temperature of 15^0 C, $s = (\rho_s/\rho - 1)$ is the specific gravity of the sediment particles, ρ_s is the mass density of the sediment, and d is the size of the sediment particles.

More details about the depth-averaged Reynolds stresses, dispersion coefficient, bedload formula, effect of the local bed inclination on sediment transport, and intensity of the secondary current are described in many articles such as those of Takebayashi et al. (2001), Luu et al. (2004), and Takebayashi (2008).

5.2.2 Defining initial channel topography

Typically, the field data define the initial channel planform and geometry. In the study area, the available field data are not enough. Therefore, in the present study, I use a method to set the channel topography based on remotely sensed data, such as the Panchromatic Remote-sensing Instrument for Stereo Mapping Digital Surface Model (PRISM-DSM) of the Japan Aerospace Exploration Agency (JAXA), which can capture a wide area within a very short time period. However, the remotely sensed data cannot give the profile of the river bottom directly.

Figure 5.1 shows a schematic diagram for reshaping the topography of the river channel, in which B_0 and h_0 are the known width and depth of the channel at a reference location, respectively, h_1 is the unknown depth to be determined, and B_1 is the width at a location where the depth is unknown. B_1 can be specified using satellite images. Assuming a steady, quasi-uniform flow and equilibrium bed-sediment transport, Yorozuya et al. (2013) proposed the following formula to specify the initial flow depth from a satellite image:

$$\frac{h_1}{h_0} = \left(\frac{B_1}{B_0} \right)^{\frac{3-6m}{7m}} \tag{5.8}$$

where m is the exponent of the non-dimensional bed shear stress related to the bed-sediment transport rate $q_{b*} \approx \tau_*^m$. In the present study, I employ 2.5 for m according to Egashira et al.'s (1991) study.

We have noted that Yorozuya et al. (2013) derived Equation (5.8) based on the equilibrium bedload transport rate. The Brahmaputra River is dominated by suspended sediment. Therefore, it is essential to test the validity of the exponent of the sediment transport rate, which is expressed by m in Equation (5.8). Figure 5.2 shows a schematic profile for suspended-sediment concentration, velocity, and the suspended-sediment transport rate in which the suspended-sediment transport rate is expressed as follows.

$$q_{ss} = \int_a^h c(z)u(z)dz \tag{5.9}$$

where $c(z)$ is the concentration profile of the suspended sediment, $u(z)$ is the velocity profile, a is the reference level, q_{ss} is the suspended-sediment transport rate, h is the flow depth, and z is the coordinate directed upward.

To evaluate Equation (5.9), it is necessary to specify the profiles for the sediment concentration and velocity. Assuming an equilibrium state of the suspended-sediment transport, Rouse (1937) derived the following profile for suspended sediment concentration:

$$\frac{c(z)}{C_{sbe}} = \left(\frac{h-z}{z} \frac{a}{h-a} \right)^{\frac{w_0}{\kappa u*}} \tag{5.10}$$

The exponent in Equation (5.10) is known as the Rouse number. Generally, values of the Rouse number greater than about 2.5 lead to a condition of less suspended sediment. In

contrast, values of the Rouse number less than about 0.25 predict grain sizes that will move as a wash load that is fully supported by the flow.

Einstein (1950) considered that the velocity distribution in open-channel flow over a sediment bed can be well described by logarithmic formulas based on von Karman's similarity theorem with constants as proposed by Keulegan (1938). For a hydraulically smooth bed, the logarithmic velocity distribution profile is as follows:

$$u(z) = 5.75u_* \log\frac{30z}{k_s} \tag{5.11}$$

Using the sediment concentration and the velocity profile, the suspended-sediment transport rate can be simplified as follows:

$$q_{ss} = 5.75ac_{sbe}u_* \frac{A^{z*-1}}{(1-A)^{z*}} \int_A^1 \left(\frac{1-\varsigma}{\varsigma}\right)^{z*} \left(\log\frac{30h}{k_s} + \log\varsigma\right) d\varsigma \tag{5.12}$$

$$q_{ss} = KC_{sbe}u_*h \tag{5.13}$$

where k_s is the roughness height, z^* is the Rouse number, A (=a/h) is the non-dimensional height of the reference level, ζ (=z/h) is the non-dimensional coordinate in the upward direction, and $K = 5.75\frac{A^{z*-1}}{(1-A)^{z*}} \int_A^1 \left(\frac{1-\varsigma}{\varsigma}\right)^{z*} \left(\log\frac{30h}{k_s} + \log\varsigma\right) d\varsigma$ is a proportionality constant.

Many researchers have conducted research and presented results on equilibrium concentration at the reference level. These results are included in many textbooks such as those of Kikkawa (1985), Ashida et al. (2008), and Graf (1998). Using the representative results, C_{sbe} is related to the relative fall velocity as follows:

$$C_{sbe} = \alpha\left(\frac{w_0}{u_*}\right)^{-\beta} \tag{5.14}$$

where α is the proportionality constant, and β is the exponent.

The dimensionless suspended-sediment transport rate (q_{s*}) can be expressed as follows.

$$q_{s*} = \alpha \tau_*^{(\beta+2)/2} \tag{5.15}$$

The value of β ranges between 2~3 (Graf, 1998; Ashida et al., 2008). In the case of β =3, the exponent of the suspended-sediment transport rate is 2.5, which is equal to the exponent of the non-dimensional bed-sediment transport rate of Egashira et al. (1991). Engelund and Hansen (1967) also proposed 2.5 as the exponent of the total sediment transport. Therefore, using m = 2.5, the depth of the flow varies to the width of the river, as follows:

$$\frac{h_1}{h_0} = \left(\frac{B_1}{B_0} \right)^{-\frac{24}{35}} \tag{5.16}$$

The width of the river channel is determined by satellite-based information such as the Panchromatic Remote-sensing Instrument for Stereo Mapping (PRISM) Digital Surface Map (DSM).

5.3 Numerical Simulation

5.3.1 Computational condition

The reach of the Brahmaputra River examined in the present study is about 90 km long and 12.50 km wide. It is divided into 11,800 computational grids with a dimension of the grids that is equal to about 250 m in the flow direction and in a transverse direction to the flow direction. The river bed slope is 0.0001. The mean diameter of the bed material is 0.00026 m. The bed material is treated as non-cohesive uniform sediment. The angle of repose of the sediment particle is 36^0. The coefficient related to the intensity

of the secondary flow is equal to 7 (Engelund, 1974). The width-to-depth ratio is higher than 1,000. Both the bedload and the suspended load are considered for computing the riverbed variation.

The time step for conducting the numerical simulations is 2 s. Three cases are simulated in which a constant flow of 65,000, 90,000 and 100,000 m^3 s^{-1}, which are equivalent to the peak flood flow with a return period of 2.33, 20, and 50 years respectively, are supplied at the upstream boundary, and the uniform flow is specified in the downstream boundary. In each computation case, the hydraulic conditions such as the width-to-depth ratio and the non-dimensional bed shear stress fulfill the criteria for the formative region of the multiple row bar according to Kuroki and Kishi (1984). The ratio of the particle-fall velocity to the shear velocity, which determines the deposition (sandbar formation), erosion (sandbar deformation), and dominant sediment transportation is less than a unity. Usually, values that are less than a unity with a decreasing trend cause erosion, whereas values that are more than a unity with an increasing trend cause deposition. The ratios of the particle-fall velocity to the average shear velocity at the beginning of each computation are 0.34, 0.28, and 0.20 respectively, which indicates the dominance of suspended sediment.

5.3.2 Initial conditions

At the beginning of the numerical simulation, the average velocity is determined using the Manning's equation and the water discharge is supplied at the upstream boundary. The average velocity is set as the initial velocity (u) in the x-direction. The initial velocity in the y-direction is set to zero ($v = 0$). The initial depth-averaged suspended-sediment concentration is specified assuming an equilibrium stage. The initial

flow depth and width of each stream in the braided channel are specified according to satellite image analysis using Equation (5.14).

5.3.3 Boundary conditions

For solving the flow equation, a constant flow and water depth are specified at the upstream and downstream boundary, respectively. In addition, at the downstream boundary, the water surface slope is kept at zero $(\partial H/\partial x = 0)$ to ensure a uniform flow. The flow depth is small near the boundary of the emerged and existing sandbars, over the partially flooded sandbars, and near the bank area. In the present study, I do not solve the momentum equations for a flow depth that is less than 0.01 m. In these circumstances, the velocity of the flow in the *x* and *y* directions is set to zero. In the other areas, such as in the fully wetted regions, the model solves the complete set of the continuity and momentum equations to find the flow depth and velocity.

5.4 Results on Channel Changes

In the present study, I use the coarse size grids to conduct the numerical simulation. The performance of the model is assessed macroscopically in terms of the formation and migration of sandbars, the formation of the braided channel, the volume of the sediment transport, the non-uniform behavior of the suspended sediment, the migration speed of the sandbars, the ratio of suspended to bedload, and the sediment concentration etc. The formation and migration of the sandbars are discussed by neglecting the bank erosion process.

5.4.1 Suspended vs. bedload transport

Many studies suggest that the Brahmaputra is a suspended-sediment dominated river due to the presence of higher finer particles in the sediment composition. Yorozuya et al. (2016) collected the data on the bedload and suspended load by means of field

investigations in the Brahmaputra River during September, 2014, and August 2015. Yorozuya et al. also collected data on the river bed profile's velocity using ADCP. Table 5.1 and Figure 5.3 show the bedload and suspended load's transport (Okada et al., 2016) in the Brahmaputra River based on the field data, which were collected by Yorozuya et al. during this study period. In the field data, the ratio of the suspended to the bedload ranges is from 10 to 25. The ratios of the suspended to the bedload transport rate, which are obtained from the results of the numerical simulation, range from 25 to 40. According to Schumm (1963), in a suspended-sediment dominated river, the rate of bedload transport is 0 – 15% of the total load. In such cases, bedload can be ignored for rough estimation, and the riverbed variations are controlled by the erosion process due to the diffusion of fine sediment from the bed boundary and the deposition of suspended-sediment particles from the water column. Therefore, the change in the riverbed elevations are determined by balancing the temporal changes in the suspended-sediment concentration, which is calculated by the mass conservation of the suspended sediment and the profile of the suspended-sediment concentration under a condition of equilibrium in which the erosion is balanced by deposition and is a function of the relative fall velocity of the particle as defined by w_0/u_*. The shear velocity that was used for computing the eddy viscosity, which determines the strength of the sediment transportation by turbulent diffusion, is calculated using Manning's equation with a roughness coefficient equal to 0.025.

The volume of the sediment transport through the river is composed of a bedload and a suspended load. The amount of cumulative transported sediment is about 570 million tons. Table 5.2 shows the results of different researchers such as Goswami (1985), Holeman (1968), Coleman (1969), and Hossain (1992) in relation to the total amount of

sediment transported annually in the Brahmaputra River. The lower and upper limit of the sediment transport are 400 million t yr^{-1} to 800 million t yr^{-1} respectively. Table 5.3 and Figure 5.4 show the results of the estimated sediment transport by Kabir and Ahmed (1996) in the Brahmaputra River; these researchers applied conventional empirical equations such as those of van Rijn, Bagnold, Englund-Hansen, Ackers-White, and Mayer-Peter-Muller and compared the results with the observed ones. In the present study, the total amount of the transported sediment is computed for the discharge of 65,000 m^3 s^{-1}. Considering that the unit weight of the sediment is 1,923.40 kg m^{-3}, the transported bedload and suspended load are 570 and 10 million tons, respectively, which is close to the results reported by many researchers. The range of sediment transport data varies widely. The reason for such variability is quite evident because of the temporal and spatial distribution of the sediment transport rate. The total sediment-transport data estimated from the simulation provide a rational view of the sediment transport of the Brahmaputra River within the stipulated time.

5.4.2 Sandbar formation and deformation

Figure 5.5 (A) shows the initial river topography with the existing sandbars delineated by S1, S2, S3, and S4. The initial topography of the river reach studied here is defined using PRISM-DSM and the method of Yorozuya et al. (2013). The water is flowing from the top to the bottom. Figures 5.5 (B), (C), and (D) give the results of the numerical simulations showing the bed evolution in terms of the formation and migration sandbars after 30 days for 65,000 $m^3 s^{-1}$, 25 days for 90,000 $m^3 s^{-1}$, and 20 days for 100,000 $m^3 s^{-1}$, respectively. The black circles in Figure 5.5 show the newly appeared sandbars. The riverbed evolution suggests that the old sandbars S1, S2, and S3 are protruding both in the flow direction and in the direction transverse to the flow direction. In each

computational case, the sandbar S4 is migrating toward the downstream direction and has a deformed shape. The bedload transport rate is small compared to the suspended-sediment transport rate. As a result, the suspended sediment controls the movement of the sandbar in the Brahmaputra River. The formation of sandbars is observed clearly in the river reach studied here. The upstream and downstream translation, the lateral extension of sandbars, and the movement of newly formed sandbars are captured successfully in the present numerical simulation. At first, sandbars are forming, and thereafter, they are migrating gradually in the downstream direction and their size is increasing with time. Figure 5.6 suggests that the river bed evolution due to erosion and deposition is dominant at the head and tail of the sandbars respectively. In the present model, bank erosion will occur in the case of a bank slope that is steeper than that of the angle of repose. However, the banks remain unchanged, which means the necessary condition to produce the bank erosion is not satisfied.

5.4.3 Temporal change in bed shear stress

Figure 5.7 (A) and (B) show the temporal variation of the flow depth and the shear velocity under a steady flow condition with a constant discharge of 65,000 $m^3 s^{-1}$ after 10, 20, and 30 days. The results are obtained from the numerical simulations. The shear velocity is computed using Manning's equation, in which the *x*- and *y*- components of the flow velocity are involved. As such, during the sandbars' movement, it is likely to develop a complex pattern of the shear velocity, especially during the riverbed evolution. In Figure 5.7 (B), it is particularly noticeable that the shear velocities are high and low at the head and tail of the sandbars respectively. Therefore, the head of the sandbars is expected to face a condition that is conducive for erosion. On the contrary, sediment is depositing at the tail part of the sandbar.

Figure 5.8 shows the temporal changes in the riverbed evolution based on numerical simulation. I focus on the sandbars S3 and S4 particularly. The upper, middle, and lower solid black lines and dotted lines represent the head, midsection, and tail of sandbars S3 and S4, respectively. Figure 5.8 suggests the relative size of the cross-sections and curvature of the bank line determine the locations of erosion and deposition areas primarily. However, the eroding areas shift gradually toward the bank region as soon as the sandbar starts to move in the downstream direction. The shear velocity is higher in the converging sections around the sandbars. The erosion follows the variation of the shear velocity.

The non-dimensional bed shear stress and relative fall velocity are the dominating factors for the bedload and the suspended-load transportation. The bed-sediment transport rate varies following the pattern of the non-dimensional bed shear stress. On the contrary, the suspended-sediment transport rate depends on the depth-averaged sediment concentration. The mass conservation of the suspended sediment includes both erosion and deposition terms. The erosion term depends on the shear velocity. The deposition term includes the depth-averaged sediment concentration. The flow and sediment transport properties in neighborhood sections influence the depth-averaged sediment concentration. Therefore, plotting the suspended-load transport rate against the relative fall velocity is scattered whereas the bedload transport follows almost a definite relationship.

5.4.4 Longitudinal bed profile and suspended-sediment concentration

Figure 5.9 shows the riverbed evolution in the flow direction and the sediment concentration along the right and left bank areas. Figures 5.9 (a-1) and (a-2) show the riverbed evolution with sediment concentration and the bedload with suspended load,

respectively, for the right bank area. Figures 5.9 (b-1) and (b-2) are the results showing the riverbed evolution with the sediment concentration and the bedload with the suspended load, respectively, for the left bank area. In cases where there is no bed deformation, it is expected that the sediment concentration will not change over time. However, in Figure 5.9 (a-2) and (b-2), both the bedload and the suspended load fluctuate with time, which is evidence of the morphological change and movement of the sandbar. Figure 5.9 (b-1) and (b-2) suggest that the bed form of the river is migrating gradually in the downstream direction. The transportation of both the bed and the suspended load are higher and lower around the trough and crest areas. The sediment concentration is higher just after the end of the crest area as well. The scale of the depth-averaged suspended-sediment concentration rate, the suspended-load transport rate, and the bedload transport rate are in the order of 10^{-3}, 10^{-3}, and 10^{-4}, which are also observed in the field investigation in the unpublished data of Yorozuya et al. (2016) and Okada et al. (2016) based on Yorozuya et al. data, also reported similar values for the suspended-sediment concentration rate, the suspended load transport rate, and the bedload transport rate. When the highly concentrated suspended sediment are transported to an area with a small w_0/u_*, the accumulation of sediment occurs, and correspondingly, deposition is dominant. The erosion is dominated in the area where the w_0/u_* is comparatively lower. The rate of the sediment transport is higher on the right bank area than the left bank area, which indicates that the right bank is likely to suffer from erosion.

5.4.5 Maximum bed scouring and aggradation

The maximum bed scouring and aggradation are about 25 m and 18 m respectively. These results describe the actual phenomenon well and are also verified by field investigation and the use of the results, which have been reported in previous studies

(Klaassen et al., 1992; Sarker et al., 2013; Nakagawa et al., 2013). To measure the speed of the sandbar migration, the position of the head, middle, and tail of the sandbars is monitored at a regular interval during numerical simulation. The speed of the migration for the new and old sandbars is about 2.0 to 10.0 m hr^{-1} and 1.6 to 3.0 m hr^{-1}. However, it depends on the size of the sandbars and the strength of the flood. The migration rate, based on the field measurement data for the Brahmaputra River, is 1.11 to 16.8 m hr^{-1} (Delft Hydraulics and DHI, 1996). The present numerical simulation covers the speed.

5.4.6 Braiding channel formation

Figure 5.10 shows the evolution of the river bed in terms of the change in the cross-section in the longitudinal direction. The top section corresponds to the section located 5km downstream from the upstream boundary of the studied reach. Thereafter, each cross-section is plotted at 10 km intervals. As such, Figure 5.10 shows the temporal change in the cross-section for 65 km of the studied reach. The cross-sectional shapes of sections a-3 and a-4 differ greatly because a-3 is located in the right side of the island and a-4 is located at the downstream end of the island. The measured cross-sections suggest that the upstream part of the study area is characterized by multiple row sandbars and thereafter converges to a single channel. The river is developing multiple row sandbars again in the downstream area. The numerical simulation results suggest the development of multiple channels in the upstream part of the study area, gradual convergence, and the formation again of multiple channels. These characteristics match the actual field condition.

5.5 Summary

In the present chapter, I discuss the formation and deformation of sandbars in the suspended-sediment-dominated Brahmaputra River in terms of remotely sensed data, field data, and numerical simulations. Results are summarized as follows.

The curvature of the riverbank and the behavior of the sandbars influence the erosion and deposition in the near-bank region. The eroding areas are shifting toward the near-bank region during the displacement of the sandbars. The suspended-sediment transport rate is 25 to 40 times higher than that of the bed-sediment transport rate. The new and old sandbars move in the downstream direction at a speed of about 2.0 to 10.0 m hr^{-1} and 1.6 to 3.0 m hr^{-1}, respectively. The movement speed depends on the size of the sandbars and the magnitude of the flood flow. The actual speed of the sandbar movement based on the observed data for the Brahmaputra River ranges from 1.11 to 16.8 m hr^{-1}. The simulated results cover the observed results.

The maximum bed scouring and aggradation are about 25 m and 18 m respectively. These results describe the actual phenomenon well and are also verified by field investigation and the use of the results, which are reported in previous studies. The scale of the depth-averaged suspended-sediment concentration rate, the suspended-load transport rate, and the bedload transport rate are 10^{-3}, 10^{-3} and 10^{-4}, respectively, which are also observed in the field investigation. The transported bedload and suspended load are 570 and 10 million tons, respectively, which is close to the results reported by many researchers.

6. Bank Erosion and Associated Bank Shifting

6.1 Introduction

It is important to study bank erosion and associated sediment issues for the planning, executing, and managing of engineering interventions and for the conducting of countermeasures to reduce damage resulting from flood hazards. According to Hasegawa (1981), the characteristics of the bank erosion are intermittent wherein four sequential steps, such as riverbed scouring near the riverbank region, collapse of bank material, deposition of collapsed material at the toe of the bank, and transport of the deposited materials, repeat in a cycle throughout the bank erosion. Therefore, bank erosion is a sporadic phenomenon (Hasegawa, 1981; Nagata, 2000; Darby et al., 2002). However, bank erosion is influenced by local factors such as the shape of the bank, the height of the bank above the water surface, and the physical properties of the bank's materials, such as the angle of repose, the sediment size, and the percentage of cohesive materials, which create difficulties when it comes to applying the same model in all conditions.

Several researchers have proposed numerical models to evaluate bank erosion. Considering the non-equilibrium sediment transport theory proposed by Nakagawa and Tsujimoto (1980) and using Hasegawa's (1991) bank erosion model, Nagata et al. (2000) proposed a numerical model to compute the temporal changes in the planform of a meandering river. Jang et al. (2005) proposed another numerical model in which they considered that scouring at the toe of a bank develops a gradient that is steeper than the submerged angle of the repose of the bank material. The sediment beyond the submerged angle of the repose collapses and deposits at the toe instantly, which enables an evaluation of bank erosion by equating the scoured and collapsed volume and resetting the gradient

so that it is equal to the angle of repose. Darby et al. (2002) developed a numerical model for evaluating the migration of the meander bends with an erodible cohesive riverbank, which includes the rotational slip and planner failure of the bank. However, it is not so easy to determine the exact timing of the supply of the sediment by the planner failure of the bank. The scouring near the riverbank caused the gradient of the riverbank to become steeper than the submerged angle of the riverbank material's repose.

In order to handle the moving boundary that originated because of the riverbank shifting toward the outer direction, Nagata et al. (2000) rearranged the grid-points at equal intervals within the left and right bank and reproduced the grids. Taking into account the riverbank shifting, Jang and Shimizu (2005) redefined the centerline of the channel, rearranged the new cross-sections perpendicular to the centerline, divided each cross-section into grid number, and generated new computational grids. Darby et al. (2002) generated a new grid when the magnitude of the widening was sufficiently large. They then computed the flow field again without bed deformation in order to stabilize the flow field's variables.

Comparing the size of the grids and the width of the river, the rate of riverbank erosion is small within a computational time step. Most of the studies related to the numerical simulations for water flow, sediment transport, and bank erosion are conducted using finer grids. Finer grids lead to the use of small computational time steps (Anderson, 1995). Finer-grids are effective in small and experimental channels for explaining and predicting riverbank erosion and channel changes. Application of such a methodology to a large river requires significant time to accomplish the simulation and enough memory space for the data storage. From the viewpoint of engineering applications, computing sediment processes with much finer grids in a large braided river may not be efficient.

Therefore, a new model is required to compute the bank erosion process in a large river such as the Brahmaputra River, which is capable of simulating the bank erosion using a coarse grid.

6.2 Bank Erosion Model Development

6.2.1 Reference quantities

To evaluate the bank erosion and associate bank shift using the two-dimensional depth-integrated governing equations, as shown in Equations (5.1) to (5.5) and the usual grid system, a specific model is needed that can predict the bank erosion by means of a reference hydraulic quantity, such as the average bed shear stress in the bank region. Figure 6.1 shows the lateral profile of bed shear stress predicted by means of the area method (Egashira et al., 1988) and the corresponding lateral bedload transport rate, as computed by Hasegawa's (1981) formula in a bank region with the cross-section illustrated by part of a circle. Hasegawa's (1981) formula is as follows:

$$q_{by} = \sqrt{sgd^3}\,\frac{\psi_d \tau_{*c}^{1.5}}{\mu_s\sqrt{\mu_s\mu_k}}\tan\theta\left[\left(\tau_*/\tau_{*c}\right)^{1/3} - \left(\tau_*/\tau_{*c}\right)^{-1/3}\right]\left(\tau_*/\tau_{*c} - 1\right) \tag{6.1}$$

where ψ_d , μ_s, and μ_k are 8.5, 1.0, and 0.8 (Hasegawa & Mochizuki, 1989), respectively, and $s = (\rho_s/\rho_w - 1)$, τ_{*c} is the non-dimensional critical bed shear stress of the sediment particles in the flat region.

The result illustrated in Figure 6.1 shows that both the bed shear stress and the lateral bedload transport rate change spatially a lot. However, the bank shifting can be evaluated in terms of the maximum of the lateral bedload transport rate ($q_{by\,\max}$), and, in addition, the bed shear stress, at the maximum point, can be connected to the average bed shear stress. Similarly, in the treatment of the bank shift resulting from the erosion and

deposition of the suspended sediment, the bank shifting can be evaluated by means of average hydraulic quantities such as the average bed shear stress in the target region.

Figure 6.2 shows the location where the maximum lateral bedload transport rate takes place. θ_r is the reference lateral bed slope at which $q_{by\,\max}$ occurs. According to the results, θ_r is independent of the bed shear stress and takes a constant value such as $\theta_r = 20^0$. This means that the $q_{by\,\max}$ can be evaluated using the bed shear stress at the lateral bed slope, $\theta_r = 20^0$. In addition, the spatial average bed shear stress in the bank region with the cross-section shape illustrated by the part of a circle, as shown in Figure 6.1, can be evaluated in terms of the bed shear stress at location θ_a, as follows:

$$\theta_a = \cos^{-1}\sqrt{\frac{\varphi\cos\varphi}{\sin\varphi}} \tag{6.2}$$

where θ_a is the location at which the average bed shear stress takes place, and φ is the angle of repose of the sediment particles.

The average bed shear stress occurs at $\theta_a = 21.6^0$ for $\varphi = 36^0$. The value of θ_a is very close to θ_r, which ranges from 20^0 to 22^0. Therefore, it can be considered that the erosion and deposition rate of the suspended sediment in the bank region can be evaluated using the bed shear stress at θ_r and using the average bed shear stress in the bank region.

6.2.2 Bank shifting due to lateral bedload transportation

To evaluate the riverbank shifting, a cross-sectional shape is assumed to maintain local similarity, which is shown in Figure 6.1 (a). Referring to the profile of the lateral bedload transport rate and assuming the sediment released by the bank collapse deposits on the inner side of point *R*, the following relationship between the bank shifting and the $q_{by\,\max}$ is proposed in the present study:

$$\frac{\partial Y_w}{\partial t} = \frac{1}{1-\lambda}\frac{q_{by\max}}{(h_f + h_r)} \tag{6.3}$$

where Y_w is the width of the water surface in the bank region, h_f is the height of the bank above the water surface, and h_r is the flow depth at the reference point.

Equation (6.3) shows that the bank shifting rate can be determined by Hasegawa's (1981) equation if $q_{by\max}$ is predicted. If the bank shifting takes place, the average bed elevation will change due to the excessive sediment supplied by the bank collapse.

$$\frac{\partial \bar{z}_b}{\partial t} = \frac{h_f}{Y_w}\frac{\partial Y_w}{\partial t} \tag{6.4}$$

where $\partial \bar{z}_b / \partial t$ is the average bed variation.

6.2.3 Bank shifting due to erosion/deposition of suspended sediment

Taking the terms that are necessary for the present discussion into consideration, in the case of the suspended-sediment-dominated river, the mass conservation of sediment at the bed layer reduces to

$$\frac{\partial z_b}{\partial t} = \frac{1}{1-\lambda}\left(D - \frac{E_n}{\cos\theta}\right) \tag{6.5}$$

In this case, the temporal change rate of the bed elevation is described as follows:

$$\frac{\partial \bar{z}_b}{\partial t} = \frac{1}{1-\lambda}\frac{1}{Y_w}\int_0^{Y_w}\left(D - \frac{E_n}{\cos\theta}\right)dy \tag{6.6}$$

in which $\bar{z}_b = \int_0^{Y_w} z_b dy / Y_w$.

Figure 6.3 shows the bank shifting process due to erosion and deposition in the bank region where suspended-sediment transport dominates. If the temporal change rate of the

average bed elevation is negative, Y_w will increase, and therefore, the bank shifting rate is described as follows:

$$\frac{\partial Y_w}{\partial t} = \frac{1}{1-\lambda}\frac{1}{h_f + h_0}\int_0^{Y_w}\left(D - \frac{E}{\cos\theta}\right)dy \tag{6.7}$$

Y_w will decrease due to sediment deposition if $\partial \bar{z}_b / \partial t$ takes a positive sign. In the reducing process of Y_w, it is assumed that sediment deposition takes place even onto the bank slope. Referring to the discussion of reference quantities in sub-section 6.2.1, it is possible to evaluate $\partial \bar{z}_b / \partial t$ and $\partial Y_w / \partial t$ using the average bed shear stress and the bed shear stress at the reference point.

6.3 Mesh Updating Algorithm

Figure 6.4 shows the schematic of the grid updating process with time by means of the stretchable grids at both boundaries of the bank area. During Δt time, the grid points located in the half gridline, the main channel line, and the bank line move to a new location corresponding to the distance of the bank shifting as determined using Equation (6.7). When the summation of the bank shifting is higher or equal to half of a grid size, which means $\Delta y'' < \Delta y/2$ where $\Delta y''$ is the remaining part of the grid in the floodplain area, as shown in Figure 6.4, the bank adjacent grid line shifts to a distance of $\Delta y/2$. If the accumulation of the bank shifting covers one bank-adjacent grid, the grid's identity number, which defines the location of the bank area, is updated. For simplicity, the bank shape is kept similar during the relocation of the grid point.

6.4 Numerical Prediction of Bank Shifting

The proposed model, as described in section 6.2, is applied to the studied reach of the Brahmaputra River. In the present study, I employ a coarse-size grid with a dimension

of about 250 m to compute the riverbank erosion, assuming a cross-sectional shape illustrated in Figure 6.1 (a). The lateral slope at the toe of the riverbank area is zero and gradually varies from zero to the angle of repose of the sediment particles at the water margin. The gradient of the lateral bedload transport rate is zero at the reference point, and the reference point is constant even with the changing hydraulic condition. The bedload transport rate is zero at the channel center and the water margin as well. Therefore, in the case of a suspended-sediment-dominated river, the bank erosion is controlled by the erosion and deposition process, in which case the bank erosion phenomena is modelled using coarse-size grids. As such, the location of the reference point is very important for selecting a suitable lateral bed slope. In this study, I use the reference lateral bed slope to modify the erosion rate term in the mass conservation of the sediment, both at the river bed level and within the flow body. It is also very important for evaluating the influence of the lateral bed slope on riverbank erosion. In the present study, I found that the reference point remained unchanged under different hydraulic conditions for the particular bank shape employed in the numerical simulation. The bank erosion is obtained using the information from the reference point.

6.4.1 Boundary condition

A constant water discharge of 65,000 $m^3 s^{-1}$ is supplied from the upstream boundary. A uniform flow condition is employed in the downstream boundary. The flow depth is small near the bank area, over the partially flooded sandbars, and near the boundary of the emerged and existing sandbars. Areas where the flow depth is less than 0.01 m are considered to be the dry bed. The x and y components of flow velocity are set to zero in the dry bed condition without solving the momentum equation. In the other areas, such

as in the fully wetted regions, the complete set of the continuity and momentum equations are solved to find the flow field variables such as the flow depth and velocity.

6.4.2 Grid deformation

Figure 6.5 shows the temporal changes in the numerical grid in a part of the study area corresponding to the changes of the boundary caused by successive bank shifting. The top figure shows the initial numerical grid, and the bottom shows the final form of the grid after one month. The sediment transported from the bank region by the action of the fluid forces is counterbalanced by the sliding of the riverbank. Therefore, a movable boundary is developed in the bank region. The banks are shifted as a consequence of the bank erosion. The magnitude of the bank erosion is small compared to the size of the grids. Therefore, the stretchable grids along both boundaries of the bank region are employed to capture this gradual shifting of the riverbank. After each computational time step, the grid points that define the bank shape are relocated to a new position in such a way that the shape of the bank are kept similar. The positions of the new location are determined using extrapolation corresponding to the magnitude of the bank shift. In the right and left bank area, which are demarcated by the black circles A and C, respectively, the bank shifting takes place toward the outer direction as a result of the erosion and deposition process. Therefore, the grid adjacent to the bank area in the floodplain and the main channel is shrinking and expanding, respectively. Figure 6.5 demonstrates that the bank shifting is higher on the right bank than on the left bank.

6.4.3 Modified erosion rate on bank erosion

Figure 6.6 shows the predicted temporal bank shift using the proposed model. The bank shifting results from the erosion and deposition of the suspended sediment. The erosion rate term is modified using the reference inclination (θ_r). The bank shifting rate

is predicted with the modified erosion rate term and without the modified erosion rate term and by assuming a profile as shown in Figure 6.1. The top two figures are the results for the left bank without and with the use of the modified erosion rate term, respectively. The bottom two figures are the results for the right bank without and with the modified erosion rate term, respectively. All the curves show that both banks are gradually shifting and that the location of the erosion peak is shifting gradually toward the downstream over time. The results suggest that the bank shifting rate predicted by the proposed model with the modified erosion rate term is higher than the result predicted without the modified erosion rate term.

6.4.4 Bank shifting from field data

Figure 6.7 shows results comparing the bank shifting obtained from the MODIS and Landsat data analysis, the measured cross-section data analysis, and the numerical simulations with the proposed bank erosion model. For remote sensing data analysis, the Moderate Resolution Imaging Spectroradiometer (MODIS) and Landsat data are used. The annual bank shifting is determined from the MODIS and Landsat image after highlighting the bank by applying the modified gradient-based method (MGBM) proposed by Biswas et al. (2016). The temporal change in the bank is also determined by superimposing the measured cross-section at selected locations. Figure 6.7 suggests that the numerical simulation with the proposed bank erosion model underestimates the bank shifting rate. However, the modified erosion rate term performs comparatively better for predicting the bank shifting in the study area. The bank shifting from numerical simulation is obtained by assuming that a flood peak of 65,000 $m^3 s^{-1}$ continues for a month. Many studies, such as a study by Klaassen et al. (1992), have suggested that the flood peak in the lower reach of the Brahmaputra River lasts for more than two months.

Therefore, the computation may underestimate the bank shifting rate. In fact, Figure 6.7 suggests that the proposed method somewhat underestimates the bank shifting rate. However, the modified erosion term performs comparatively well for predicting the bank shifting in the Brahmaputra River.

6.5 Summary

In the present chapter, I discusses the bank erosion and sandbar behaviors in rivers where suspended-sediment transportation dominates. The results are summarized as follows.

A bank erosion model that includes the influence of the lateral bed slope on the erosion rate of the suspended sediment is proposed, and it is connected to the depth-integrated two-dimensional numerical model. The stretchable grids are proposed to treat the bank shifting caused by sediment erosion and deposition using a reference hydraulic quantity and a coarse grid system. The proposed numerical model is applied to the lower reach of the Brahmaputra River to predict bank shifting and sandbar behaviors.

The location of the reference point at which average bed shear stress occurs is specified uniquely even when it changes widely, which enables us to treat bank erosion using the coarse grid system with the stretchable grids. The proposed numerical model, which includes the bank erosion model, underestimates somewhat the bank shifting rate, and it predicts the migration of the sandbars, suspended loads, and bedload fairly well.

7. Conclusions and Policy Implications

7.1 Conclusions

In the present research, I have discussed channel changes in a large braided river dominated by suspended sediment. For evaluating the channel changes numerically, I have used a two-dimensional depth-integrated governing equations to obtain information for river management. The erosion term in the governing equations depends on the turbulent characteristics near the bed and is conventionally evaluated in the vertical direction. The present research introduces a treatment to evaluate the suspended sediment transport by turbulent diffusion in the direction perpendicular to the bed boundary in the laterally slopped bank area. The governing equations are modified with the proposed treatment, are applied to the studied reach of the Brahmaputra River to test the validity of the proposed modification.

In Chapter 1, I discussed general information on channel changes and their impact on the socio-economic conditions of the inhabitants along erosion-prone rivers in Bangladesh. It was identified that the prediction of channel changes by means of numerical simulations is essential for planning, executing, and managing engineering interventions and for conducting countermeasures to reduce property damage resulting from riverbank shifting and flood hazards. Review studies suggest that a number of numerical models are available for the meandering rivers dominated with bedload. Similar models for suspended-sediment-dominated, large, braided rivers are not as common.

In Chapter 2, the morphological characteristics of the Brahmaputra River within the studied reach is described in terms of the flow, sediment transport, bedform, and geometry

of the cross-sections and the bed and bank materials. The characteristics of the flow are estimated from statistical analysis of the hydrological data. The results suggest that the mean of the annual peak flood and the highest flood flow is about 65,000 m^3 s^{-1} and 102,000 m^3 s^{-1}, respectively. The discharge differs widely throughout the years in the studied reach of the Brahmaputra River. The maximum discharge is 3 to 30 times higher than that of the minimum discharge. About 540 million tons of sediment are carried by the river, and most of this remains under suspension during transport by the water. The river possesses high width-to-depth ratio, a huge drainage basin, and a high flow discharge, which meets the criteria for the large river. The river encompasses the braided channel with multiple row bars based on the criteria proposed by Kuroki and Kishi (1984).

In Chapter 3, I described the analytical procedure for the derivation of a new erosion term based on the mechanism of sediment transportation by turbulent diffusion. The effect of the lateral bed slope on the erosion and deposition of suspended sediment in the laterally slopped bank area is described by means of a modified erosion term. The analytical solution for the lateral profile of the suspended sediment concentration in an idealized flow field results in two peaks, which suggest that sediment diffusion takes place from the bank area to the channel center from both sides of the channel. Numerical computations with a simple channel that has a circular shape also produce a similar lateral profile for the suspended sediment concentration. Therefore, the criteria for the formation process of an equilibrium cross-sectional shape proposed by Parker (1978) may not be attained in the river's reach dominated by suspended-sediment. In fact, the numerical results related to bed evolution suggest that the ridge is formed due to sediment deposition, that the eroded area is forming inside of the ridge area corresponding to the positions of the two peaks of sediment concentration, and that the deposition area is

created in the channel center region by sediment transportation from both sides. The scoured area is shifting toward the bank area in the case of computation with the proposed modified erosion rate term, and is deeper than that of the scoured hole computed without the modified erosion rate term.

In Chapter 4, I discussed a modification of the gradient-based method (GBM) for detecting the channel changes automatically using remote sensing data such as MODIS images. The index-based method (IBM) generally employs trial-and-error method to find a suitable threshold that is difficult to apply in the studied reach due to insufficient data availability. The proposed modified gradient-based method (MGBM) can successfully highlight the edges and can identify the sandbars without using any threshold. The proposed method uses the daily surface reflectance with a 250 m resolution and successfully maps the channel changes continuously in a daily scale, which is very useful to overcome the limitation of the temporal resolution of the satellite image.

In Chapter 5, I described the application of the two-dimensional depth-integrated governing equations with a modified erosion term for studying the formation and migration of sandbars numerically using a coarse-size grid. The results suggest that phenomena such as movement of sandbars in the upstream and downstream direction, the lateral extension of old sandbars, and the movement of newly formed sandbars are captured well in the present numerical simulation. It was found that the migration speed for the new and old sandbars was about 2.0 to 10.0 m hr^{-1} and 1.6 to 3.0 m hr^{-1}. However, this depends on the size of the sandbars and the magnitude of the flooding event. The migration rate based on the field measurement data in the Brahmaputra River is 1.11 to 16.8 m hr^{-1}. About 25 m of riverbed scouring and 18 m of bed aggradation are observed from the numerical simulation. In addition, the formation of braided channel, the

suspended-sediment concentration, and the longitudinal bed profile are well computed. However, the riverbank remains unchanged even with 25 m of bed scouring. Therefore, it may be difficult to evaluate the riverbank's shifting with the coarse-size grid.

In Chapter 6, I introduced a bank erosion model for a suspended-sediment-dominated large braided river, which employs a coarse-size grid to evaluate bank erosion. To apply the coarse size grid, a location corresponding to the maximum lateral bedload determined by means of Hasegawa's formula was used as the reference for the lateral bed slope. The average bed variation is determined using the hydraulic variables from the reference point. I found that the reference point is fixed for different hydraulic conditions, which allow for the application of the coarse grid in order to assess bank erosion. The bank erosion model and the modified erosion rate term are introduced into Takebayashi et al.'s (2000) two-dimensional depth-integrated model. I also found that the modified erosion rate term was suitable for covering the bank shifting in the Brahmaputra River. The stretchable grid is successful at capturing the gradual shifting of the bank resulting from the erosion and deposition of suspended sediment.

Since most of the rivers in Bangladesh are braided, dominated by suspended sediment, and densely inhabited on their riverbanks, special attention is required for the evaluation of the sediment transport in the near bank area and for the planform changes. This is important for effective management of the river. In the present research, I introduce a methodology to improve the predictions. Such a model provides a valuable and easy-to-use tool to analyze the problems related to sediment transport and to plan suitable countermeasures.

7.2 Policy Implications

In Bangladesh, problems related to sediment transport can broadly be categorized into two major classes. The first and the most formidable problem relates to the erosion of sediment from the riverbank area, which has remained one of the most unique ongoing problems in Bangladesh. The bank erosion causes land loss and impacts society negatively. The other issue relates to sediment deposition, which causes a loss of navigability and disrupts the fresh water supply to branch channels. The degree of the severity of the problems related to deposition is not limited to a point but extends to a greater region. However, the present status of the knowledge base in Bangladesh is never adequate to manage these issues efficiently.

The National Water Policy (1999) and the National Water Management Plan (2001) of Bangladesh emphasize the execution of structural countermeasures such as revetment, groyne, and spur-dykes to control the riverbank erosion and to undertake dredging for the revival of the river system. However, due to the limited financial budget, the bandage-type approach is adopted, focusing on the most affected area arbitrarily rather than taking a whole reach into consideration after analyzing it scientifically. It is also essential to evaluate the impact on the other parts of the river after implementing the structural countermeasures. However, a gap exists in relation to the availability of a scientific tool that can be applied rapidly to assess the impact of these countermeasures.

In the present study, I developed a tool to treat the sediment issues in the near-bank region, which can be a good option for filling the gap in the availability of the scientific tool. Generally, in the planning and designing of the hydraulic structures and local erosion protection, the stability of the slope is prioritized by computing the scour depth at the toe. The hydraulic variables related to the design of the river bank protection works are

maximum discharge, water level at maximum discharge, shape of the river cross-section, flow velocity, wave height, silt factors, anticipated maximum scour, wind speed and wave characteristics. The discharge is obtained from the analysis of hydrological data, especially through extrapolation of stage discharge relations at water level stations. In the case of braided river such as the Brahmaputra, the design discharge for a channel is determined based on the bankfull discharge and braiding index. The flow velocity, wave height and median diameter of the bed materials is selected based on the recommendation from the Guidelines and Manual for Standardized Bank Protection Structures (FAP 21, 1994). Lacey's formula is common to apply in finding the scour depth. Thereafter, empirical equations are employed to find the size of the protection materials. However, to design the countermeasures, the geometry of the eroding section needs to be considered, which can be done by numerical simulation with the modified erosion rate term.

The bank erosion model proposed in this study suggests that the location of the maximum erosion is gradually shifting toward the downstream direction. Presently, policymakers plan countermeasures that focus only on the location of the maximum erosion and implement these countermeasures to safeguard this location. The influence of these countermeasures may aggravate conditions in the upstream area. In such case, a structure such as a spur-dyke, in which the stream line and the sediment transport direction are changed considerably, may be ineffective. The change in the sediment transport needs to be studied by means of a numerical simulation with a bank erosion prediction tool. The proposed bank erosion model is able to fulfill the gap, as it uses coarser size grids and is able to conduct numerical simulation for the whole river reach within a reasonable time and can produce results that are consistent with the field condition.

The long-term plan for river managers in Bangladesh is to tame the Brahmaputra River by adopting the node and bend control approach. In order to implement the method of sediment transportation, it is important to study the channel changes and the formation and migration of sandbars. The present tool will be useful for treating these issues.

Developing a real-time forecast of the riverbank erosion is desirable. Presently, the Centre for Environmental and Geographic Information Services (CEGIS) predicts bank erosion on the basis of the shape of sedimentary features such as the contraction bar, the sharpened bar, the sand-wing, the sand tongue, and the bankside bar, which are characterized by pointed edges (CEGIS, 2002) and can mainly be observed, in the dry season, in satellite images using satellite imagery. The prediction is conducted once a year, which is useful for managing the budget. The real time change is difficult to include in this process. The present tool can be useful for developing a real-time bank shifting tool that will be useful for disaster management.

In the present study, I proposed the modified gradient-based method (MGBM), which is successful at identifying the sandbar and riverbank efficiently without using any threshold. The method will be useful for monitoring both the flood and the sandbars. The challenge for conducting numerical simulation in a suspended-sediment-dominated, large river is the availability of data with which to create the initial channel topography. By combing the MGBM to the hydraulics of water flow and sediment transport, a reasonable solution can be derived for developing the initial channel topography.

7.3 Recommendation for Future Study

In the present research, I have studied the evolution of the riverbed in the laterally slopped area and have considered the transport of suspended sediment by means of erosion and deposition only. The lateral bedload transport also needs to be considered to

evaluate riverbed evolution. Secondly, the stable channel section is desirable for executing river management structures. The modified erosion rate term may be introduced in the stable channel theory proposed by Parker (1978) for evaluating its effect on the shape of the formation of a stable cross-section for suspended-sediment-dominated rivers. In the present study, I treated only an idealized flow field to compute the riverbed evolution. The bed shear stress is determined by neglecting the temporal riverbed variations. Therefore, the proposed erosion term and the generality of the present results need to be tested through experimentation in the laboratory and using a suitable physical model.

References

Ahmad, Q. K., & Ahmed, A. U. (2003). Regional cooperation in flood management in the Ganges–Brahmaputra–Meghna region: Bangladesh perspective. *Natural Hazards*, 28, 181–198.

Anderson, J. D. (1995). *Computational fluid dynamics: The basics with application*. New York: McGraw-Hill International Editions, Mechanical Series.

Ashida, K. (1964). On river bed variations and stable channels in alluvial streams. *Bulletin of the Disaster Prevention Research Institute, Kyoto University, 14*(1), 23–45.

Ashida, K., Egashira, S., & Liu, B. Y. (1991). Numerical method on sediment sorting and bed variation in a meander channel. *Annual Journal of Hydraulic Engineering, JSCE, 35*, 383–390.

Ashida, K., Egashira, S., & Nakagawa H. (2008). *River morph-dynamics for 21st century*. Kyoto: Kyoto University Press.

Ashida, K., & Michiue, M. (1972). Study on hydraulic resistance and bedload transport rate in alluvial streams. *Transactions of JSCE, 206*, 59–69.

Ashworth, P. J., & Lewin, J. (2012). How do big rivers come to be different? *Earth-Science Reviews, 114*, 84–107.

Baki, A. B. M., & Gan, T. Y. (2012). Riverbank migration and island dynamics of the braided Jamuna River of the Ganges–Brahmaputra basin using multi-temporal Landsat images. *Quaternary International, 263*, 148-161. doi:10.1016/j.quaint.2012.03.016

Best, J. L., & Bristow, C. S. (1993). Braided rivers: Perspectives and problems. In J. L. Best & C. S. Bristow (Eds.), *Geological Society, Special Publication, 75*, 1–11.

Biswas, R. K., Egashira, S., & Yorozuya, A. (2015). Influence of lateral bed slope on erosion deposition process in suspended-sediment dominated river. *Journal of Japan Society of Civil Engineers, 71*(4), 871–876.

Biswas, R. K., Yorozuya, A., & Egashira, S. (2016). Modified gradient based method for mapping sandbars in mega-sized braided river using MODIS image. *Annual Journal of Hydraulic Engineering, JSCE, 60*, 931–936.

Blondeaux, P., & Seminara, G. (1985). A unified bar-bend theory of river meanders. *Journal of Fluid Mechanics, 157*, 449–470.

Brice, J. C., Blodgett, J. C., et al. (1978). *Countermeasures for hydraulic problems at bridges*. Federal Highway Administration Report Vols. 1 & 2. (FHW Publication No. ARD-78-162). Retrieved on 05, 25, 2016 from: http://ntl.bts.gov/lib/46000/46500/46529/FHWA-RD-78-163.pdf.

Bristow, C. S. (1993). Sedimentary structures exposed in bar tops in the Brahmaputra River, Bangladesh. *Geological Society, London, Special Publications, 75*, 277–289.

Center for Environmental and Geographic Information Services (2001). New prediction method for the morphological changes of the Jamuna River. *Bi-Annual Bulletin of Environment and GIS Project for Water Sector Planning, 1*(2), 1–2. Retrieved on 05, 25, 2016 from: http://www.cegisbd.com/pdf/July2001.pdf.

Center for Environmental and Geographic Information Services (2007). Long-term erosion process of the Jamuna River. Main Report. Bangladesh: Ministry of Water Resources.

Chowdhury R., & Ward N. (2004). Hydro-meteorological variability in the greater Ganges-Brahmaputra-Meghna basins. *International Journal of Climatology, 24*, 1495–1508.

Coleman, J. M. (1969). Brahmaputra River: Channel processes and sedimentation. *Sedimentary Geology, 3*, 129–239.

Crosato, A. (1989). Meander migration prediction. *Excerpta, 4*, 169–198.

Darby, S. E., Alabyan, A. M. & Van de Wiel, M. J. (2002). Numerical simulation of bank erosion and channel migration in meandering rivers. *Water Resources Research, 38*(9), 1163, doi:10.1029/2001WR00602,2002.

Delft Hydraulics and Danish Hydraulic Institute. (1996). Sedimentological characteristics of the main rivers of Bangladesh. *Government of the People's Republic of Bangladesh, FAP24 River Survey Project*, Final Report, Annex 4.

Dietrich, W. E., Smith, J. D., & Dunne, T. (1979). Flow and sediment transport in a sand bedded meander. *Journal of Geology, 87*, 305–315.

Duan J. G. (2004). Simulation of flow and mass dispersion in meandering channels. *Journal of Hydraulic Engineering, 130*(10), 964–976.

Duan, J. G., & Julien, P. Y. (2010). Numerical simulation of meander evolution. *Journal of Hydrology, 391*, 34–46.

Egashira, S., Kuroki, M., Sawai, K., & Yamasaka, M. (1988). Methods to evaluate the bed shear stress in open channel flow. *Proceedings of the 32nd Japanese Conference on Hydraulics*, 503–521.

Egashira, S., Ashida, K., Takahama, J., & Tanonaka, S. (1991). Derivation of bed-load formula from a view point of continuum body. Proc. of Hydraulic Engineering, JSCE, 35, 441-446 (in Japanese).

Einstein, H. A. (1950). *The bed-load function for sediment transportation in open channel flows*. United States Department of Agriculture, Soil Conservation Service (Technical Bulletin No. 1026).

Engelund, F. (1974). Flow and bed topography in channel bends. *Journal of Hydraulic Division, Proceedings of ASCE, 100*, 1631–1648.

Engelund, F., & Hansen, E. (1967). A monograph on sediment transport in alluvial Streams. *Teknisk Forlag*, Copenhagen, Denmark.

FAP 1 (1994). River training studies of the Brahmaputra River, Master Plan Report, Annex 4, Design and Construction. *Bangladesh Water Development Board, Ministry of Water Resources*, Government of Bangladesh.

FAP 21 (1994). Morphological predictions for test areas, bank protection and river training pilot project. *Bangladesh Water Development Board, Ministry of Water Resources*, Government of Bangladesh.

Food and Agriculture Organization. (2000). *Global river sediment yield database*. Retrieved on 25 July 2015 from: http://www.fao.org/nr/water/aquastat/sediment/index.stm

Flood Forecasting and Warning Centre. (2013). Annual flood report 2012. Retrieved on 25 July 2016 from: http://www.ffwc.gov.bd/index.php/reports/annual-flood-reports

Fujita, Y., & Muramoto, Y. (1982). The widening process of straight stream channels in alluvial rivers. *Bulletin of the Disaster Prevention Research Institute, Kyoto University, 32*(2), 115–141.

Gao, B. (1996). NDWI-A normalized difference water index for remote sensing of vegetation liquid water from space. *Remote Sensing and Environment, 58*, 257–266.

Graf, W. H. (1998). Fluvial hydraulics: Flow and transport processes in channels of simple geometry. New York: John Wiley & Sons.

Goswami, D. C. (1985). Brahmaputra River, Assam, India: Physiography, basin denudation and channel aggradation. *Water Resources Research, 21*(7), 959–978.

Haque, C. E. (1988). Human adjustments to river bank erosion hazard in the Jamuna floodplain, Bangladesh. *Human Ecology*, *16*(4), 421–437.

Hasegawa, K. (1981). Bank erosion discharge based on a non-equilibrium theory. *Proceedings of the JSCE, Tokyo, 316*, 37–50.

Hasegawa, K., & Mochizuki, A. (1989). Formation process of an equilibrium cross section in a straight channel of sand-silt river. In *4th International Seminar on River Sedimentation, Beijing, China*, 417–424.

Holeman, J. N. (1968). Sediment yield of major rivers of the world. *Water Resources Research, 4*(4), 737–1968.

Howard, A. D. (1992). Modelling channel migration and floodplain sedimentation in meandering stream. In *Lowland Floodplain Rivers: Geomorphological Perspective*, P. A. Carling and G. E. Petts (Eds.), 1–41. New York: John Wiley & Sons Ltd.

Hossain, M. M. (1992). Total sediment load in the Lower Ganges and Jamuna. *Journal of Institute of Engineers, 20*(3), 7–1.

Hutton, D., & Haque, C. E. (2004). Patterns of coping and adaptation among erosion-induced displacees in Bangladesh: Implications for hazard analysis and mitigation. *Natural Hazards, 29,* 405–421.

Hutton, D., & Haque, C. E. (2004). Human vulnerability, dislocation and resettlement: Adaptation processes of river-bank erosion-induced displacees in Bangladesh. *Disasters, 28*(1), 41–62.

Ikeda, S. (1975). On secondary flow and bed profile in alluvial curved open channel. In *Proceedings of 16th Congress IAHR, 3,* 105–112.

Ikeda, S., Parker, G., & Sawai, K. (1981). Bend theory of river meanders. Part 1: Linear development. *Journal of Fluid Mechanics, 112,* 363–377.

Ikeda, S. & Izumi, N. (1991). Stable channel cross sections of straight sand rivers. *Water Resources Research, 27*(9), 2429–2438.

Islam, M. R., Begum, S. F., Yamaguchi, Y., & Ogawa, K. (1999). The Ganges and Brahmaputra rivers in Bangladesh: Basin denudation and sedimentation. *Hydrological Processes, 17,* 2907–2923.

Islam, M. R., Yamaguchi, Y., & Ogawa, K. (2001). Suspended sediment in the Ganges and Brahmaputra rivers in Bangladesh: Observation from TM and AVHRR data. *Hydrological Processes, 15,* 493–509.

Islam, S. R. (2006). Integrated flood management in deltas and low-land river regions: country paper; Bangladesh. In A. Van Aplphen, A. van Beek, & A. Taal (Eds.), *Floods: From Defence to Management.* London: Taylor & Francis Group.

Itakura, T., & Kishi T. (1980). Open channel flow with suspended sediments, *Journal. Hydraulics Divisions, Procedures of the American Society of Civil Engineers, 106*(HY8), 1325–1343.

Mahanta, C., et al. (2014). Physical assessment of the Brahmaputra River. IUCN, International Union for Conservation of Nature, Dhaka, Bangladesh.

Jang, C., & Shimizu, Y. (2005). Numerical simulation of relatively wide, shallow channels with erodible banks. *Journal of Hydraulic Engineering, 131*(7), 565–575.

Ji, L., Zhang, L., & Wylie, B. (2009). Analysis of Dynamic Threshold for the Normalized Difference Water Index, Photogrammetric Engineering and Remote Sensing, 75(11), 1307-1317.

Johannesson, H., & Parker, G. (1985). *Computer simulated migration of meandering rivers in Minnesota*. (Project Report: No. 242), Retrieved from University of Minnesota, St. Anthony Falls Hydraulic Laboratory website on 05 25 2016: https://conservancy.umn.edu/handle/11299/113348.

Jullien, P. Y. (1992). Study of bed form geometry in large river. *Colorado State University and Delft Hydraulics*. Retrieved on 05 12 2015 from: http://repository.tudelft.nl/assets/uuid:bcb47286-6371-4645-b9ac-0a25cdcb448f/Q1386.pdf.

Kabir, M. R., & Ahmed, N. (1996). Bed shear stress for sediment transportation in the River Jamuna. *Journal of Civil Engineering, 24(1)*, 55–68.

Keulegan, G. H. (1938). Laws of turbulent flow in open channels. *Journal of Research of the National Bureau of Standards, 21*, 708–741.

Kikkawa, H. (Ed.). (1985). Sediment hydraulics. Tokyo: Ma-ruzen Ltd.

Kikkawa, H., Ikeda, S., & Kitagawa, A. (1976). Flow and bed topography in curved open channels. *Journal of Hydraulic Division, Proceedings of ASCE, 102*.

Kitanidis, P., & Kennedy, J. F. (1984). Secondary current and river-meander formation. *Journal of Fluid Mechanics, 144*, 217–219.

Klaassen, G. J., & Vermeer, K. (1988). *Confluence scour in large braided rivers with fine bed material*. Paper presented at the Proceedings of the International Conference on Fluvial Hydraulics, Budapest.

Klaassen, G. J., & Masselink, G. (1992). Planform changes of a braided river with fine sediment as bed and bank materials. In *5th international symposium on river sedimentation*. Karlsruhe, Germany.

Klaassen G. J., Mosselman, E., & Brühl, H. (1993). On the prediction of planform changes in braided sand-bed rivers. *Proceedings of the 1st conference on advances in hydro-science and engineering, USA*

Kovacs, A., & Parker, G. (1994) A new vectorial bedload formulation and its application to the time evolution of straight river channels. *Journal of Fluid Mechanics, 267*, 153–183.

Kuroki, M., & Kishi, T. (1984). Regime criteria on bars and braids in alluvial straight channel. *Proceedings of JSCE, 42*, 87–96.

Kwak, Y., Park, J., & Fukami, K. 2014. Estimating floodwater from MODIS time series and SRTM DEM data. *Artificial Life and Robotics, 19*(1), 95–102.

Lane, E. W., & Kalinske, A. A. (1941). Engineering calculation of suspended sediment. *Trans. A.G.U., 22*.

Lane, S. N., Parsons, D. R., Best, J. L., Orfeo, O., Kostaschuk, R. A., & Hardy, R. J. (2008). Causes of rapid mixing at a junction of two large rivers: Rio Parana and

Rio Paraguay, Argentina. *Journal of Geophysical Research, 113*, doi:10.1029/2006JF000745.

Latrubesse, E. M. (2008). Patterns of anabranching channels: The ultimate end-member adjustment of mega rivers. *Geomorphology, 101*, 130–145.

Leopold, L. B., & Wolman, M. G. (1957). River channel patterns: Braided, meandering and straight. Professional Paper: 282-B. Retrieved on 06, 20, 2016 from: http://pubs.usgs.gov/pp/0282b/report.pdf.

Lewin, J., & Ashworth, P. J. (2014). Defining large river channel patterns: Alluvial exchange and plurality. *Geomorphology, 215,* 83–98.

Li, M., Zang, S., Zhang, B., Li, S., & Wu, C. (2014). A review of remote sensing image classification techniques: The role of spatio-contextual information. *European Journal of Remote Sensing*, 47, 389–411.

Lira, J. (2006). Segmentation and morphology of open water bodies from multispectral images. *International Journal of Remote Sensing, 27*(18), 4015–4038.

Luu, L. X., Egashira, S., & Takebayashi, H. (2004). Investigation of Tan Chau reach in lower Mekong using field data and numerical simulation. *Annual Journal of Hydraulic Engineering, JSCE, 48*.

Luu, L. X., Takebayashi, H., Egashira, S., & Ide, S. (2005). Study on bed deformation in lower Mekong River. *Proceedings of Annual Fluid Mechanics Conference*, Tokyo.

Luu, L. X., Egashira, S., & Takebayashi, H. (2006). A new treatment of the exchange layer thickness to evaluate sediment sorting and armoring. *Journal of Applied Mechanics, JSCE, 9*, 1025–1030.

McFeeters, S. K. (1996). The use of the normalized difference water index (NDWI) in the delineation of open water features. I*nternational Journal of Remote Sensing, 17*(7), 1425–1432.

Milliman, J. D., & Meade, R. H. (1983). World-wide delivery of river sediment to the ocean. *Journal of Geology, 91*(1), 1–20.

Molinas, A., & Wu, B. (2010). Transport of sediment in large sand-bed rivers. *Journal of Hydraulic Research, 39*(2), 135–146.

Mosley, M. P. (1983). Response of braided rivers to changing discharge. *Journal of Hydrology (NZ), 22*(1), 18–67.

Mosselman, E., Huisink, M., Koomen, E., & Seymonsbergen, A. C. (1993). Morphological changes in a large sand-bed river. *Proceedings of the Third International Geography Conference*, Hamilton, Canada.

Mosselman, E. (1995). A review of mathematical models of river planform changes. *Earth Surface Processes and Landforms, 20*, 661–670.

Muramoto, Y., & Fujita, Y. (1978). The classification of meso-scale river bed configuration and the criterion of its formation. *Annual Journal of Hydraulic Engineering, JSCE, 22*, 275–282.

Nagata, N., Hosoda, T., & Muramoto, Y. (2000). Numerical analysis of river channel processes with bank erosion. *Journal of Hydraulic Engineering, 126*(4), 243–252.

Nakagawa, H., & Tsujimoto, T. (1980). Sand bed instability due to bed load motion. *Journal of Hydraulic Division, ASCE, 106*(12), 2029–2051.

Nakagawa, H., Zhang, H. Baba, Y., Kawaike, K., & Teraguchi, H. (2013). Hydraulic characteristics of typical bank-protection works along the Brahmaputra/Jamuna River, Bangladesh. *Journal of Flood Risk Management, 6*, 345–359.

Northwest Hydraulic Consultants. (2013). Main river flood and bank erosion risk management program final report, annex e: River and charland morphology and river engineering. Bangladesh Water Development Board, Ministry of Water Resources, Government of the Peoples Republic of Bangladesh.

NWPo. (1999). National water policy. *Ministry of Water Resources*, Government of the People's Republic of Bangladesh.

NWMP. (2001). National water management plan. Volume 1: Summary, *Ministry of Water Resources*, Government of the People's Republic of Bangladesh.

Okada, S., Yorozuya, A., Koseki H., Kudo, S., & Muraoka, K. (2016, September). Comprehensive measurement techniques of water flow, bedload and suspended sediment in large river using Acoustic Doppler Current Profiler. *Proceedings of the International Symposium on River Sedimentation*. Stuttgart, German

Olaode, A., Naghdy, G., & Todd, C. (2014). Unsupervised classification of images: A review. *International Journal of Image Processing 8*(5): 325–342.

Oya, M. (1979). An applied geomorphological study on the selected bridge site along Brahmaputra-Jamuna River in Bangladesh. *Geographical Review of Japan, 52*(8), 407–425.

Parker, G. (1978). Self-formed straight rivers with equilibrium banks and mobile bed. Part 1. The sand-silt river, *Journal of Fluid Mechanics, 89*, 109–125.

Parker, G., Sawai, K., & Ikeda, S. (1982). Bend theory of river meanders. Part 2. Nonlinear deformation of finite-amplitude bends. *Journal of Fluid Mechanics, 115*, 303–314 doi:10.1017/S0022112082000767.

Peters, J. J. (1993). Morphological studies and data needs. *Proceedings International Workshop on Morphological Behavior of Major Rivers in Bangladesh, Dhaka*.

Potter, P. E. (1978). Significance and origin of big rivers. *The Journal of Geology, 86*(1), 13–33.

Rouse, H. (1937). Nomogram for the settling velocity of spheres. In *Division of Geology and Geography, Exhibit D of the Report of the Commission on Sedimentation, 1936–1937*. 57–64.

Rubey, W. W. (1933). Settling velocities of gravel, sand and silt particles. *American Journal of Science, 25*, 325–338.

Ruben, D. L., Szupiany, R., Abad, J. D., & Farias, H.D. (2015). Dynamics of flow structure, suspended sediment and morphology of large meandering rivers. *E-Proceedings of the 36th IAHR World Congress, The Hague, the Netherlands*.

Saito, Y. (2001). *Deltas in Southeast and East Asia: Their evolution and current problems*. Paper presented at the Proceedings of the APN/SURVAS/LOICZ Joint Conference on Coastal Impacts of Climate Change and Adaptation in the Asia–Pacific Region, Kobe.

Sambrook Smith, G. H., Ashworth, P. J., Best, J. L., Lunt, I. A., Orfeo, O., & Parson, D. (2009). The sedimentology and alluvial architecture of a large braid bar, Rio Paraná, Argentina. *Journal of Sedimentary Research, 79*, 629–642.

Sarker, M. H. (2009). *Morphological response of the Brahmaputra-Padma-Lower Meghna river system to the Assam earthquake of 1950*. (Doctoral Thesis, University of Nottingham, Nottingham, England). Retrieved on 09 20 2015 from http://eprints.nottingham.ac.uk/14566/1/606302.pdf

Sarker, M. H., Huque, I. A., Alam, M., & Koudstaal, R. (2003). Rivers, chars and char dwellers of Bangladesh. *International Journal of River Basin Management, 1*(1), 61–80.

Sarker, M. H., Akhter, J., & Ferdaous, M. R. (2011). River bank protection measures in the Brahmaputra-Jamuna River: Bangladesh experience. *Proceedings of the International Conference on Water and Flood Management, Dhaka*.

Sarker, M. H., Throne, C. R., Aktar, M. N., & Ferdous, M. R. (2013). Morpho-dynamics of the Brahmaputra–Jamuna River, Bangladesh. *Geomorphology, 215*, 45-59.

Schumm, S. A. (1963). A Tentative Classification of Alluvial River Channels. Geological Survey Circular 477, Washington, USA.

Schumm, S. A. (1969). River Metamorphosis. Journal of the Hydraulic Division, Proceedings of the ASCE, 95(HY1), 255-273.

Schumm, S. A. (1981). Evolution and response of the fluvial system, sedimentologic implications. *Soc. Econ. Paleontol. Mineral. Spec. Publ. 31*, 19-29.

Schumm, S. A., & Winkley, B. R. (1994). The character of large alluvial rivers. In S. A. Schumm & B. R. Winkley (Eds.), *The variability of large alluvial rivers*. 1–9.

Shimizu, Y., & Itakura, T. (1991). Calculation of flow and bed deformation with a general non-orthogonal coordinate system. *Proceedings of the XXIV IAHR Congress, Madrid, Spain*, 41–48.

Subramanian, V., & Ramanathan, A. L. (1996). *Nature of sediment load in the Ganges-Brahmaputra river systems in India sea-level rise and coastal subsidence*. Springer. DOI:10.1007/978-94-015-8719-8_8

Sun, D., Yu, Y., & Goldberg, M. D. (2011). Deriving water fraction and flood maps from MODIS images using a decision tree approach. *IEE Journal of Selected Topics in Applied Earth Observations and Remote Sensing, 4*(4). 814–825.

Takebayashi, H. (2008). Instability of Stream Geometry. *Fourth International Conference on Scour and Erosion, Tokyo, Japan*.

Takebayashi, H., Egashira, S., & Nakagawa, H. (2000). Formative condition and mechanism of a self-formed channel in straight river course. *Annual Journal of Hydraulic Engineering, JSCE, 44*, 771–776.

Takebayashi, H., & Egashira, S. (2001). Formative process and domain of a self-formed channel. *Proceedings of the JSCE, 677/II-55*, 75–86.

Takebayashi, H. & Okabe, T. (2002). Geometric characteristics of braided channel on non-uniform sediment bed. *International Congress: INTERPAEVENT 2002 in the Pacific Rim-Matsumoto/Japan, 1*, 79–89.

Takebayashi, H., Egashira, S. & Okabe, T. (2003). Braided streams formed on bed beds with non-uniform sediment. *Proceedings of the 3rd IAHR Symposium on River, Coastal and Estuarine Morphodynamics*, Matsumoto,787–798.

Takebayashi, H., Fujita, M., & Harsanto, P. (2010). Bank erosion model along bank composed of both cohesive and non-cohesive layer. *Annuals of Disaster Prevention Research Institute, Kyoto University, 53B*, 527–536.

Takebayashi, H., & Fujita, M. (2012). Numerical model of bank erosion process of rivers in wetland. *Proceedings of the 9th ISE, Vienna*.

Vernon, D. (1991) *Machine vision: Automated visual inspection and robot vision*. London: Prentice Hall Int. (UK) Ltd.

World Bank. (2015). *Environmental impact assessment (EIA) of river management improvement program, Phase I (RMIP-I), Volume I*. Bangladesh Water Development Board. Retrieved on 06 30 2016 from:

http://documents.worldbank.org/curated/en/993651468205481925/pdf/E47510V10P149700Box385438B00PUBLIC0.pdf

World Meteorological Organization. (2006). *Technical regulations. Volume III. Hydrology*, (2006 edition, supplement no. 1 I.2008). Retrieved on 06 30 2016 from: http://www.wmo.int/pages/prog/hwrp/publications/technical_regulations/WMO_N49_TechnReg_Vol3.pdf

Xiao, X., Boles, S., Frolking, S., Salas, W., Moore, B., Li, C., He, L., & Zhao, R. (2002). Observation of flooding and rice transplanting of paddy rice fields at the site to landscape scale in China using vegetation sensor data. *International Journal of Remote Sensing*, *23*(5), 3009–3022.

Xu, H. (2006). Modification of normalized difference water index (NDWI) to enhance open water features in remotely sensed imagery. International Journal of Remote Sensing 27(14), 3025-3033.

Yorozuya, A., Rahman, M. S., & Egashira, S. (2012). Study on meso scale bed-form in Ganges reach dominated by suspended sediment. In *River Flow 2012* (pp. 837–843). London: Tailor & Francis Group.

Yorozuya, A., Islam, M. S., Kamoto, M., & Egashira, S. (2013). Influence of Jamuna Bridge on river morphology. In Fukuoka et al. (Eds.) *Advances in river sediment research*. London

Zhang, B., Li, S., Wu, C., Gao, L., Zhang, W., & Peng, M. (2012). A neighborhood-constrained k-means approach to classify very high spatial resolution hyperspectral imagery. *Remote Sensing Letters, iFirst*, 1–10.

Figure 1.1 Riverbank erosion prone areas in Bangladesh

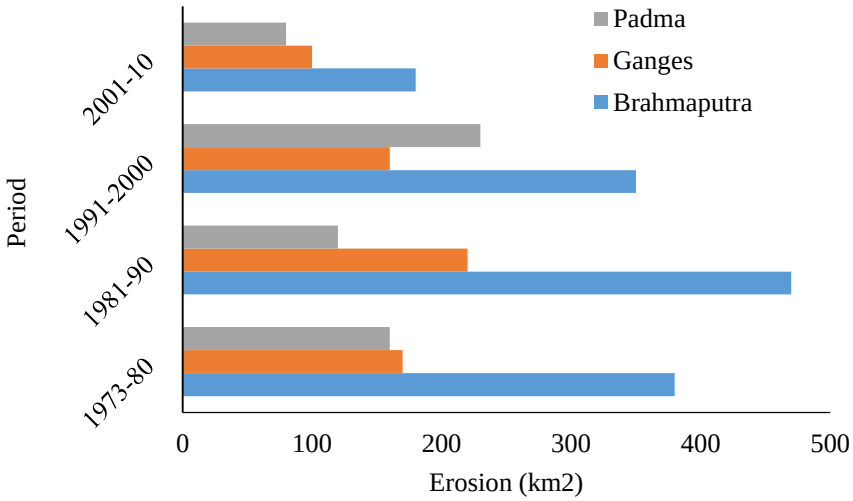

Figure 1.2 Riverbank erosion in decadal scale along the major rivers in Bangladesh (NHC, 2013)

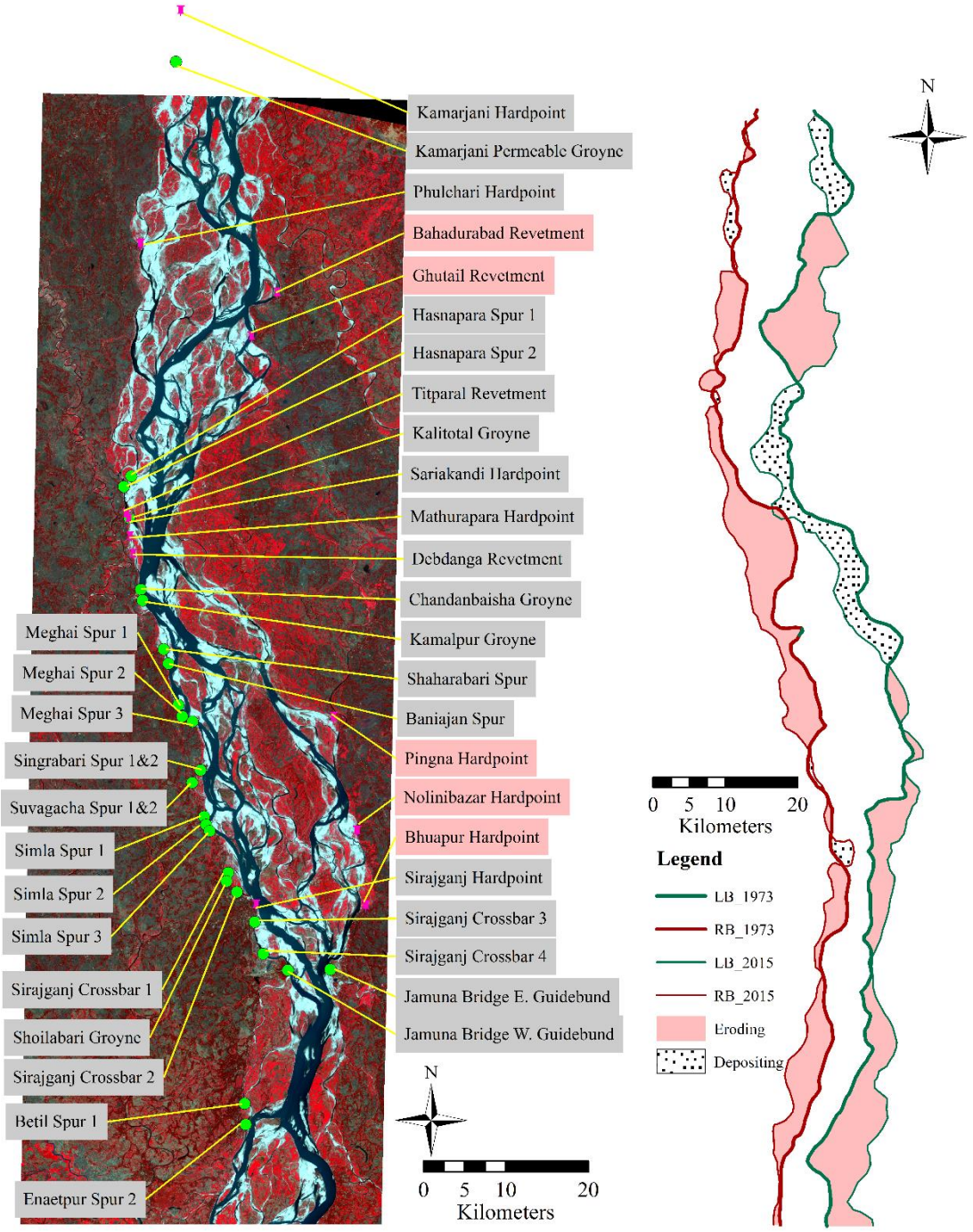

Figure 1.3 Riverbank changes from 1973 to 2015 (right) and locations and types of structural countermeasures from 1995 onward (left) in the Brahmaputra River

Figure 1. 4 Damage spur in the Brahmaputra River (photographs taken on 12 September 2015)

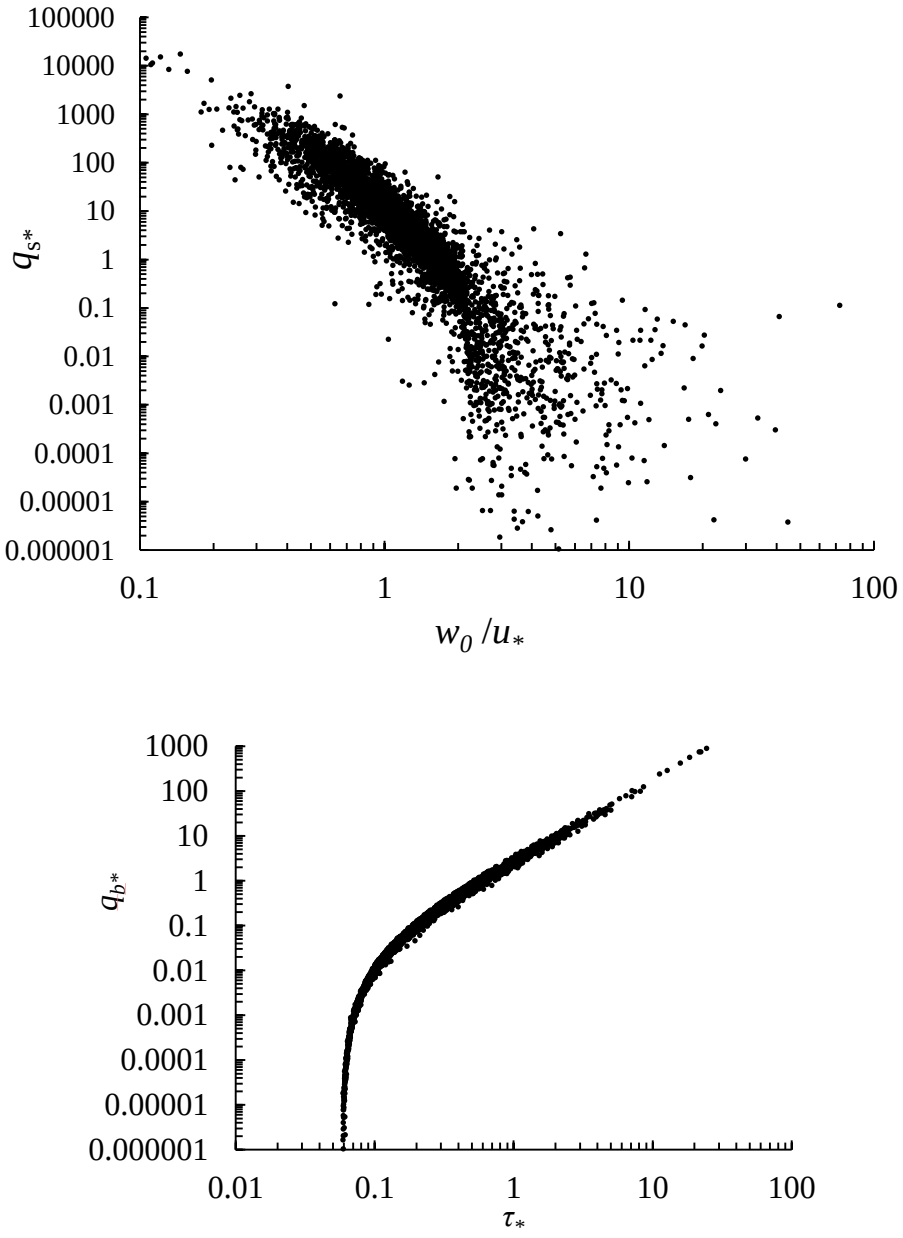

Figure 1.5 Suspended and bedload transport rate for different hydraulic conditions

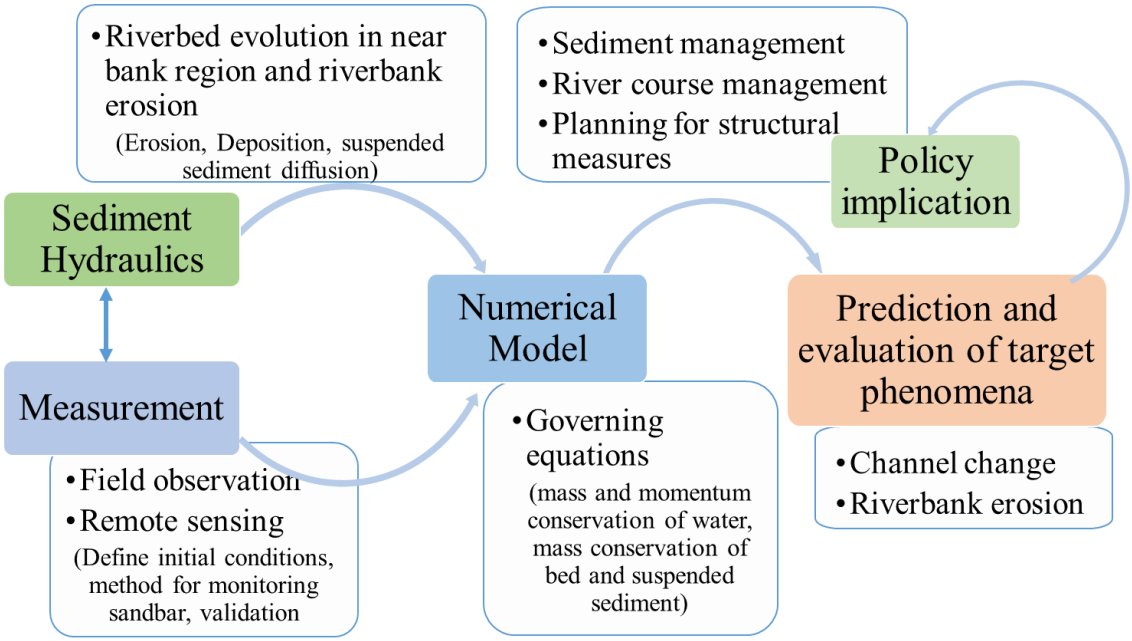

Figure 1.6 Flowchart of the general methodology applied in this study

Note. Based on Author (2016)

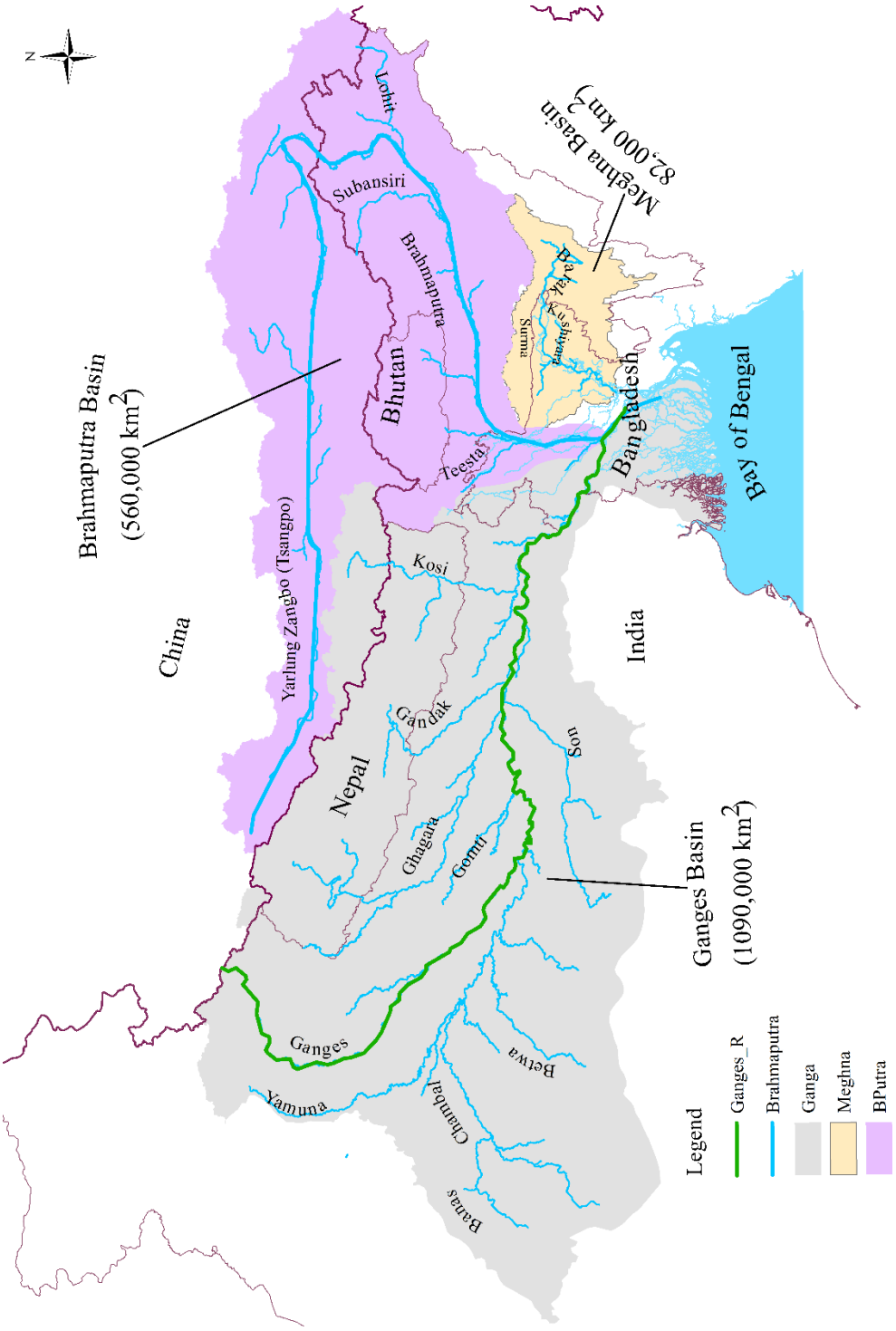

Figure 2.1 Location of Bangladesh in the Ganges, Brahmaputra and Meghna rivers basin

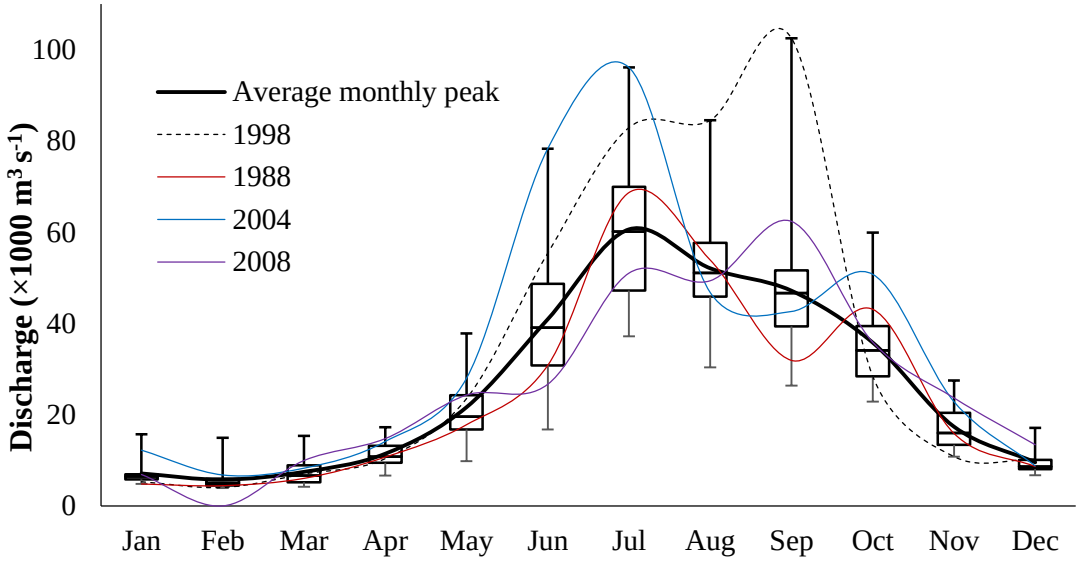

Figure 2.2 Hydrograph in the Brahmaputra River. Box-and-whisker plots indicate minimum and maximum (whiskers), 25th and 75th percentiles (box ends), and median (black solid middle bar). Solid black curve line represents average value

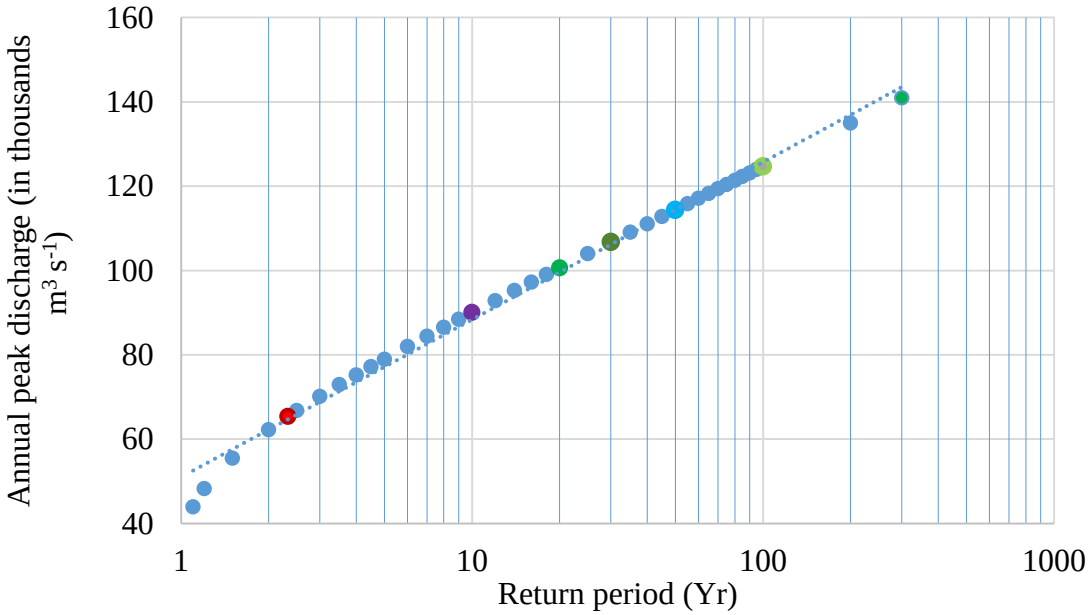

Figure 2.3 Exceedance probability of annual peak discharge in the Brahmaputra River

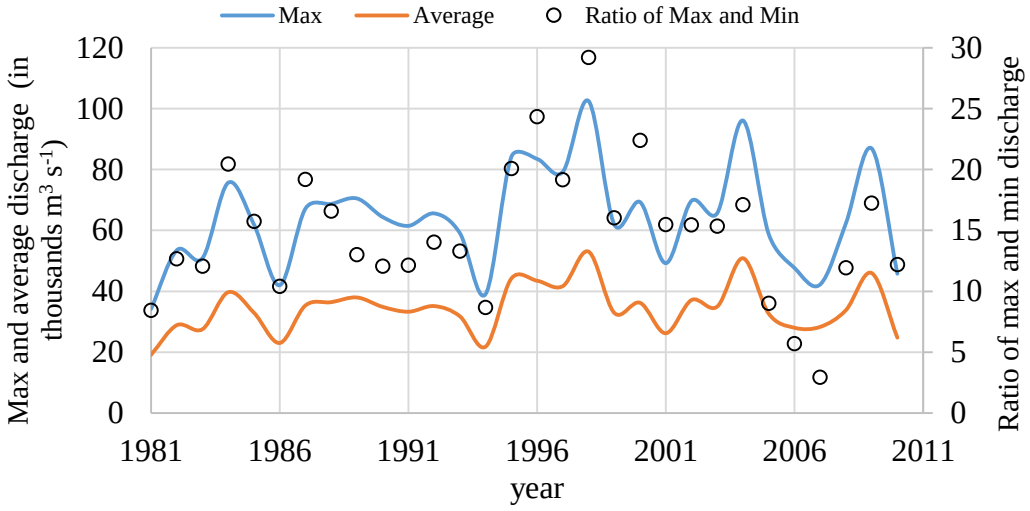

Figure 2.4 Inter-annual variability of flow discharge in the Brahmaputra River

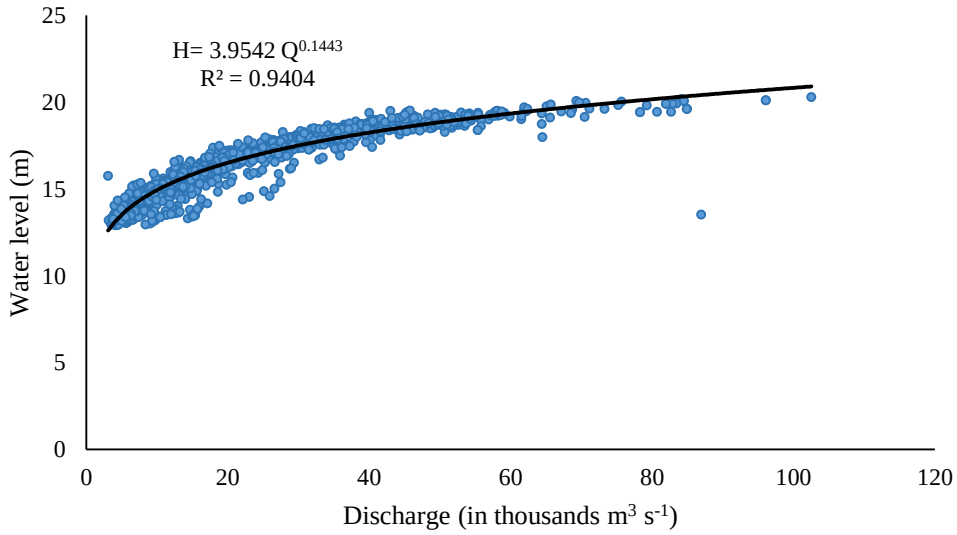

Figure 2.5 Stage versus discharge relationship in the Brahmaputra River

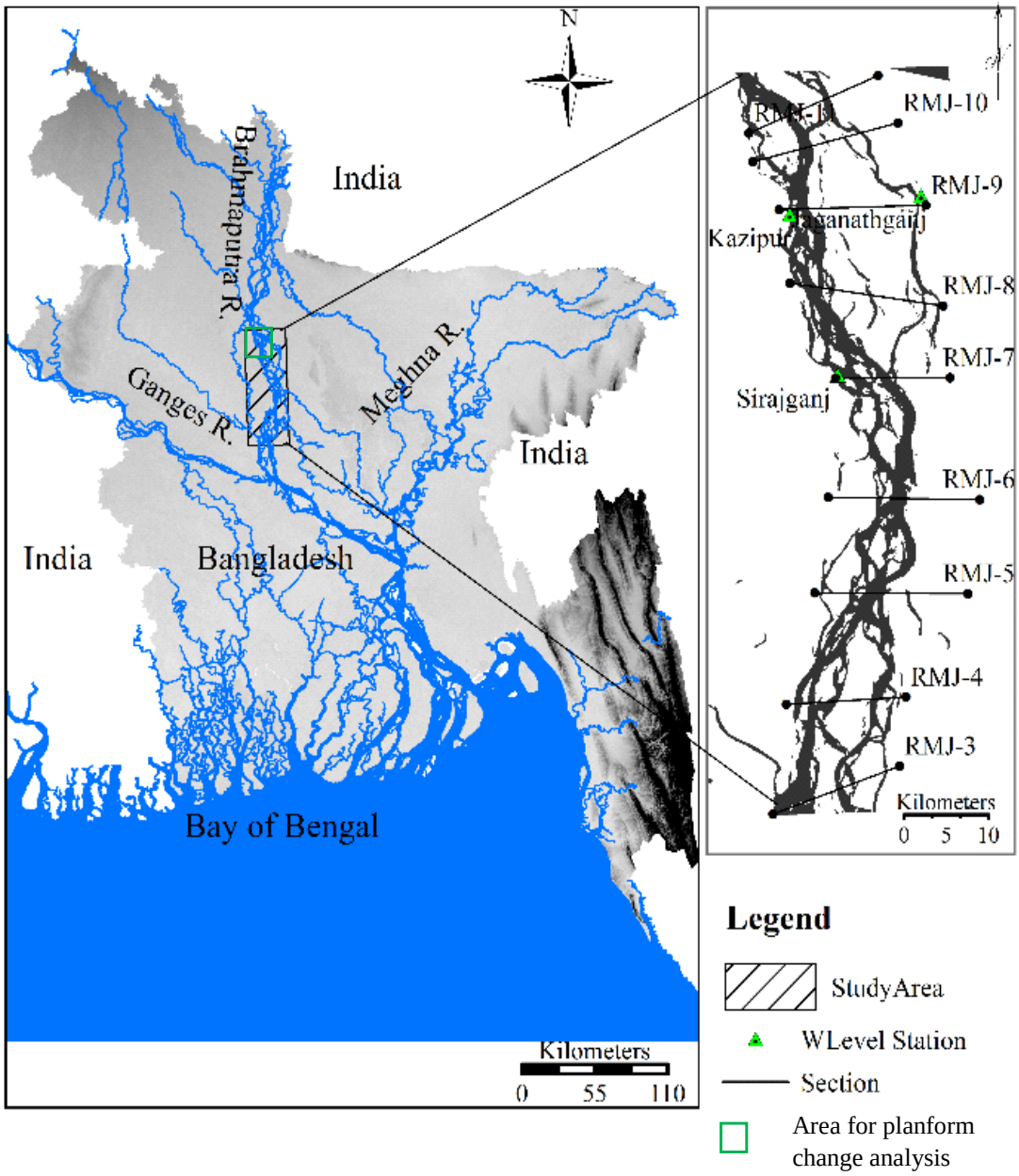

Figure 2.6 Study area and braided planform based on PRISM-DSM of JAXA of the Brahmaputra River

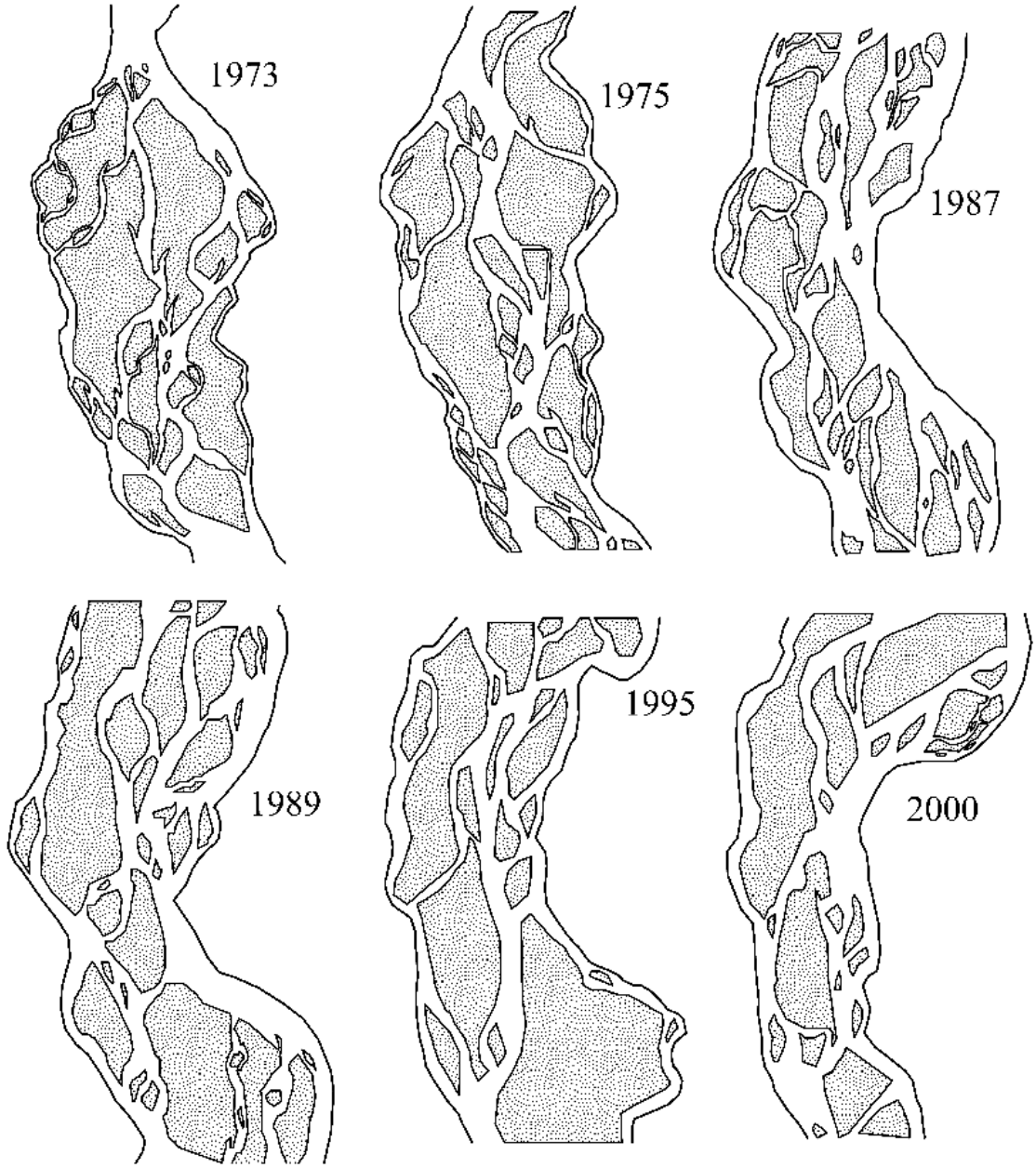

Figure 2.7 Planform changes in a part of the Brahmaputra River in Bangladesh from satellite image analysis

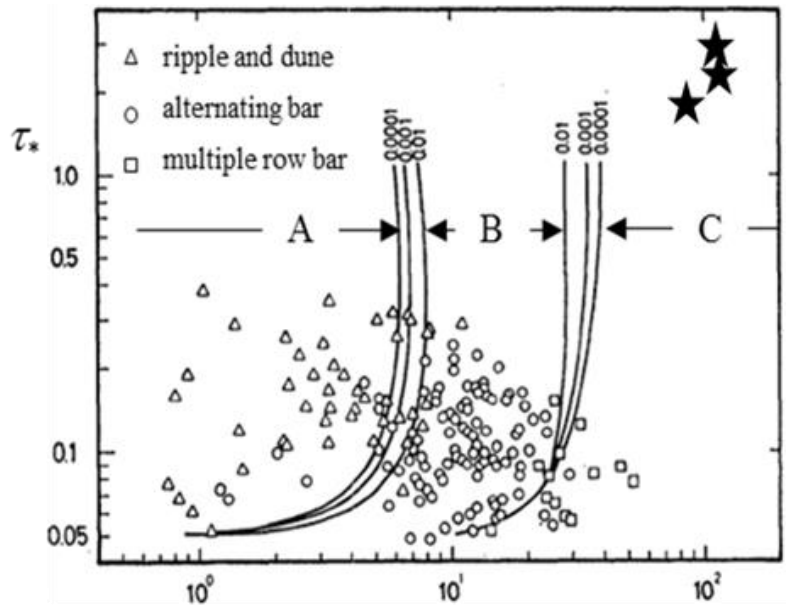

$BI_0^{0.2}/h$

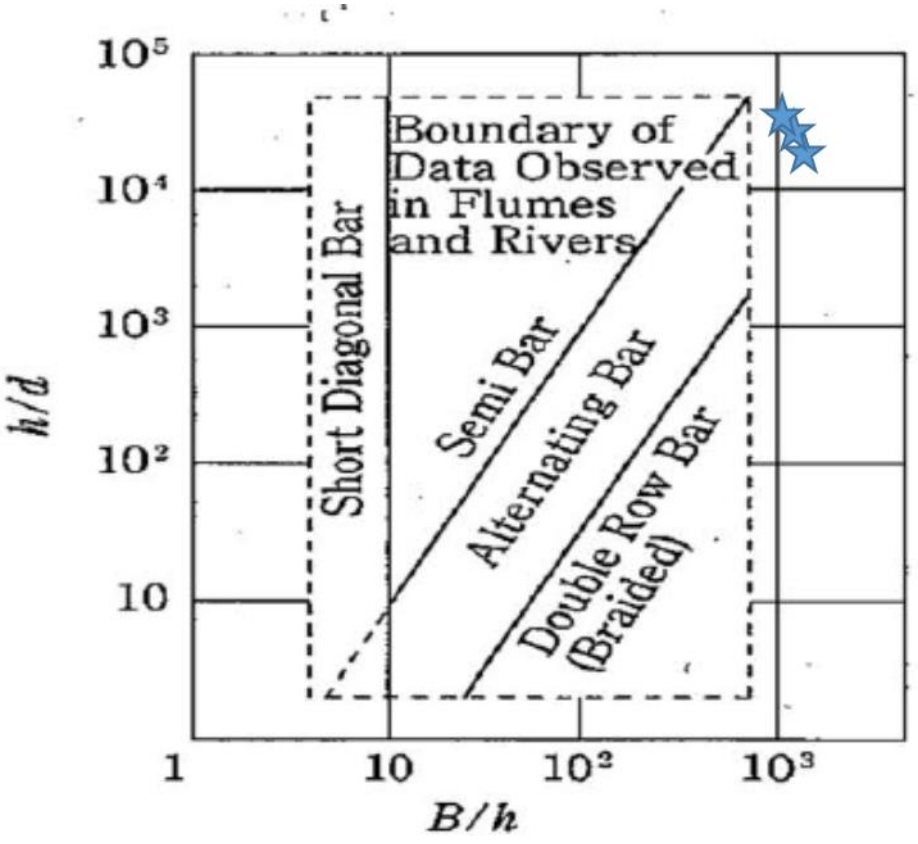

Figure 2.8 Formation region of mesoscale bed form (*at* top: after Kuroki and Kishi, 1984 and *at* the bottom after Muramoto and Fujita, 1978)

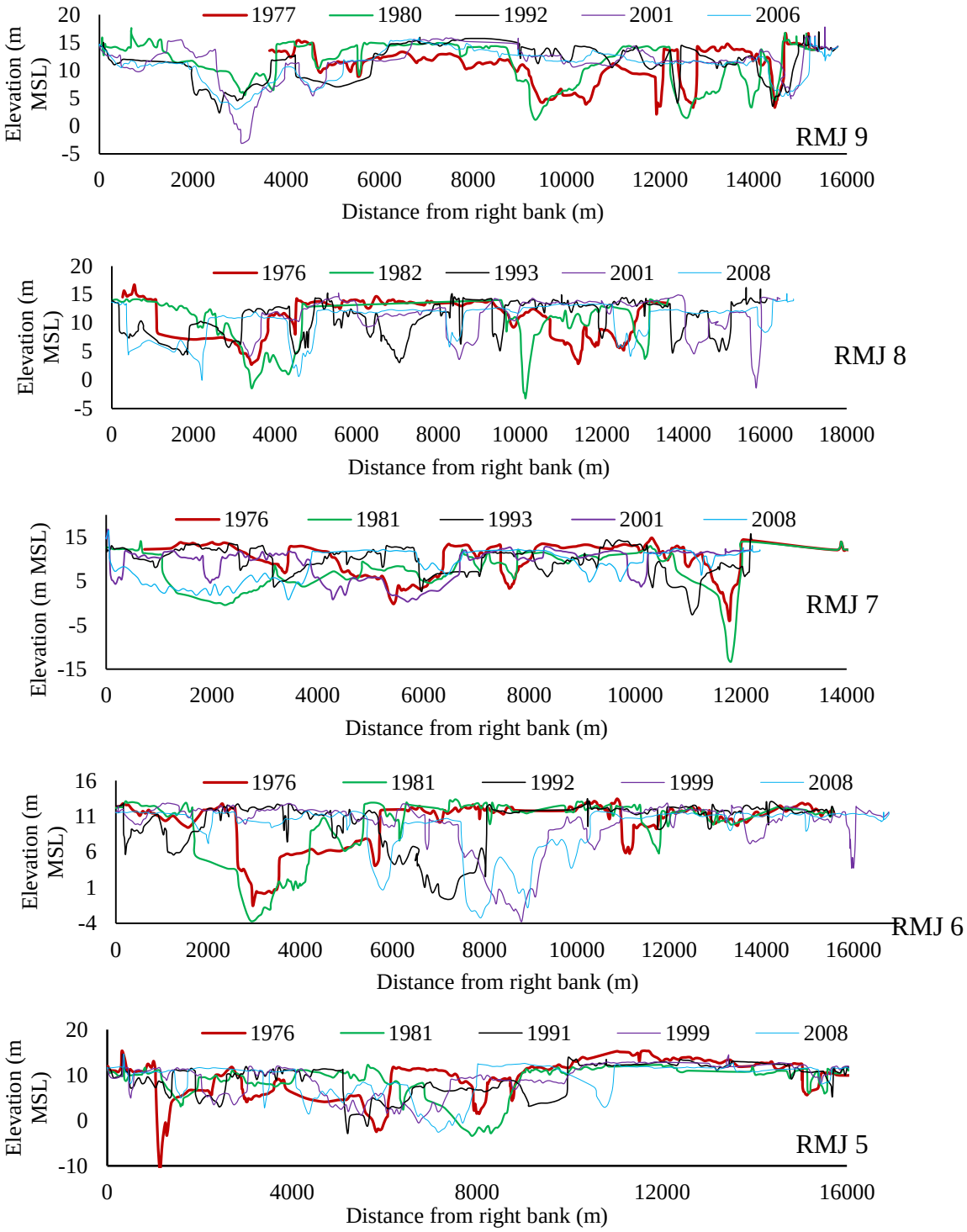

Figure 2. 9 Temporal planform changes in Brahmaputra River based on measured cross-section data of BWDB

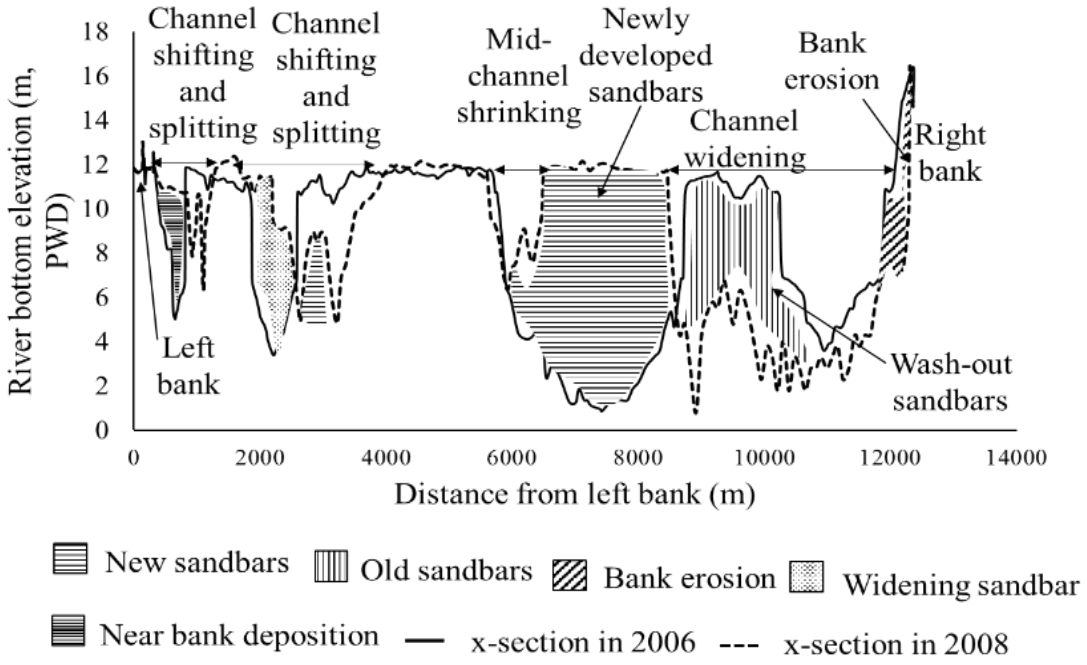

Figure 2.10 Typical planform changes in Jamuna River from measured cross-sections.

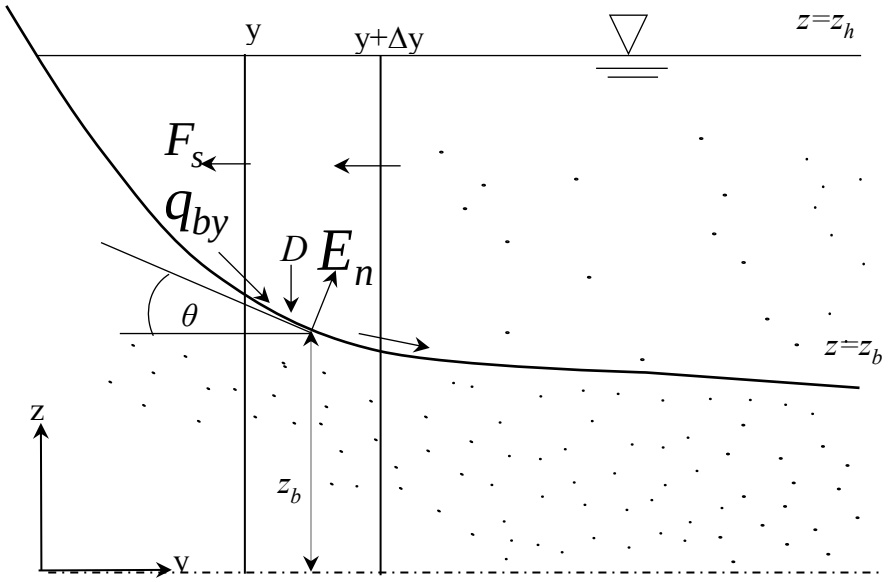

Figure 3. 1 Definition sketch for sediment budget, turbulent diffusion and bed variation

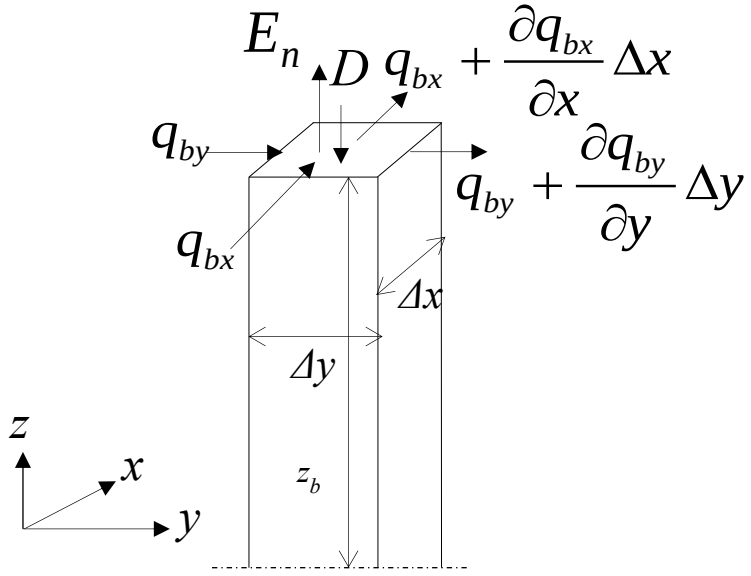

Figure 3.2 Schematic diagram for conventional sediment budget at bed layer

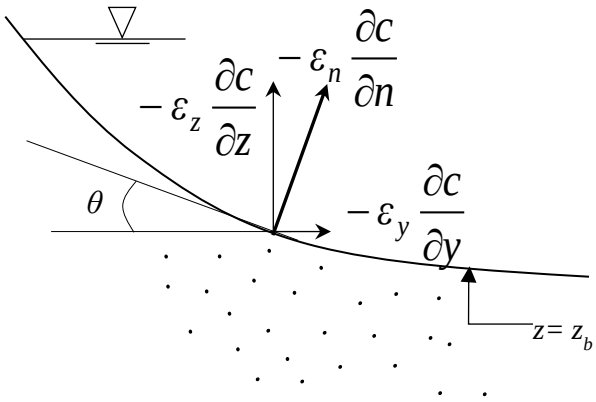

(a) Turbulent diffusion at riverbed surface

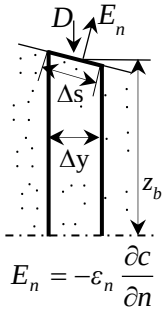

(b) Erosion-deposition at the bed surface

Figure 3.3 Schematic diagram for sketch for turbulent diffusion and erosion-deposition processes at the inclined bed surface

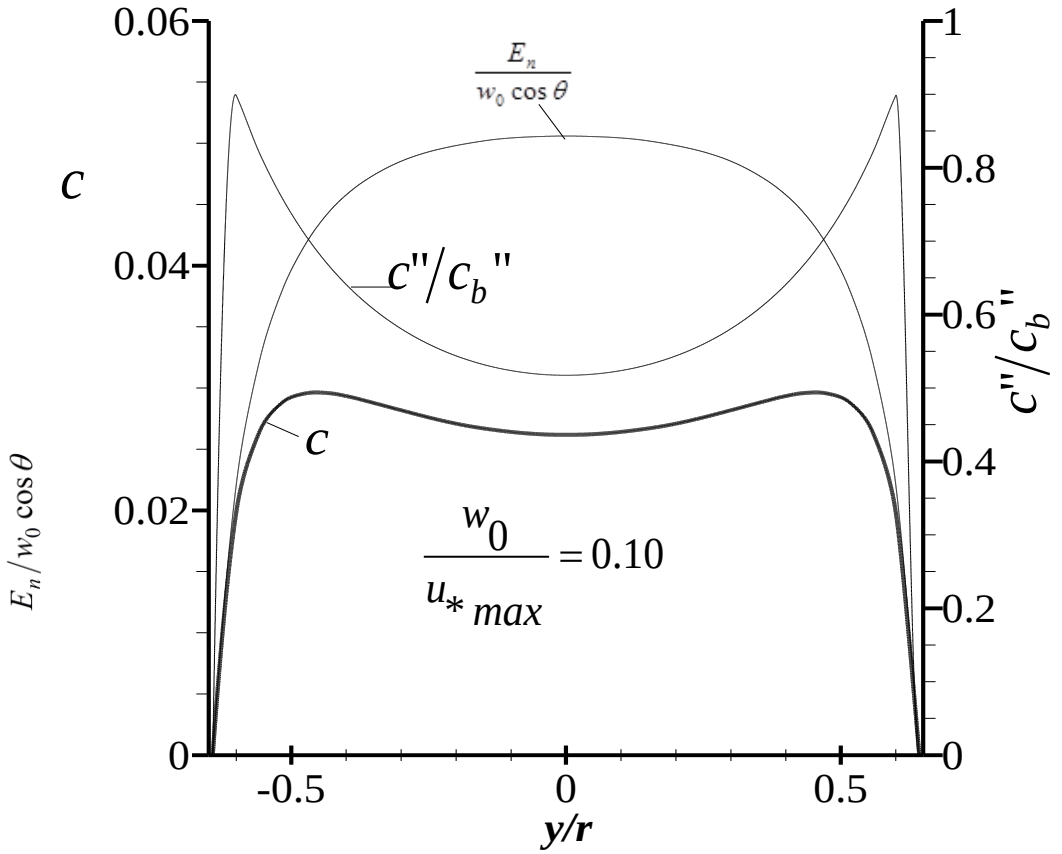

Figure 3.4 Lateral sediment concentration profile (theoretical)

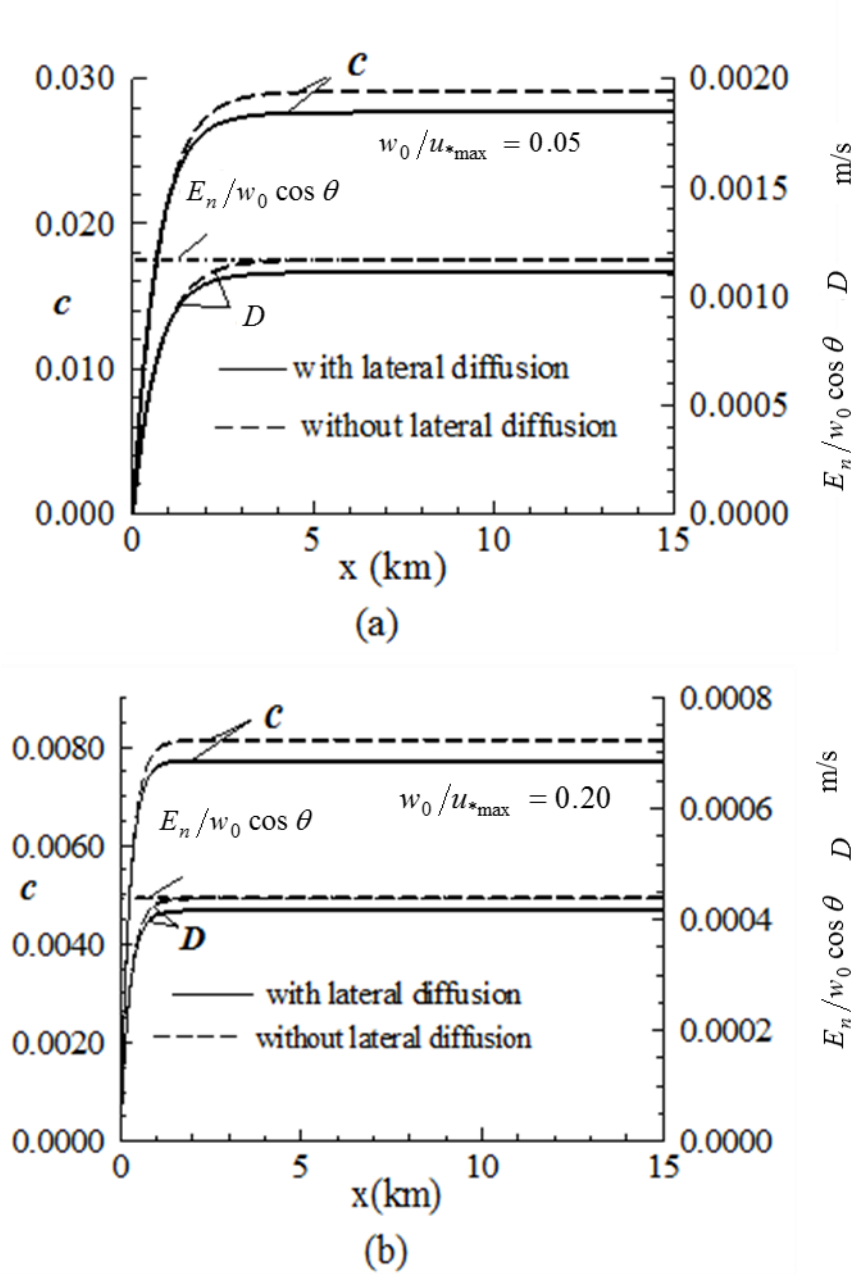

Figure 3.5 Longitudinal profile for sediment concentration, erosion and deposition

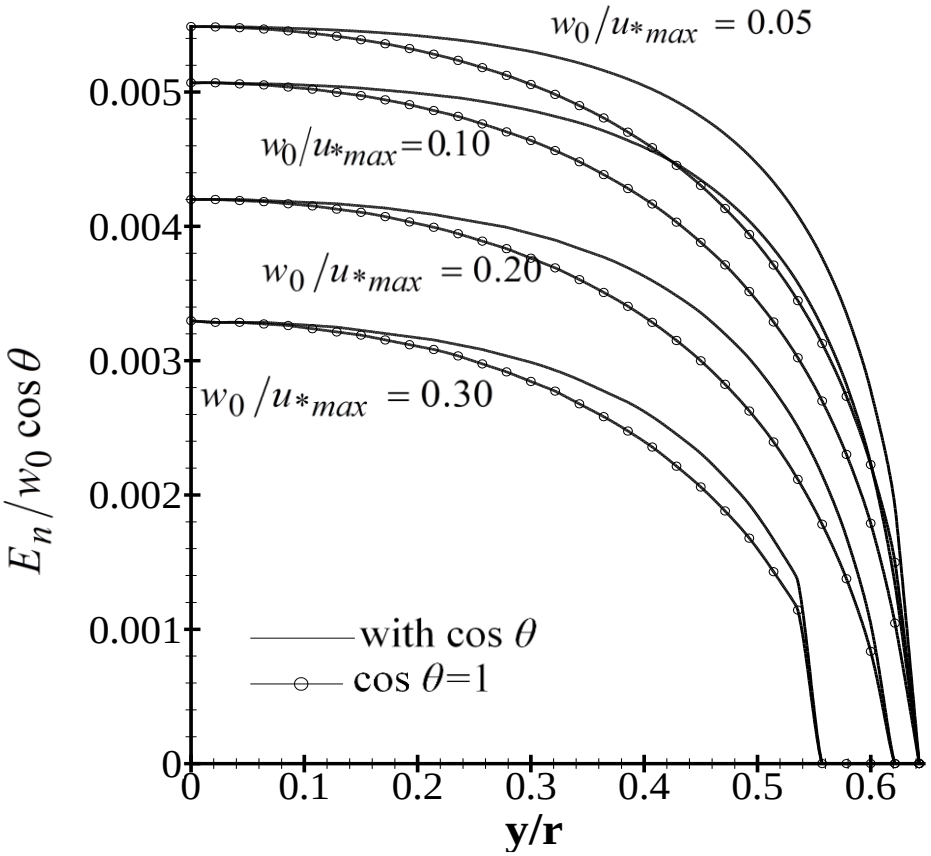

Figure 3.6 Erosion rate term with and without lateral bed slope

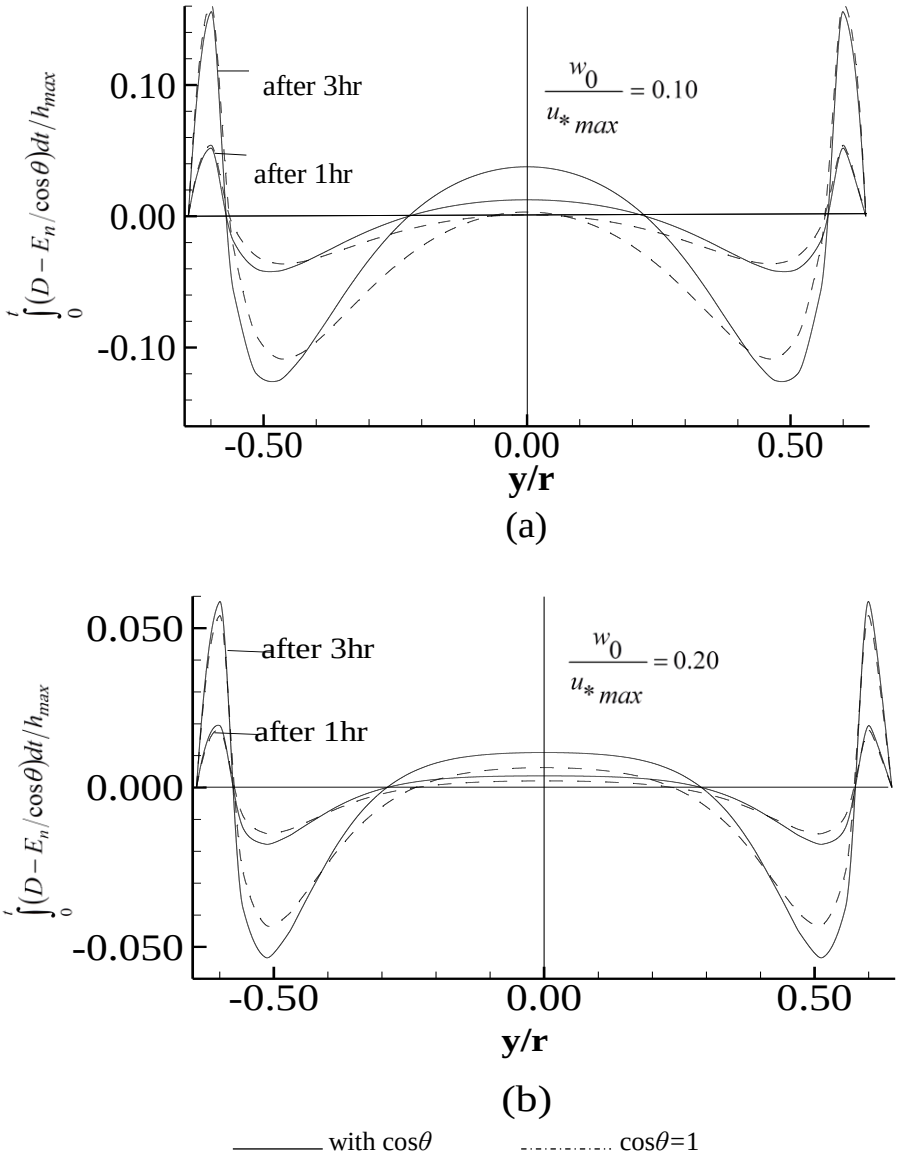

Figure 3.7 Effect of lateral bed slope on river bed evolution

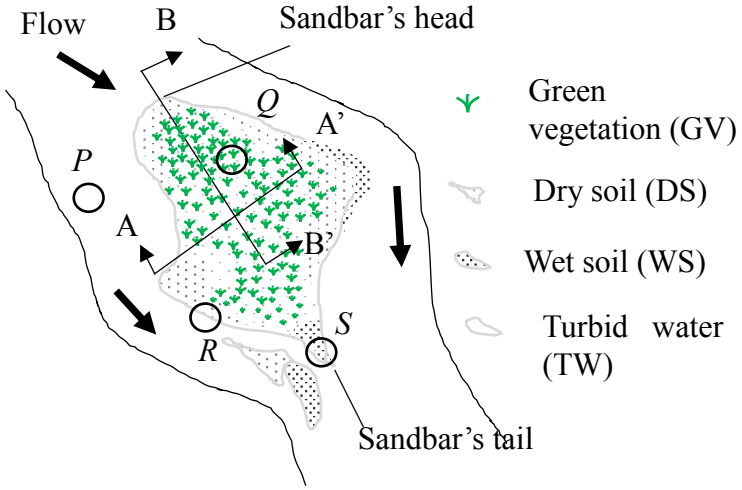

Figure 4.1 Schematic diagram of surface types in a braided river

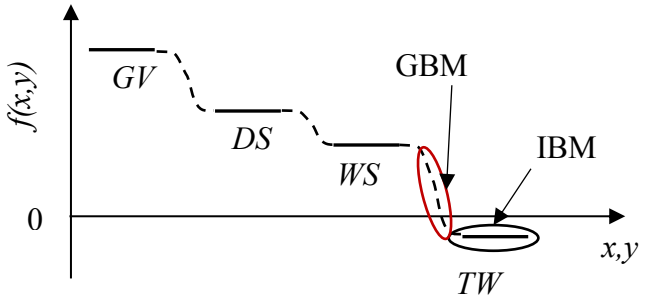

Figure 4.2 Schematic diagram for focused areas of index and gradient based method

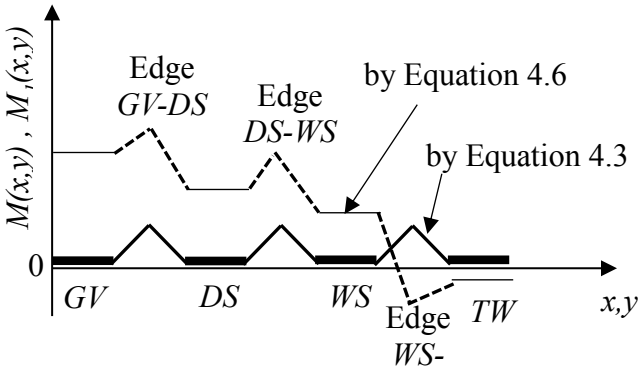

Figure 4.3 Effect of weightage average in the GBM for edge detection

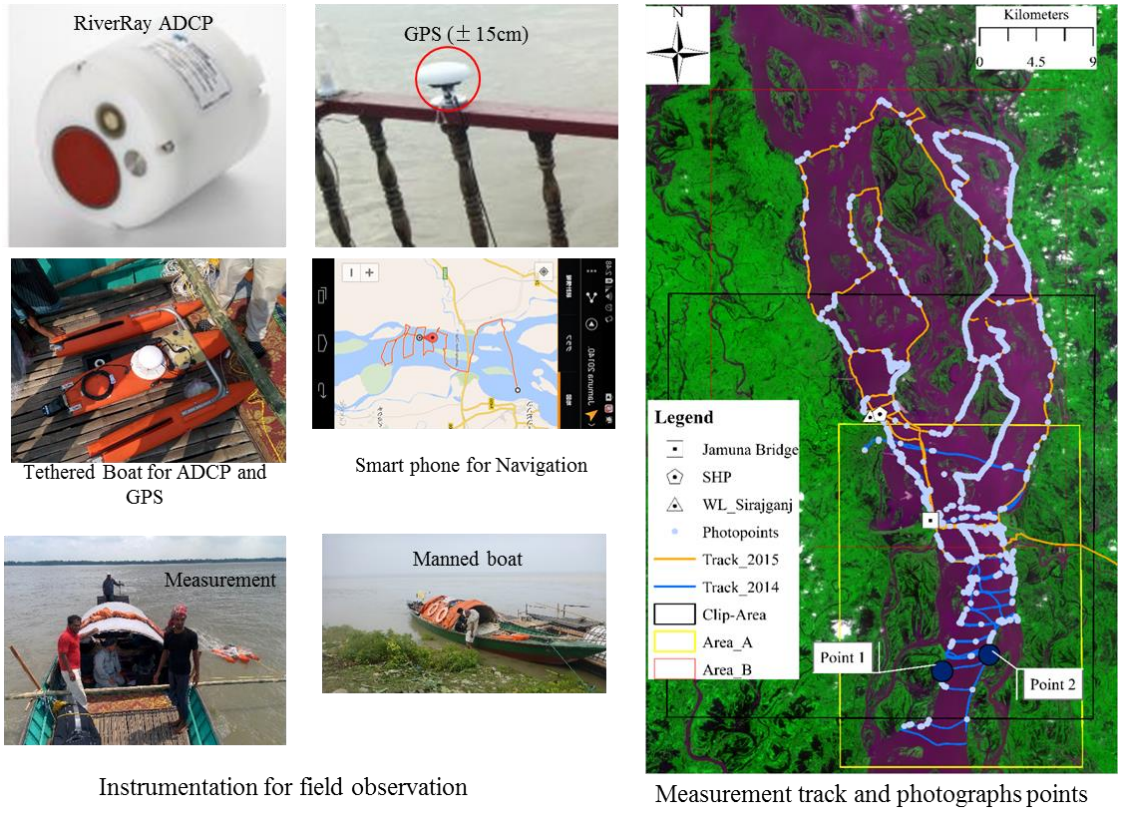

Figure 4.4 Schematic of the principle of MGBM

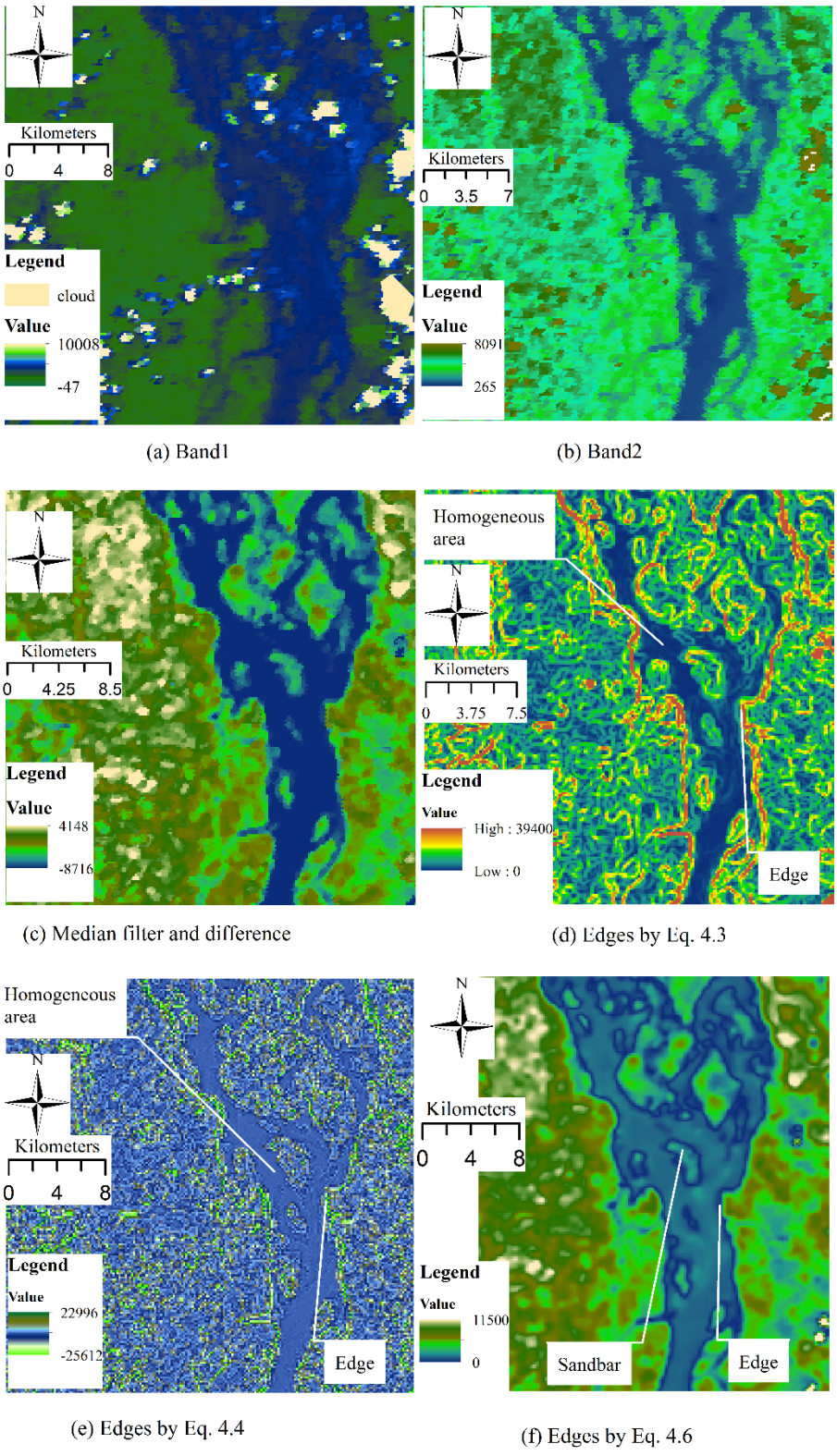

Figure 4.5 Performance of first and second order gradient and proposed modification on edge detection using MODIS image

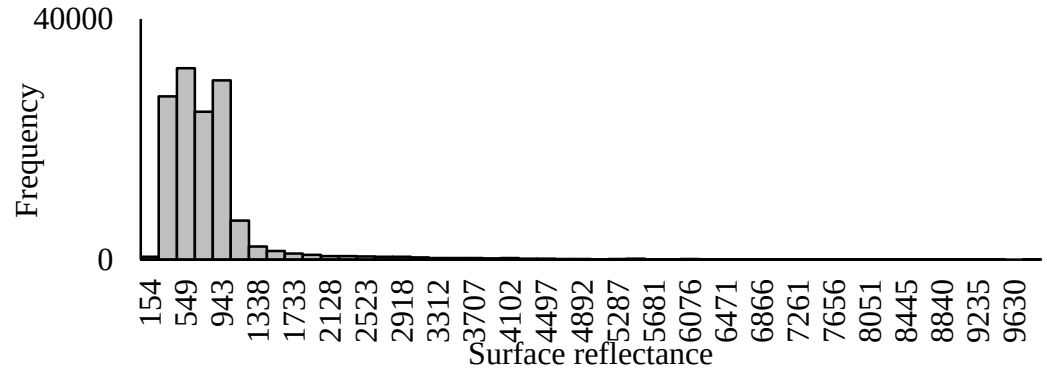

(a) MODIS Band 1

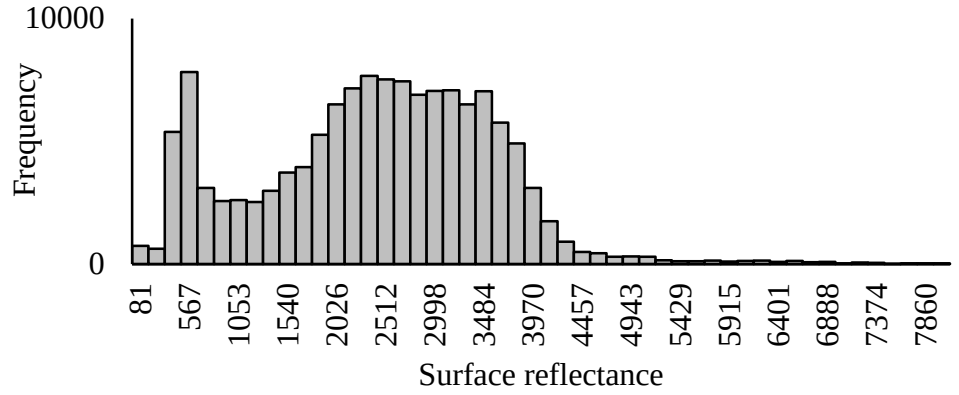

(b) MODIS Band 2

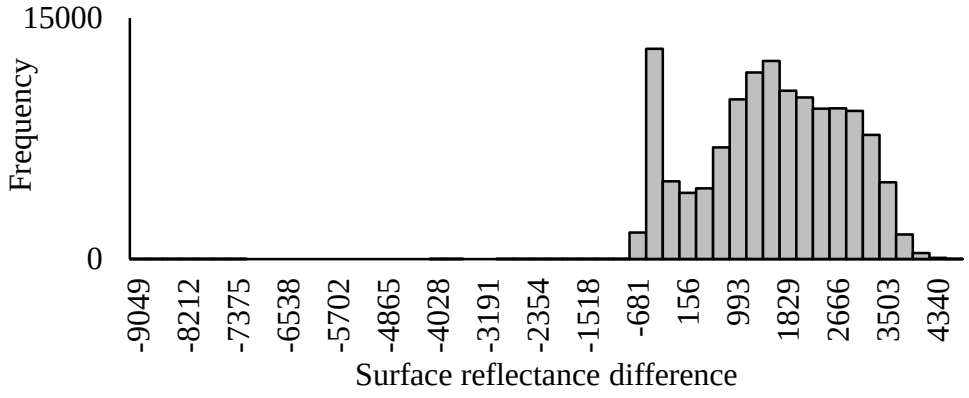

(c) Median filter and difference of MODIS Band 2 and 1

Figure 4.6 Histogram for MODIS image (a) band 1, (b) band 2 and (c) boundary enhancement after taking difference between band 2 and 1

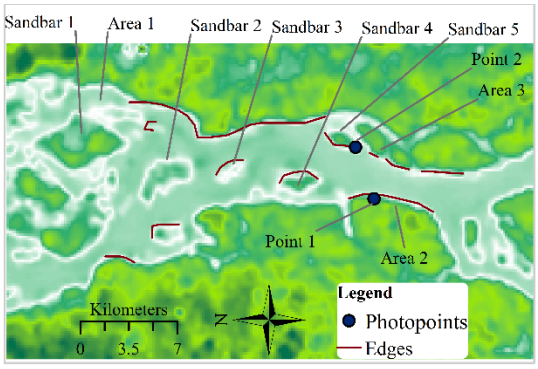

(a) by Eq. 4.6 for 2014

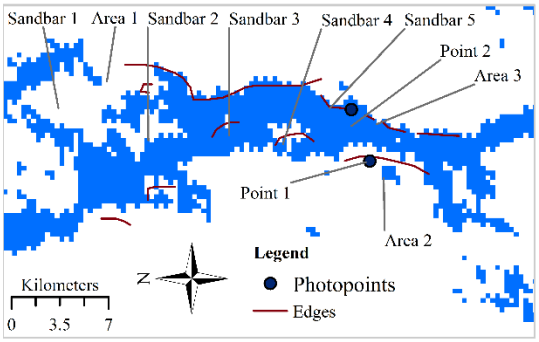

(b) by Eq. 4.1 for 2014

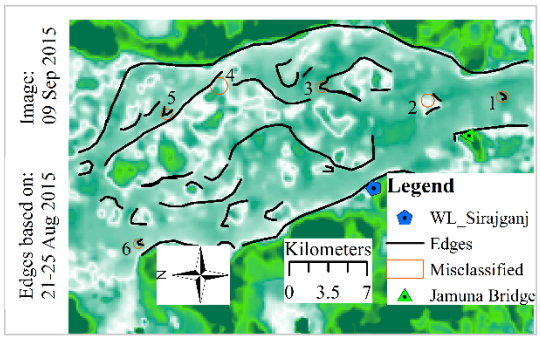

(c) by Eq. 4.6 for 2015

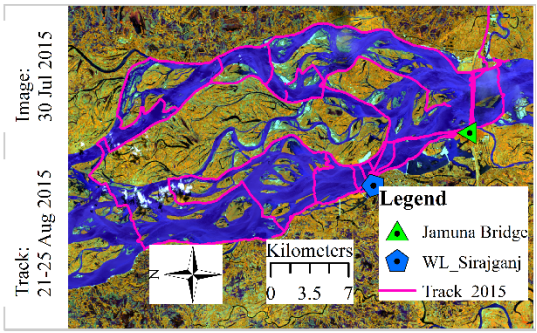

(d) Landsat image

Figure 4.7 Sandbars identified by MGBM and MLSWI, and verification by field investigations

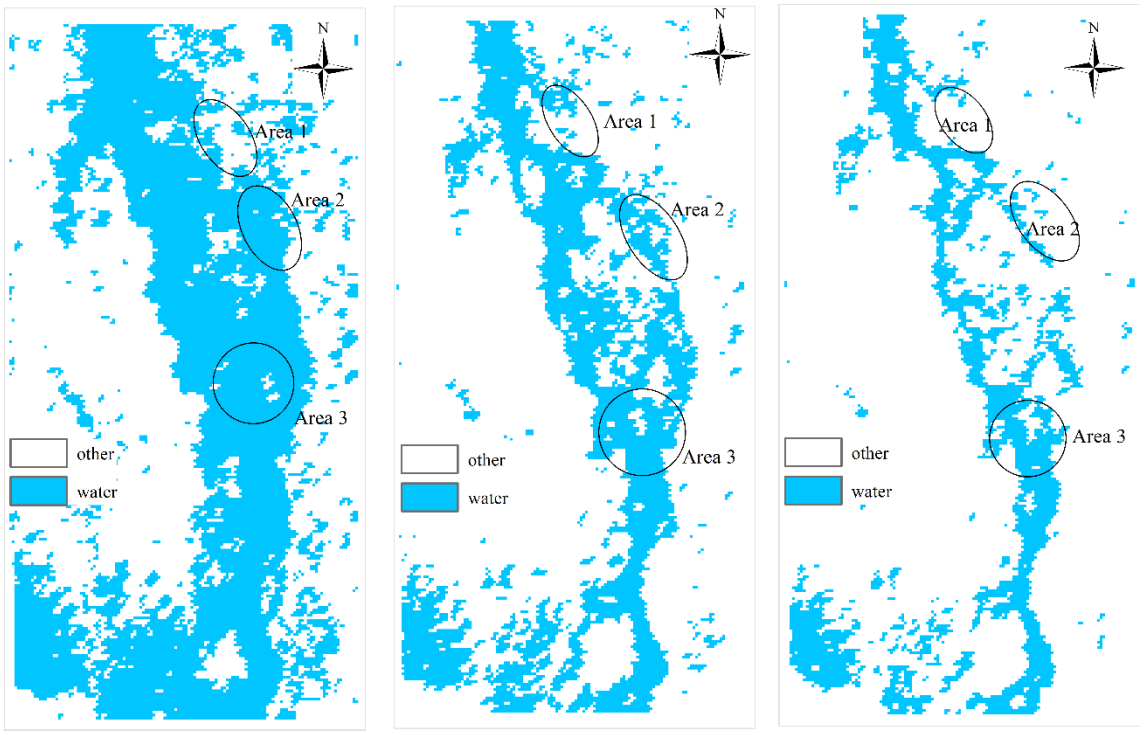

(a) MLSWI>0.70 (b) MLSWI>0.80 (c) MLSWI>0.84

Figure 4. 8 Threshold sensitivity of MLSWI based water identification

Figure 4. 9 Photographs of existing features for verification of edge identification

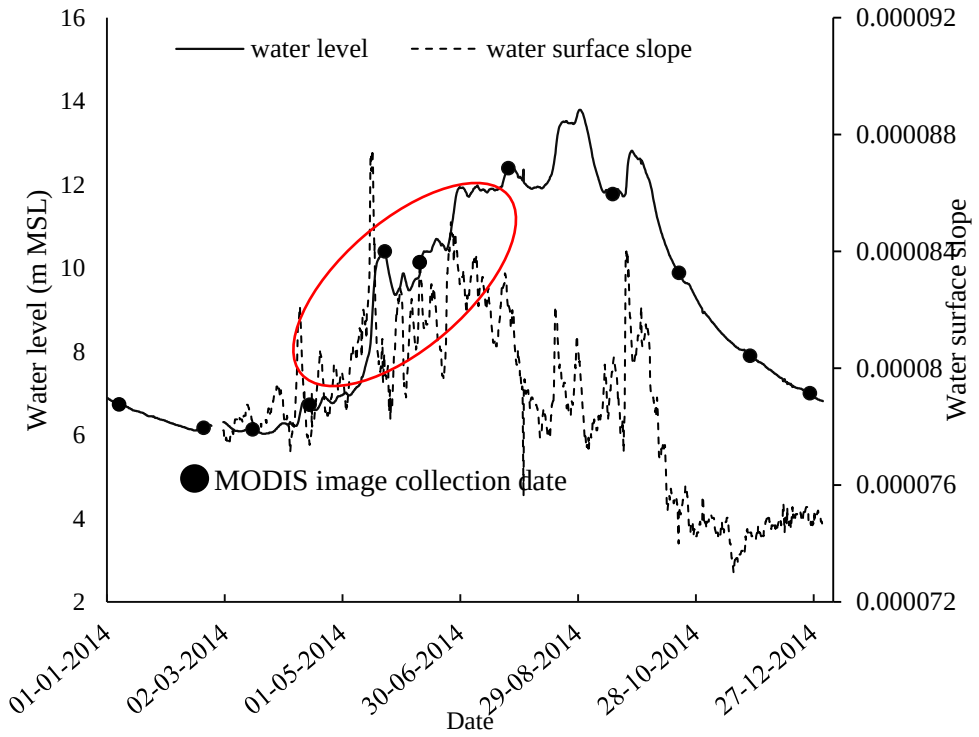

Figure 4. 10 Temporal variation in water level and water surface slope

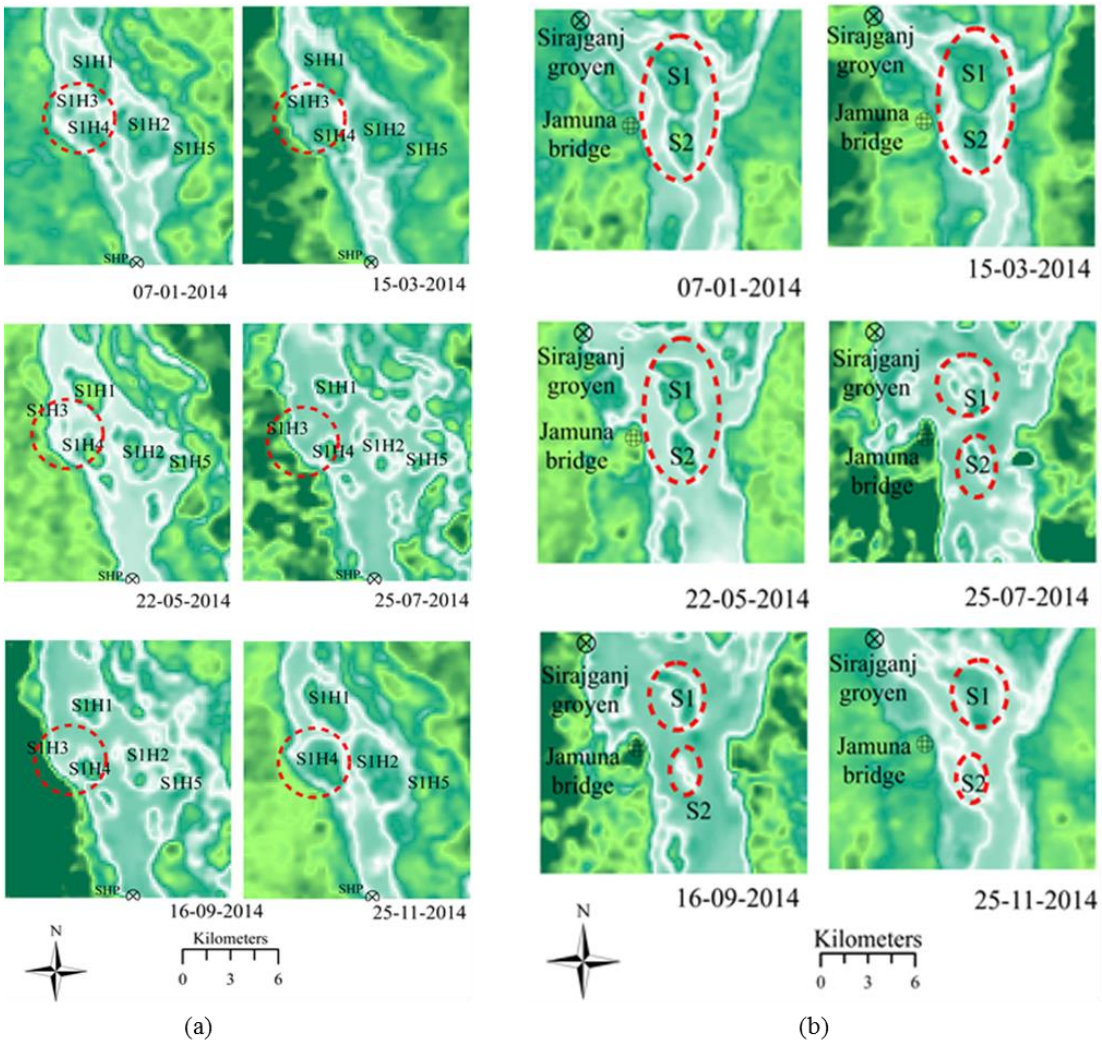

Figure 4. 11 Temporal change in sandbars in the Jamuna River (a) around the Sirajganj Hard Point (SHP) area *and* (b) around Jamuna Bridge area

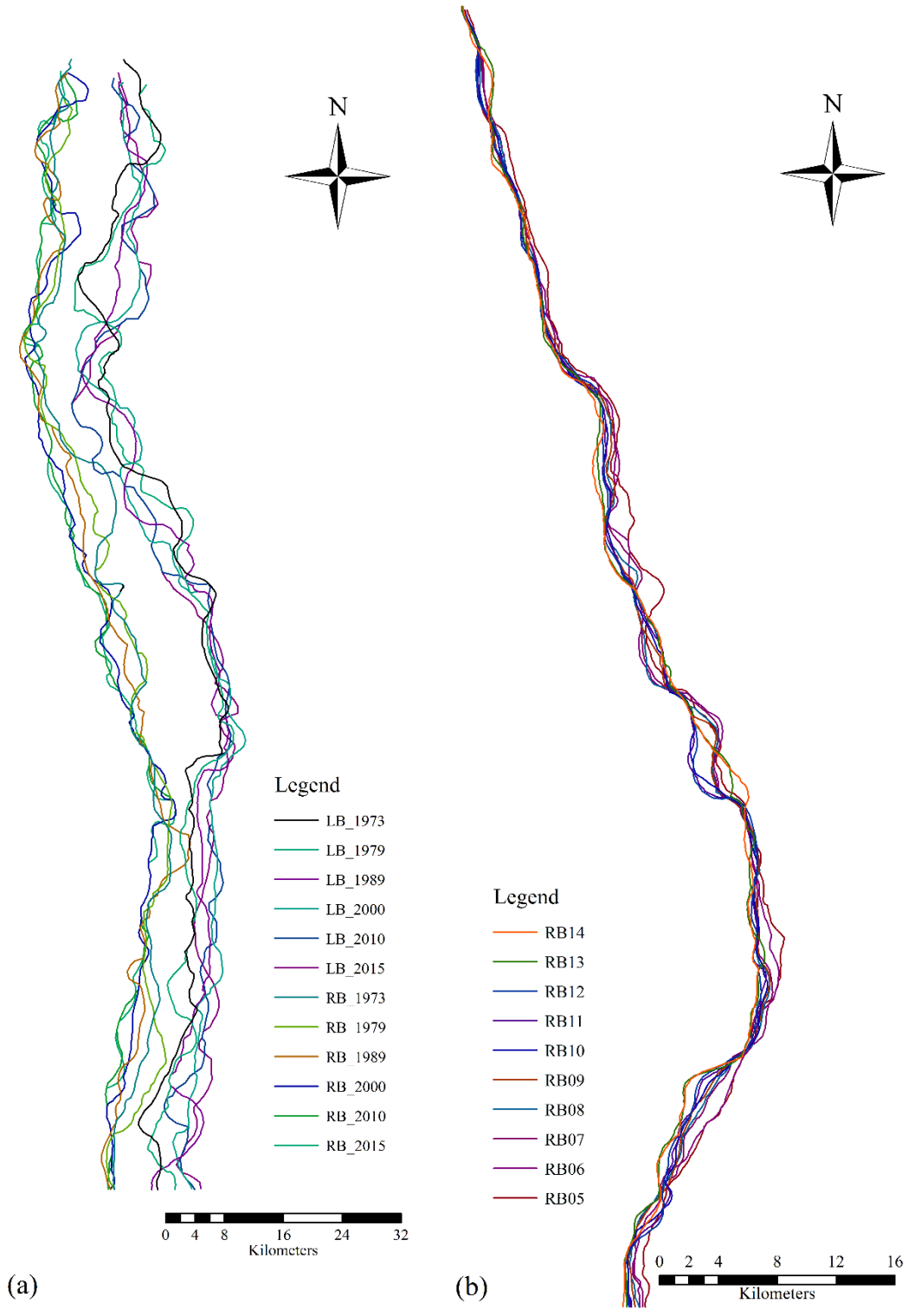

Figure 4. 12 Bank shift in Jamuna River (a) in decadal scale from Landsat (b) from MODIS using MGBM

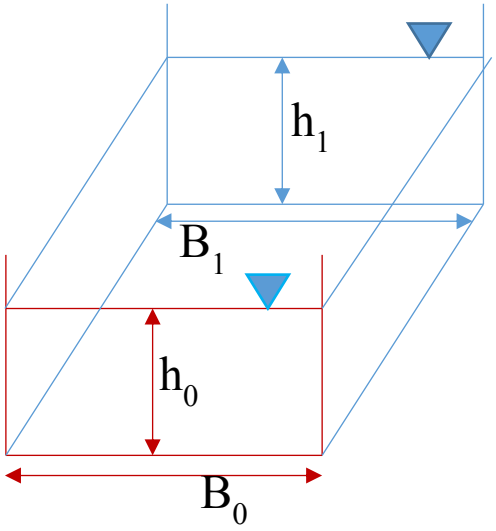

Figure 5. 1 Schematic diagram for reshaping cross-section

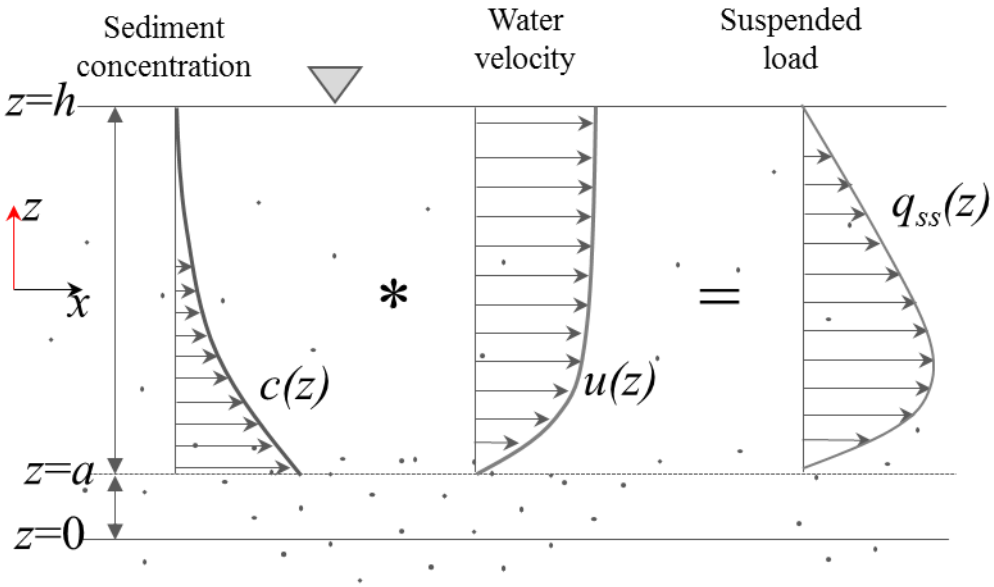

Figure 5. 2 Schematic profile of suspended sediment concentration, velocity and suspended load transport.

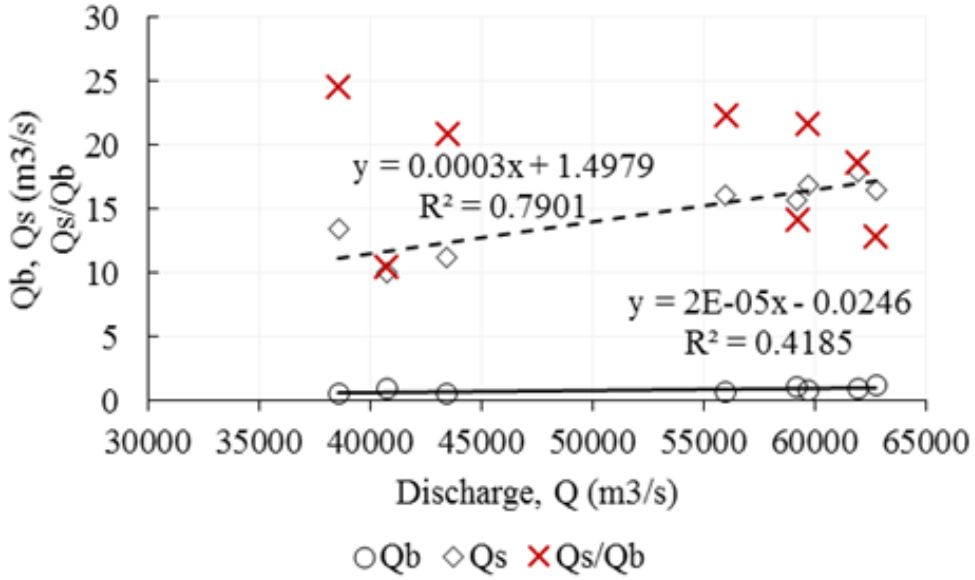

Figure 5.3 Field data on bedload and suspended load in Brahmaputra River

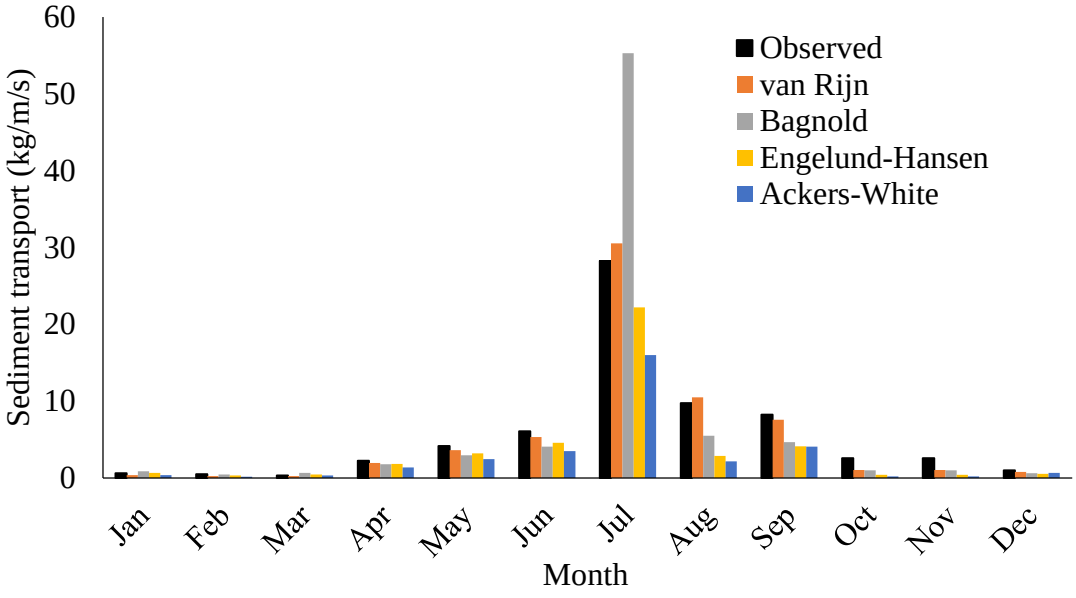

Figure 5.4 Sediment transport in Brahmaputra River using conventional formula

Note. Based on Kabir and Ahmed (1996)

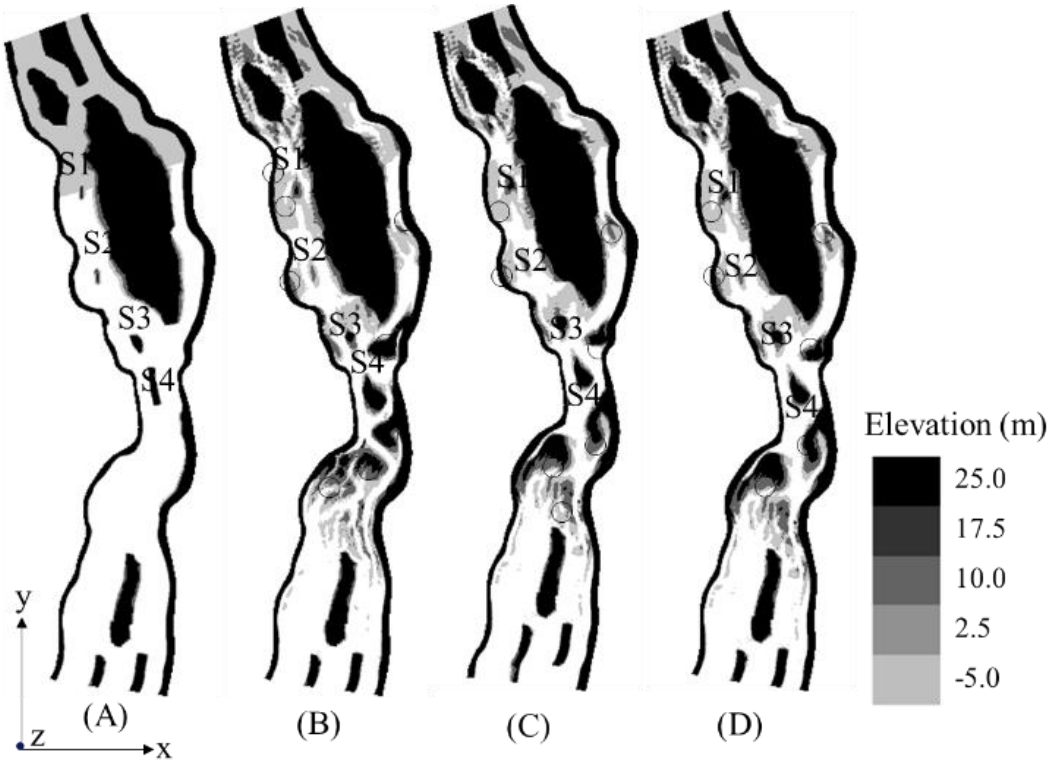

Figure 5.5 Formation and migration of sandbar from numerical simulations

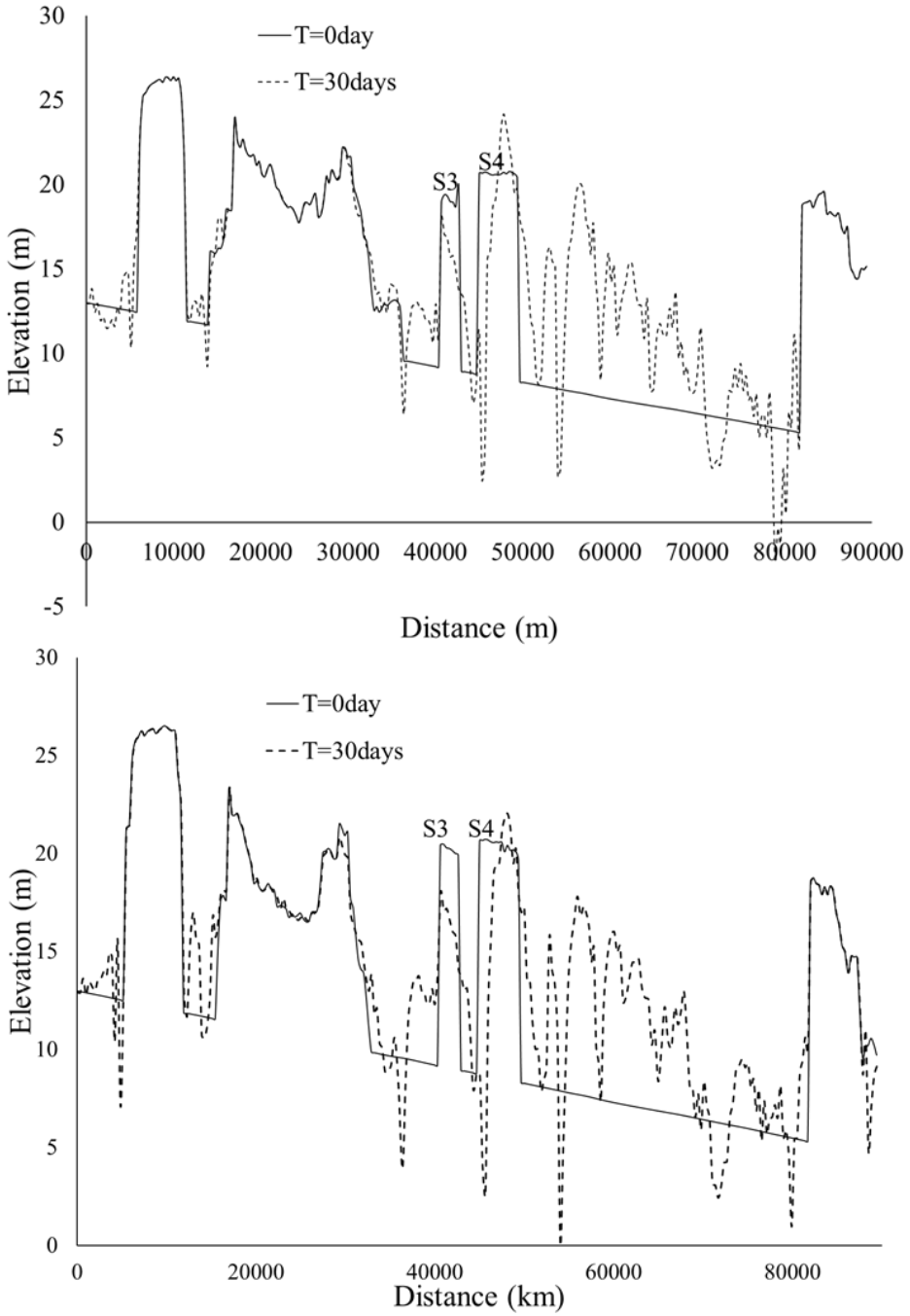

Figure 5.6 Longitudinal profile of temporal variation of elevation along the middle part of sandbars S3 (top) and S4 (bottom)

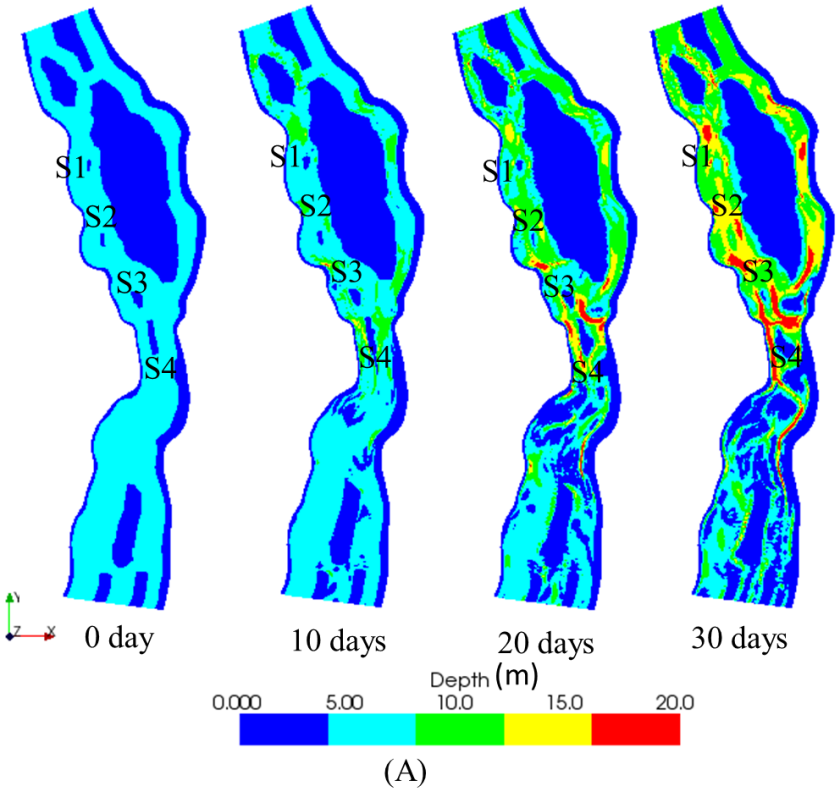

(A)

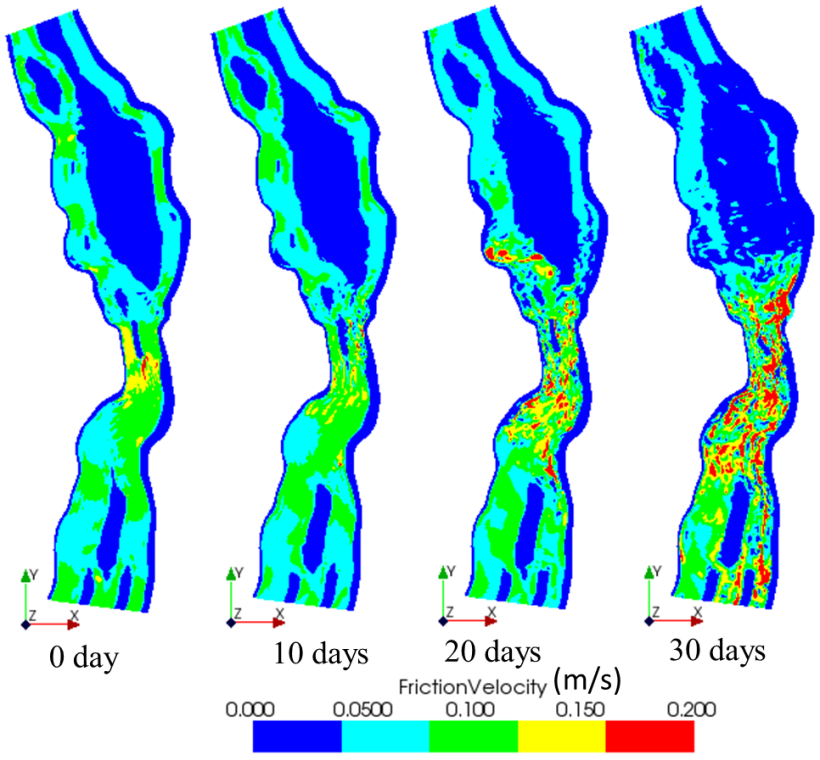

(B)

Figure 5.7 2D distribution of temporal change in depth of flow and shear velocity

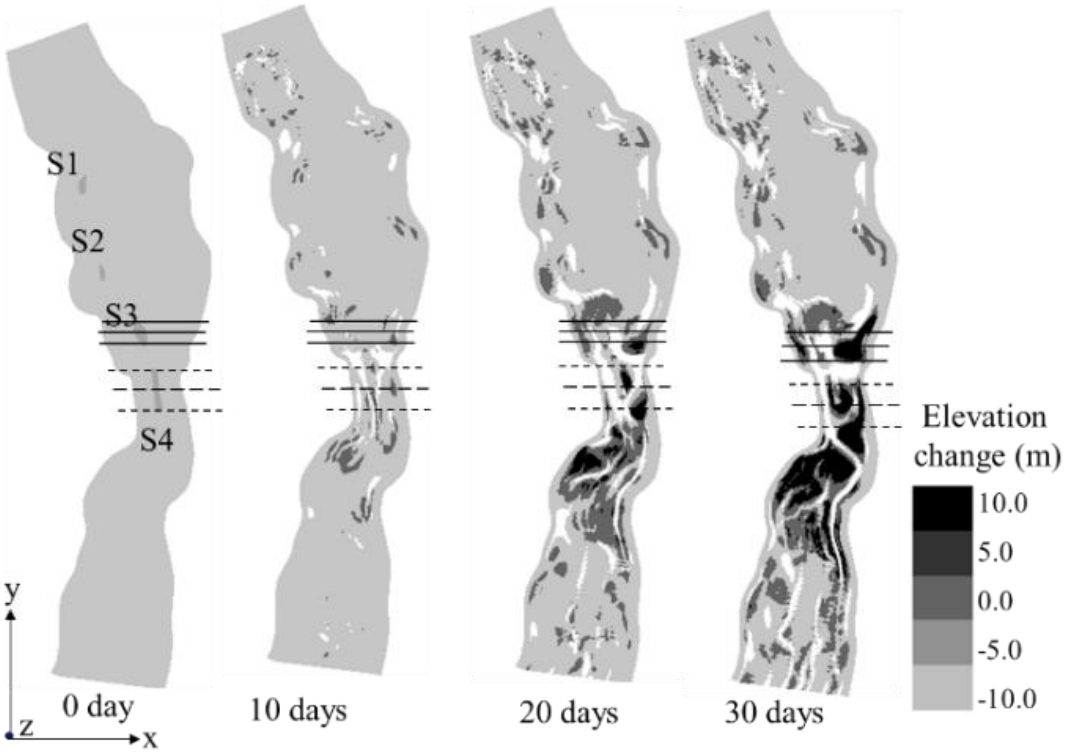

Figure 5.8 Change in riverbed evolution with time from numerical simulation

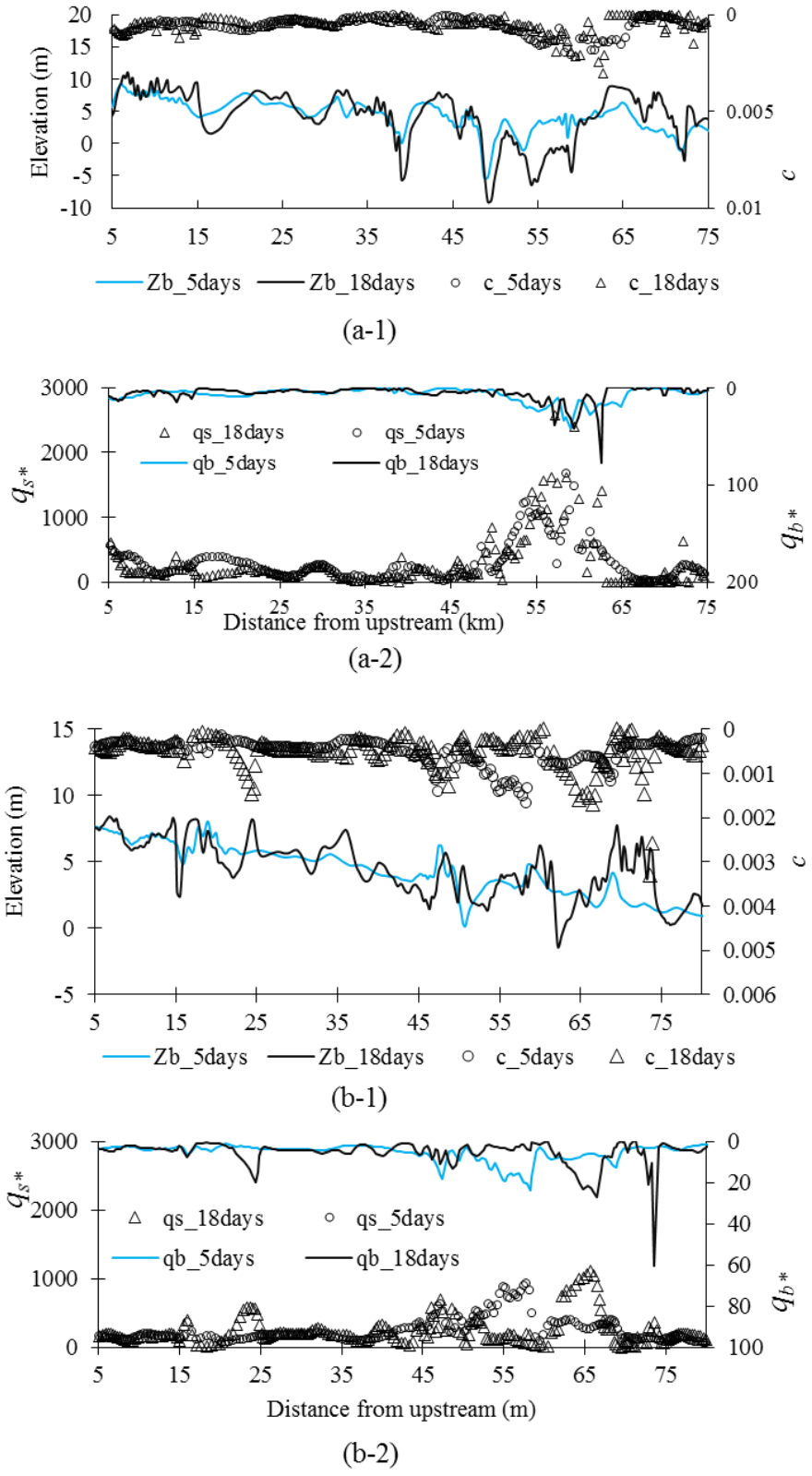

Figure 5. 9 Longitudinal riverbed profile and sediment transport (a-1), (a-2): along right bank; and (b-1), (b-2): along left bank

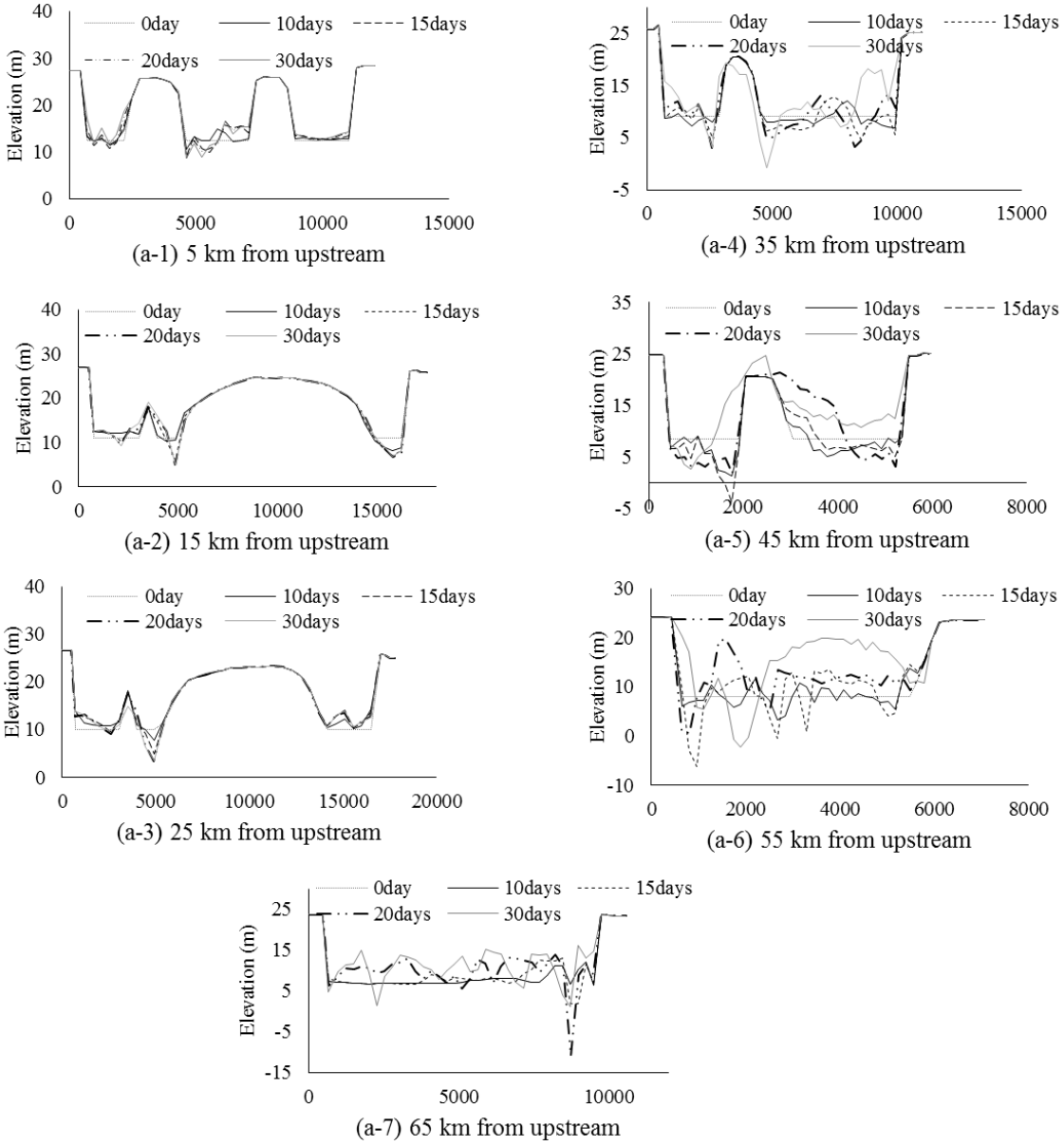

Figure 5.10 Temporal variation in the channel shape (a-1: 5km from the most upstream end and thereafter each section at 10km interval, in all cases, x-axis: distance from right bank in meter)

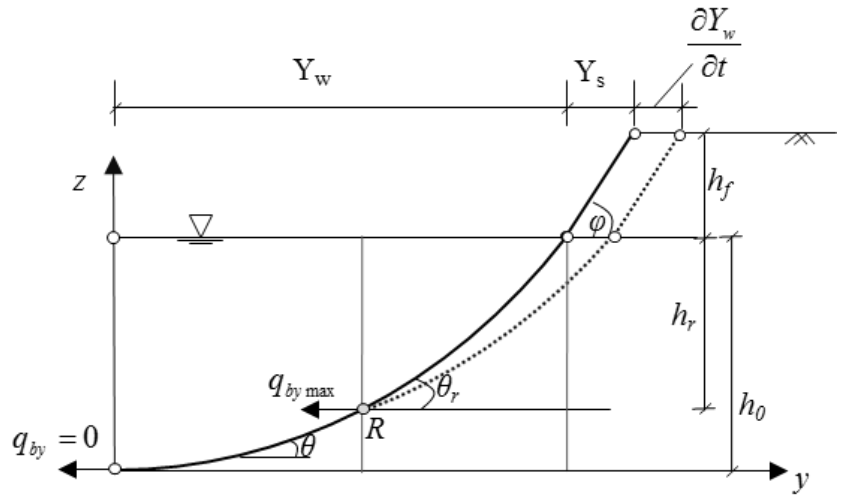

(a) Schematic of cross-section and bank shift

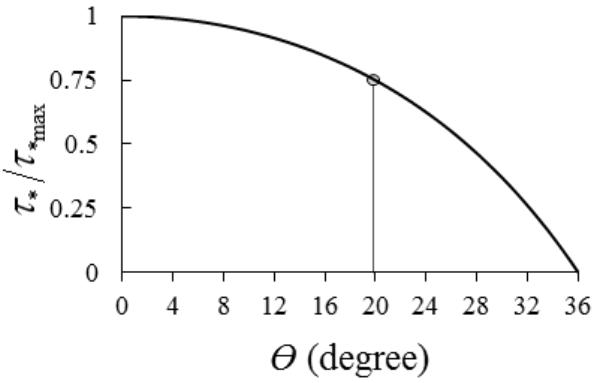

(b) Bed shear stress distribution

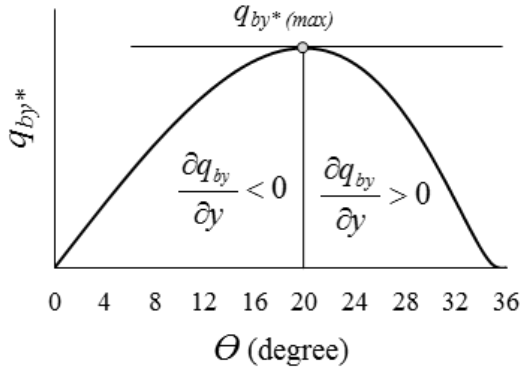

(c)Profile of lateral bedload transport rate

Figure 6.1 Schematics of lateral bedload transport in a bank region

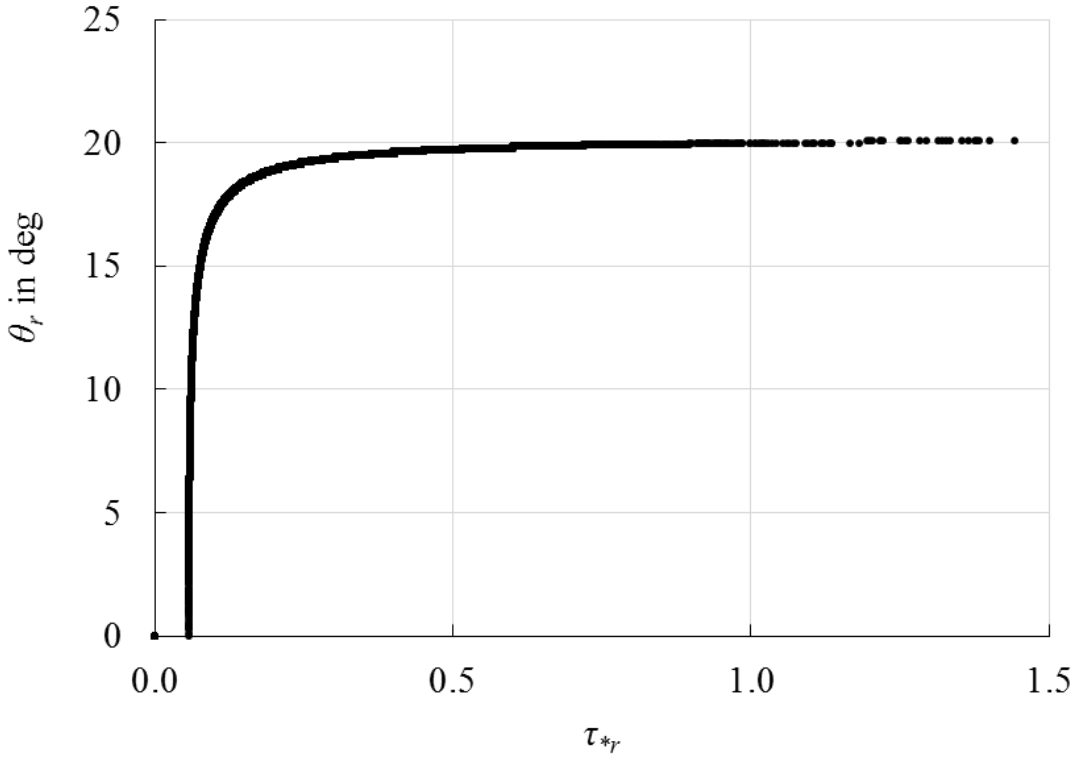

Figure 6.2 Reference lateral bed slope for different hydraulic condition

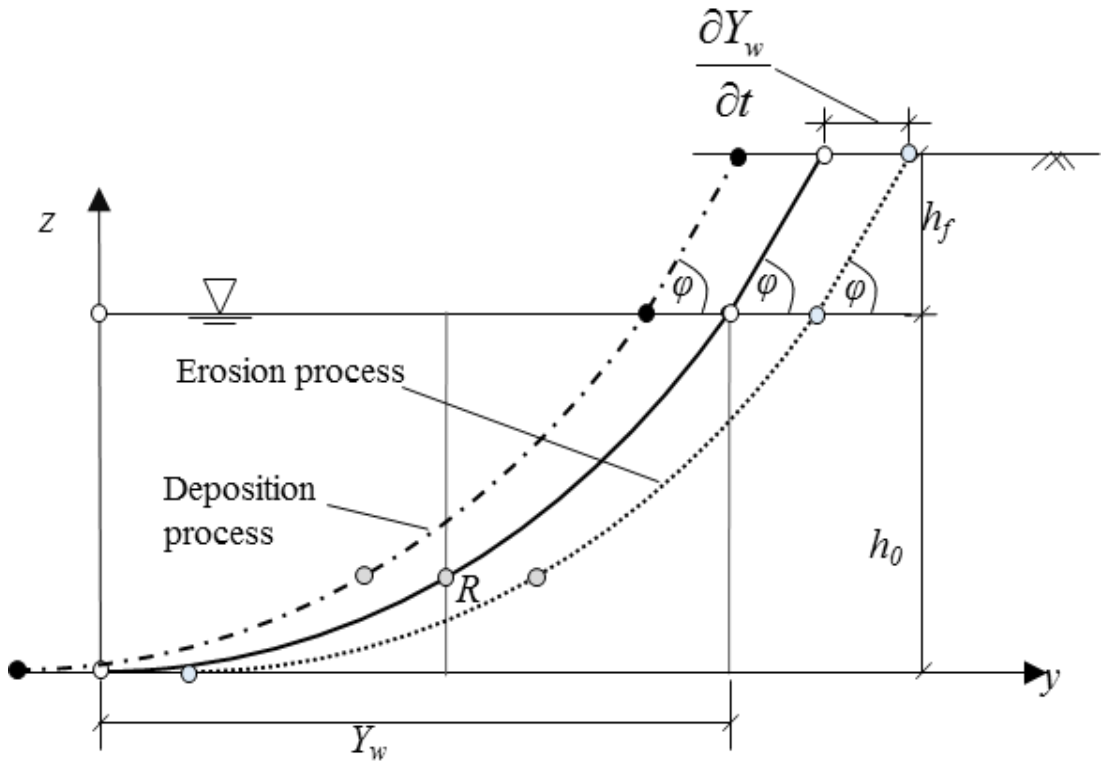

Figure 6.3 Schematic of bank erosion in the flow where suspended sediment dominates.

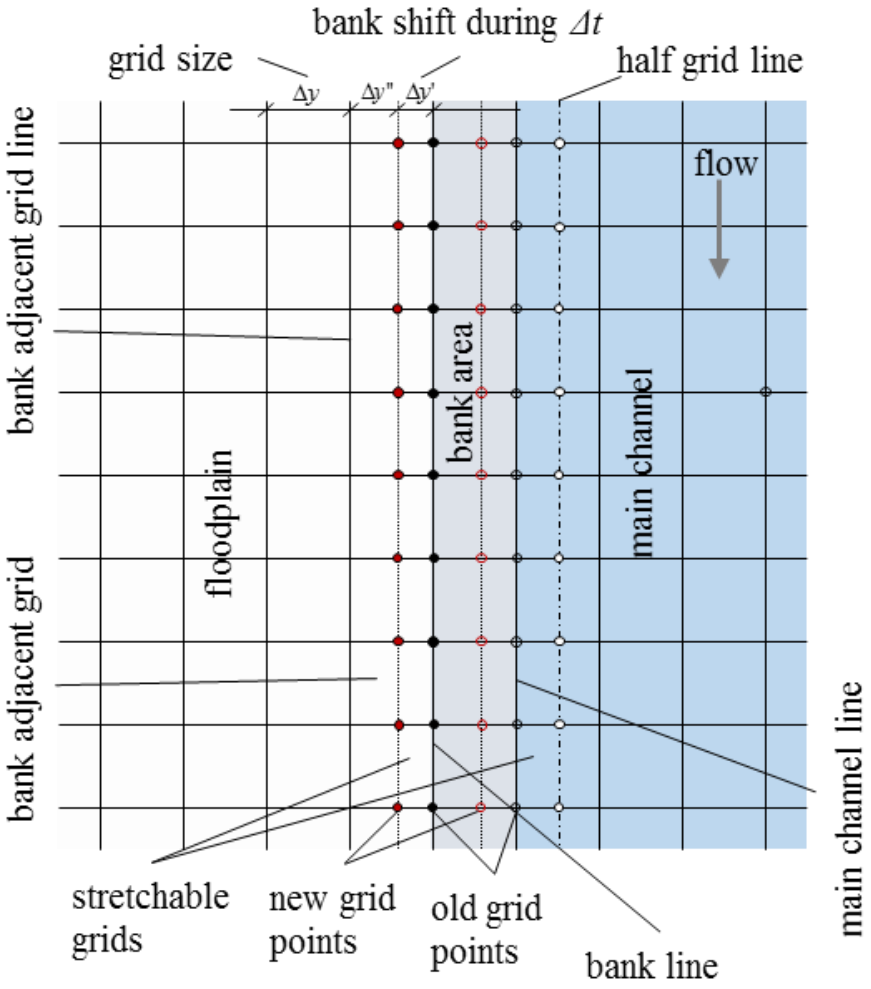

Figure 6.4 Schematic of stretchable grid for grid updating

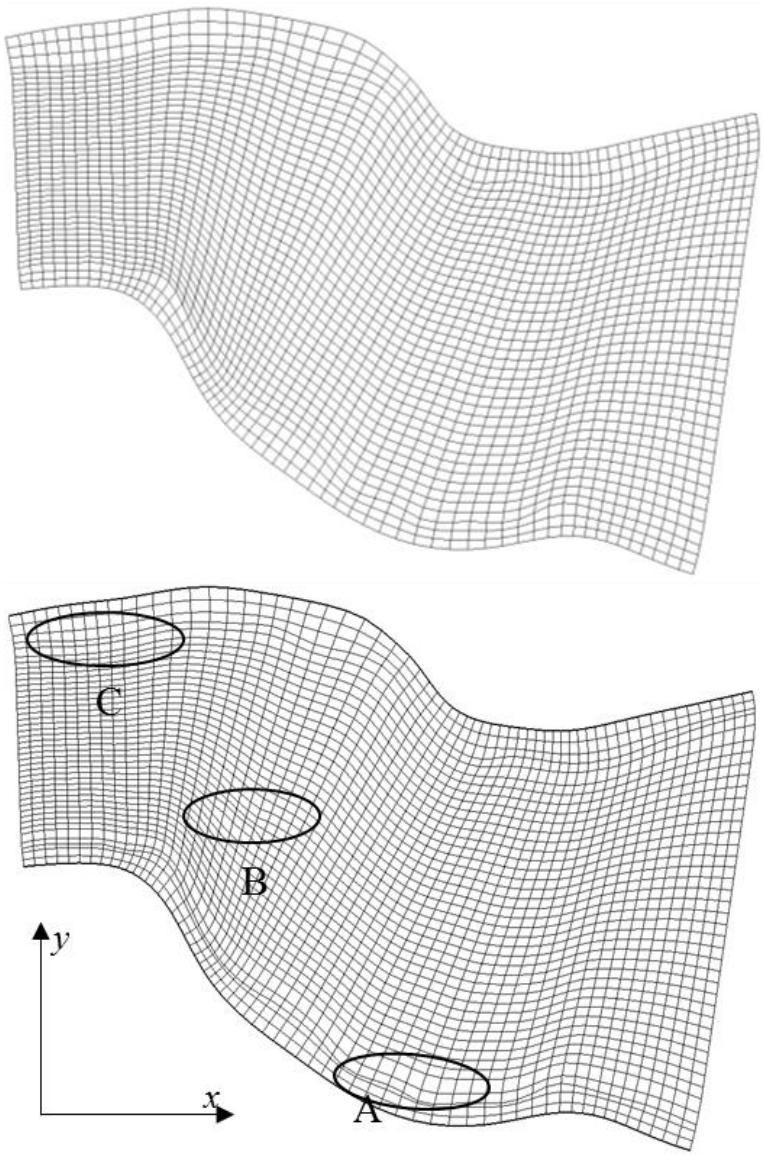

Figure 6.5 Grid deformation at the bank area.

(Top: original, Bottom: after one month)

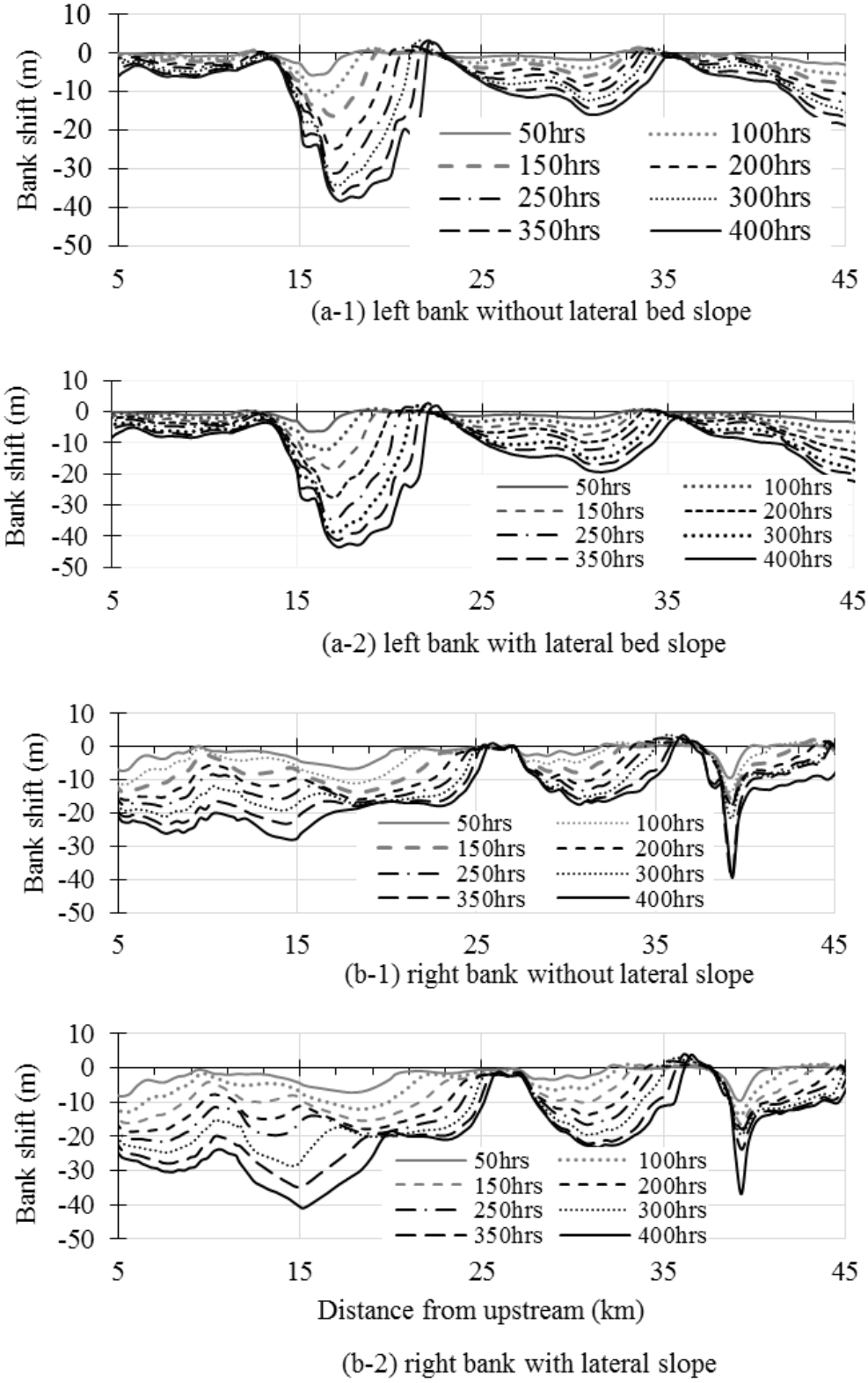

Figure 6.6 Effect of modified erosion rate term on bank erosion

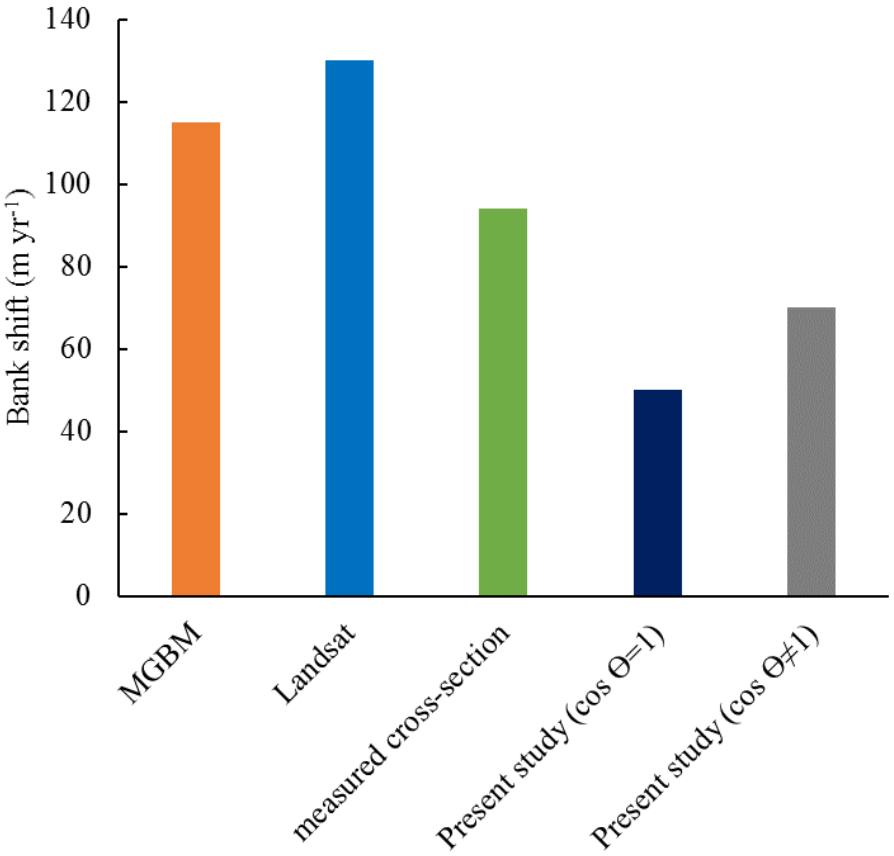

Figure 6.7 Bank shift from numerical simulation with proposed model, satellite imagery, and measured cross-section

Table 2.1 Calculated Values for Formation Region of Bed Forms

Discharge (m^3/s)	**Width (*B*) (m)**	**Depth (h) (m)**	**Non-dimensional bed shear (τ_*)**	***B/h***	h/d_{50}	$BI_0^{0.2}/h$	**Region of bed form**
20,000 (average pre-monsoon)	9 000	8.50	1.95	1.06×10^3	3.22×10^4	170	Multiple row bar [a] Alternate bar [b]
65,000 (average flood)	13 500	11.20	2.57	1.20×10^3	4.24×10^4	191	Multiple row bar [a] Alternate bar [b]
90,000 (10-year return period)	14 500	12.00	2.75	1.20×10^3	4.55×10^4	191	Multiple row bar [a] Alternate bar [b]

Note. d_{50} = 0.264 mm, Average bed slope I_0 = 0.0001, Manning's n = 0.025. Author's calculations based on data from Kuroki and Kishi [a] (1984) and Muramoto and Fujita [b] (1978).

Table 5.1 Ratio of *S*uspended to *B*edload *F*rom *F*ield *I*nvestigation

	Q ($m^3 s^{-1}$)	Q_b ($m^3 s^{-1}$)	Q_s ($m^3 s^{-1}$)	Q_s/Q_b
Case 1	38,574	0.55	13.51	24.56
Case 2	40,756	0.95	10.00	10.53
Case-3	43,480	0.54	11.27	20.87
Case-4	56000	0.72	16.10	22.36
Case-5	59,211	1.11	15.73	14.17
Case-6	59,690	0.78	16.93	21.71
Case-7	62,766	1.28	16.51	12.90
Case-8	61,942	0.96	17.95	18.70

Note. Q = discharge, Q_b = Bedload, Q_s = Suspended load.

Table 5.2 Sediment *T*ransport in the Brahmaputra River *B*ased on *P*ast *S*tudies.

Sl. No.	Q_{ss} (million t yr^{-1})	Remarks
1	402	Goswami, 1985
2	800	Holeman, 1968
3	617	Coleman, 1969
4	541	BWDB, 1972
5	650	Hossain, 1992

Note. Q_{ss} = volume of sediment transport.

Table 5. 3 Sediment Transport Using Different Methods

Month	**Observed**	**van Rijn**	**Bagnold**	**Engelund-Hansen**	**Ackers-White**
Jan.	0.64	0.909	0.678	0.398	0.909
Feb.	0.525	0.456	0.333	0.178	0.456
Mar.	0.36	0.671	0.476	0.334	0.671
Apr.	2.272	1.817	1.851	1.394	1.817
May	4.183	2.962	3.227	2.455	2.962
Jun.	6.095	4.108	4.602	3.515	4.108
Jul.	28.25	55.257	22.23	15.988	55.257
Aug.	9.775	5.491	2.894	2.163	5.491
Sep.	8.265	4.664	4.148	4.111	4.664
Oct.	2.611	1.025	0.417	0.209	1.025
Nov.	2.611	1.025	0.417	0.209	1.025
Dec.	1.008	0.649	0.556	0.665	0.649

Unit: kg/m/s

Note. Author's calculations based on Kabir and Ahmed (1996).